Old Dominion University

ODU Digital Commons

Electrical & Computer Engineering Theses & Dissertations

Electrical & Computer Engineering

Spring 2012

Image-Guided Robotic Dental Implantation With Natural-Root-Formed Implants

Xiaoyan Sun
Old Dominion University

Follow this and additional works at: https://digitalcommons.odu.edu/ece_etds

 Part of the Biomedical Engineering and Bioengineering Commons, Computer Engineering Commons, and the Computer Sciences Commons

Recommended Citation

Sun, Xiaoyan. "Image-Guided Robotic Dental Implantation With Natural-Root-Formed Implants" (2012). Doctor of Philosophy (PhD), Dissertation, Electrical & Computer Engineering, Old Dominion University, DOI: 10.25777/8zjf-s774
https://digitalcommons.odu.edu/ece_etds/188

This Dissertation is brought to you for free and open access by the Electrical & Computer Engineering at ODU Digital Commons. It has been accepted for inclusion in Electrical & Computer Engineering Theses & Dissertations by an authorized administrator of ODU Digital Commons. For more information, please contact digitalcommons@odu.edu.

IMAGE-GUIDED ROBOTIC DENTAL IMPLANTATION WITH NATURAL-ROOT-FORMED IMPLANTS

by

Xiaoyan Sun
B.S. June 2004, Zhejiang University, China
M.S. June 2007, Peking University, China

A Dissertation Submitted to the Faculty of
Old Dominion University in Partial Fulfillment of the
Requirements for the Degree of

DOCTOR OF PHILOSOPHY

ELECTRICAL AND COMPUTER ENGINEERING

OLD DOMINION UNIVERSITY
May 2012

Approved by:

Frederic D. McKenzie (Director)

Jen-Kuang Huang (Member)

Yuzhong Shen (Member)

Jiang Li (Member)

ABSTRACT

IMAGE-GUIDED ROBOTIC DENTAL IMPLANTATION
WITH NATURAL-ROOT-FORMED IMPLANTS

Xiaoyan Sun
Old Dominion University, 2012
Director: Dr. Frederic D. McKenzie

Dental implantation is now recognized as the standard of the care for tooth replacement. Although many studies show high short term survival rates greater than 95%, long term studies (> 5 years) have shown success rates as low as 41.9%. Reasons affecting the long term success rates might include surgical factors such as limited accuracy of implant placement, lack of spacing controls, and overheating during the placement.

In this dissertation, a comprehensive solution for improving the outcome of current dental implantation is presented, which includes computer-aided preoperative planning for better visualization of patient-specific information and automated robotic site-preparation for superior placement and orientation accuracy. Surgical planning is generated using patient-specific three-dimensional (3D) models which are reconstructed from Cone-beam CT images. An innovative image-guided robotic site-preparation system for implants insertion is designed and implemented. The preoperative plan of the implant insertion is transferred into intra-operative operations of the robot using a two-step registration procedure with the help of a Coordinate Measurement Machine (CMM).

The natural-root implants mimic the root structure of natural teeth and were proved by Finite Element Method (FEM) to provide superior stress distribution than current

cylinder-shape implants. However, due to their complicated geometry, manual site-preparation for these implants cannot be accomplished. Our innovative image-guided robotic implantation system provides the possibility of using this advanced type of implant.

Phantom experiments with patient-specific jaw models were performed to evaluate the accuracy of positioning and orientation. Fiducial Registration Error (FRE) values less than 0.20 mm and final Target Registration Error (TRE) values after the two-step registration of 0.36±0.13 mm (N=5) were achieved. Orientation error was 1.99±1.27° (N=14). Robotic milling of the natural-root implant shape with single- and double-root was also tested, and the results proved that their complicated volumes can be removed as designed by the robot. The milling time for single- and double-root shape was 177 s and 1522 s, respectively.

Copyright, 2012, by Xiaoyan Sun, All Rights Reserved.

This dissertation is dedicated to my past 24 years as a student,

the uncertain future,

and the long journey to go.

ACKNOWLEDGMENTS

I would like to thank my advisor, Dr. Frederic D. McKenzie, for his advising and guidance during my stay at Old Dominion University. This dissertation could not been accomplished without his efforts. I also want to thank all of my committee members, Dr. Jen-Kuang Huang, Dr. Yuzhong Shen and Dr. Jiang Li, for their suggestions and advice on this project.

I would like to thank Yongki Yoon for his long standing cooperation on this project with patience and kindness and Krzysztof Rechowicz for his help on model printing and instructions on 3D model modification. Thanks to Mr. Harold Clukey and Mr. Larry Clukey for their initial idea about this project.

My deepest gratitude to my family, who gave me unconditioned love and support all the time, no matter where I am and no matter what decision I make. My special thanks to my husband, who is my biggest supporter and my best friend.

Thanks to all my friends, for their company, no matter if they are here or somewhere far away.

NOMENCLATURE

CS	Coordinate System
VCS	Virtual Coordinate System
RCS	Reference Coordinate System
OCS	Operation Coordinate System
CMM	Coordinate Measurement Machine
CBCT	Cone-Beam Computed Tomography
FRP	Fixed Registration Points
MELFA	Mitsubishi Electric Factory Automation
VD	Volume Decomposition
FEM	Finite Element Method
FLE	Fiducal Localization Error
FRE	Fiducial Registration Error
TRE	Target Registration Error
VF	Virtual Fixture

TABLE OF CONTENTS

Chapter Page

LIST OF TABLES

LIST OF FIGURES

Figure Page

Figure Page

CHAPTER 1

INTRODUCTION

Dental implantation is now recognized as the standard of care for tooth replacement [1-2]. The loss of teeth can harm one's ability of eating, alimentation, speech and appearance, thus significantly affecting the patient's quality of life. According to the American Dental Association, there are approximately 45 million tooth removals in the United States every year [3]. The dental implant market worldwide expects strong growth through 2015 to reach $4.2 billion at a compound annual growth rate (CAGR) of 6% [4], or a global market of $7.9 billion with a CAGR of 13% according to another source [5].

With such a huge need for dental implantation, however, there are still several problems that need to be improved. Although many studies show high short term survival rates greater than 95%, long term studies (> 5 years) using Albrektsson, et al. [6] criteria have shown success rates as low as 41.9% [4-7]. Reasons for such low success rates might include inappropriate planning, limited accuracy of implant placement, instability and hygiene factors during the procedure. Robotic placement of the implants can improve accuracy and natural-root-formed implants can improve stability, thereby providing the foundation for long term success rates under any criteria.

1-1 Thesis Statement

To improve the outcome of current dental implantation, an innovative image-guided robotic system can be developed enabling more accurate and controlled site-preparation of implants including novel natural-root-formed implants for superior biomechanics. Better results than current manual methods within the sub-millimeter range needed for implant placement can be achieved.

1-2 Challenges

One of the important factors that affect the final outcome of dental implantation is successful insertion of the implant into the patient's jawbone. An ideal placement of a dental implant considers the bone density and neighboring anatomical structures for the site-preparation, in particular, the schneiderian membrane of the maxillary sinus in the upper jaw and the mandibular nerve in the lower jaw. The development of imaging technologies provides the information desired for the ideal implantation. Cone-Beam Computer Tomography (CBCT) provides superior 3-dimensional (3D) imaging quality especially for bones, with a significantly lower radiation dose than previously used panoramic radiographs or normal CT [8-9], thereby becoming very attractive for preoperative planning in dental applications. Much pre-surgical planning software is commercially available on the market, for example, BioDental Model System from Biomedical Modeling, Inc., SimPlant from Materialise, Implant Guidance System from DENX, and so on [10]. With the planning software, 3D anatomical information is visualized and a preoperative surgical plan can be generated accordingly.

Appropriate surgical planning is valuable only if the exact transfer of the plan to the intra-operative implant placement is achieved. In fact, it has been the most challenging part of implant dentistry. Currently, two major categories of methods are applied for the transfer: navigation and drill guide. Navigation provides the surgeon with the location of the surgical tool in real time, relative to the important anatomical structures of the patient. It is usually achieved by using an optical or electro-magnetic tracking system. Another category is the drill guide (template). It is a small device with several holes on it, whose position and orientation are manufactured according to the preoperative plan. Both methods are proved to provide better results than conventional free-hand implant placement [11-14], which solely depends on the experience of the surgeon. On the other hand, these two methods are not perfect. For example, navigation utilizing optical tracking can be obstructed by objects along the light path, and electro-magnetic tracking might be influenced by the metal objects in the surrounding area. Most crucially, both the navigation and drill guide methods still require manual drilling for the site-preparation of the implant, with which errors caused by human factors like limited identification accuracy, trembling, and fatigue, etc. are hardly avoidable. Therefore, the accuracy introduced by the computer-aided preoperative planning could be impaired, and even the patient's safety might be endangered.

Looking at the implant itself, research indicated that the design of an implant including geometry, material, surface treatment, etc. can affect the outcome of implantation. A typical dental implant is usually in a cylinder shape mostly because of its easy-to-prepare feature. Finite Element Method (FEM) analysis indicated that the optimal designs for implant load distributions followed closely the natural root forms [15-16].

Nevertheless, the authors dismissed such designs because they are "difficult to manufacture" [16] and site-preparations would be manually impossible.

1-3 Proposed approaches & innovation

In this dissertation, a comprehensive solution is given regarding the challenges in dental implantation as defined in Section *1-2*. A preoperative planning software based on patient-specific CBCT images is implemented to generate appropriate surgical plan and support our novel implants, and a two-step registration strategy which provides an accurate transfer of the surgical planning to the actual operation of the robot while ensuring the patient's safety, are designed. An image-guided robotic site-preparation methodology is developed, which will control proper spacing and orientation on the bone according to the preoperative planning. The development of novel implants in an optimized natural-root form is proposed, which we believe can achieve superior stability and uniform load distribution than current cylinder-shaped implants. With such novel implants, CBCT image-based preoperative surgical planning and image-guided robotic operation to allow precise preparation of the natural-root form that is not manually possible, a comprehensive system to improve the outcome of dental implantation is presented. With this design, the following contributions can be anticipated:

Wholly integrated image-guided, robotic system for dental implantation with a clinically acceptable overall accuracy

- No 1: *Provide a novel two-step registration procedure to transfer the surgical plan to the robot operation*

A wholly integrated image-guided robotic system for dental implantation is presented. Computer-aided technology and a robot-assisted method are combined to provide an advanced application for dental implantation. In the system, instead of registering the image coordinate system and the surgery coordinate system directly, a novel two-step registration procedure was designed to transfer the preoperative planning to the robotic operation. A coordinate measurement machine (CMM) was used to act as a reference coordinate system thus unnecessary and potentially hazardous contact between the robot and the patient was avoided.

- No 2: *Use image-guided robotic dental implantation with sub-millimeter accuracy*

The overall accuracy is one of the most crucial considerations for all kinds of surgery systems. Usually, a sub-millimeter accuracy is regarded as clinically acceptable for dental implantation systems. Among all factors that may affect the system accuracy, registration error plays a very important role. As a result of proper system design and the usage of a high accuracy CMM, phantom experiments indicated an error of 0.36±0.13 mm and 1.99±1.27 ° on position and orientation after registration, respectively, proving that a sub-millimeter accuracy was achieved in our system.

Automated robotic site-preparation methodology for natural-root-formed implants

- No 3: *Implement an innovative automated site-preparation methodology for dental implants using a robot*

A robot-based site-preparation methodology for dental implants was given to control proper spacing, orientation, and thermal effects on bone. A robot with six degrees of freedom (DOF) was introduced into the system and acts as a high-accuracy milling machine. Researchers from other groups already proposed similar robot-assisted systems. However, most of these systems involve "tele-operation" (remote control mode) or "hands-on" (cooperative control mode) for the robot, in which case, a human still needs to control the surgical operation to a great extent. The application is among the limited applications that apply a robot in the system in a totally automated way, which might open a new era for the dental implantation. In addition, the novel natural-root-formed implants have a more complicated geometry than current cylinder-shape implants, which makes manually site-preparation impossible. The volume of certain natural-root-formed implants is removed by calling some pre-defined subroutines, which makes the application of the novel natural-root-formed implants possible.

- No 4: *Establish a standardized set of proven (via FEM) natural-root-formed implant designs that can achieve superior load distribution over current dental implant designs*

The idea of implants with natural-root form was initially proposed by Quality Dental Lab (QDL). It was implemented by generating a standardized set of implants based on

the shapes of natural teeth, and optimized according to the simulation result of Soft Kill Option (SKO) optimization implemented by Yongki Yoon from the Department of Mechanical and Aerospace Engineering of Old Dominion University. These implants mimic the root structure of natural teeth, and have been proven through FEM (implemented by Yongki Yoon) to provide superior stress distribution than current cylinder-shape implants. Although it still needs to be proven by animal experiments, it is believed that a natural-root-formed implant can achieve the stability and uniform load distribution necessary for immediate loading.

- No 5: *Provide a volume decomposition algorithm for robot milling sequences generation*

The 6 DOF robot works as a milling machine in the system. However, milling the volume (geometry) that needs to be removed for the insertion of a certain implant in a point-by-point basis requires large data storage in the robot, which can cause memory outage of the robot and lead to operation termination. A novel algorithm was implemented to generate the robot milling sequence for each natural-root-formed implant, utilizing a volume decomposition concept. The volume is decomposed into the combination of several pre-set standard shapes. In this way, only several parameters are needed to define the milling sequence, and it also allows the most efficient reutilization of the robot sub-routines.

1-4 Organization of this dissertation

The rest of the dissertation is organized as follows: In ***Chapter 2***, a wide review of related topics of the application will be given, and the related works are introduced in ***Chapter 3***. In ***Chapter 4***, a description of the novel natural-root-formed implants were designed is provided: where the idea came from, the theoretical proof, and what results achieved. ***Chapter 4*** illustrates the design and architecture of our application at the system level, including the major components, system operation flow and the architectures of hardware and software. The detailed description of each component of the system is provided in ***Chapter 6***, which includes the planning, registration and robot operation. Later in ***Chapter 7***, the methods and materials for the experiments conducted to test the feasibility and accuracy of the system are explained, and the experiment results are provided in ***Chapter 8***. ***Chapter 9*** gives the conclusion of this dissertation.

CHAPTER 2

BACKGROUND

According to American Association of Oral and Maxillofacial Surgeons, "69% of adults ages 35 to 44 have lost at least one permanent tooth" and "26% of adults have lost all of their permanent teeth" by age 74 [17]. A missing tooth not only will affect one's appearance, speaking ability and eating ability, but also causes bone loss and tooth decay. Without a tooth, adjacent teeth tend to shift closer and cause "crooked teeth" which are harder to clean. Additionally, the bone surrounding the area begins to deteriorate and gums begin to shrink, thus affecting long term quality of life.

Several options are available for replacing missing teeth, including dental bridges, removable dentures and dental implants (Fig. 1). A dental bridge is made up of two crowns and a false tooth/teeth in between that bridges the gap created by one or more missing teeth. It may require the shaping or cutting down of adjacent healthy teeth underneath bilateral crowns. "Recurrent decay, periodontal (gum) disease and other factors often doom fixed bridgework to early failure." [17] A removable denture can be a partial (Fig. 2 b-1) or complete (Fig. 2 b-2). It is removable because it sits over a patient's gums but without secure connection to the jawbone. Dentures are probably the cheapest and the most convenient way of dealing with a missing tooth. However, its outcome is not satisfactory neither esthetically nor functionally. As the patient's jawbone shrinks over time, the denture becomes loose and could cause problems such as gum damage, nerve injury, and difficulties in chewing and speaking. Dental bridges and

dentures usually need to be replaced every 7 to 15 years, and the failure rate is up to 30% after 5 to 7 years [17]. Dental implants are "frequently the best treatment option for replacing missing teeth", according to American Association of Oral and Maxillofacial Surgeons [17]. It has been almost a half century of clinical research since Branemark, et al. reported the osseointegration property of titanium [18]. A dental implant is an artificial piece which substitutes for the root part of a missing tooth. Currently, most dental implants are Branemark osseointegrated titanium implants. As seen in Fig. 1, it is the only way which substitutes the root portion of a missing tooth. Its presence and osseointegration in the jawbone prevents the bone loss caused by the missing teeth, and a success rate of around 95% was reported by many researchers [19-20]. However, different voices do exist. Long term studies (> 5 years) using Albrektsson et al. [6] criteria have shown success rates as low as 41.9% [4-7].

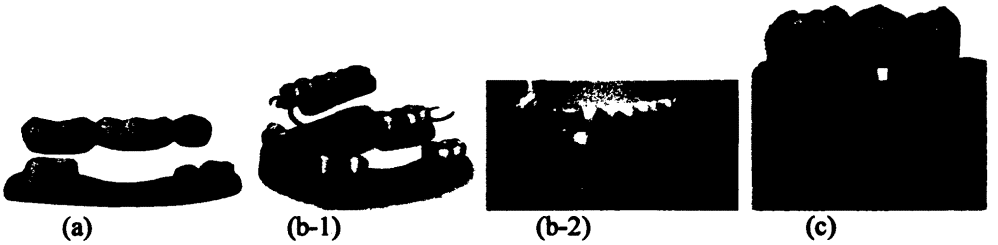

Fig. 1. Solutions for replacing missing teeth [21]. (a) dental bridge; (b-1) partial denture; (b-2) complete denture; (c) dental implant

2-1 Design of a dental implant

A human tooth is composed of two parts: crown and root. The latter is the lower part of a tooth, which serves to anchor the crown in position. Nearly all the dental implants available today are endosseous implants. When a tooth or several teeth are missing, a dental implant is the manmade piece that substitutes for the root part of the missing tooth/teeth. For the majority of implant designs, a two-piece design is utilized: an implant which is the portion embedded and osseointegrated with the jawbone and an abutment affixed to the implant with a screw (Fig. 2). Such a design is based on the two-stage surgery concept, which places the osseous component (implant) first and the restorative component (abutment) a certain time later (usually several months) with another small surgery. As noticed by many researchers, this two-piece design does introduce problems like screw-loosening and infection within the micro-gaps between the two parts [1-22].

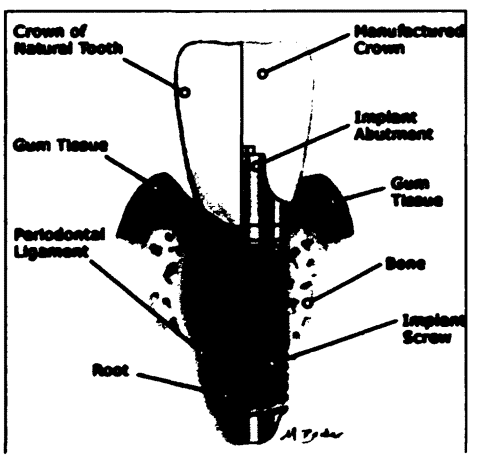

Fig. 2. Natural tooth and dental implant [21]

Research has indicated that "contamination of the implant-abutment junction, the microgap, and violation of the biological width are the causes for the initial bone loss" [23]. A one-piece design that encompasses the abutment together with the implant or in other words, without the abutment, was designed in order to minimize marginal bone loss. Research has shown that one-piece implant has comparable results as the two-piece ones in simulation [24], and a "biologic width"—the vertical dimension of healthy periodontal soft tissues, more similar to natural teeth dimensions as compared to two-piece implants [25]. Nevertheless, one-piece implants are not widely accepted in the dental industry although they are actually commercially available. A typical example is NobelDirect by Nobel Biocare (Kloten, Switzerland), which was launched in 2004. It incorporates both an implant and an integral fixed abutment in one piece, and was designed to "simplify use and ensure long-term healthy, beautiful teeth" [26]. However, many clinical cases reported poor clinical outcomes with an excessively high amount of marginal bone loss surrounding the implant and lower success rates [27-28]. In a one-year prospective study, 20% of analyzed 550 NobelDirect showed a marginal bone loss of >3 mm, while the success rate (under grade 1 criteria) was 46.1% compared to 85.5% of the two-piece implants [23]. Although some other studies reported a survival rate of 97.9% after three years [29], and even a success rate (33 months) of 100% with a mean marginal bone loss of 0.53 ± 0.37 mm at the 12-month follow-up visit [30]. Nobel Biocare has been sued by a California dentist seeking class-action status on behalf of dentists whose patients have suffered complications such as bone loss. In fact, in 2005 to 2006, the Swedish Medical Products Agency investigated NobelDirect after receiving complaints about the same problem, however, its continued sales was approved after the

investigation [31]. Other one-piece implants available in market include Zimmer One-Piece Implant by Zimmer Dental Inc. (Carlsbad, CA USA) [32], One-piece 3.0 by BioHorizons, Inc. (Birmingham, AL USA) [33], etc.

Research indicated that the shape of dental implants has an effect on implant biomechanics [34]. Today, screw- or cylinder-shaped implants are the standard for dental implantation. While such designs mimic the structure of natural roots and ease the drilling procedure into the bone, it is hard to achieve the ideal stability provided by natural human roots, especially for molars, thus leading to loosening and fracture [35]. Attempts were made by placing two single screw-type implants instead of a single implant in large molar case [35]. Results indicated that it was a "more functional and biomechanically sound method of molar replacement"[35]. Balshi, et al. conducted a three years follow-up, which showed a cumulative success rate of 98.6% and less complications but with increased bone loss [36]. Leung, et al. implemented the first *in vitro* study using the connection of two mini-implants with a mini plate [37], which proved to be a stable system. All these trials attempted to get an implant more similar to the shape of a natural root of a human tooth, and showed very encouraging preliminary results. In fact, an optimum design problem indicated that the optimum shape of an implant was somehow close to a natural root shape [15], and the conclusion was also supported by FEM results [16]. However, such designs were not pursued because they are "difficult to manufacture [16]", thus site-preparation would be manually impossible.

2-2 Image-guided dental implantation

Image-guided technology has been applied in dental surgery and has shown the capability of optimizing preoperative planning and improving the quality of the intra-operative performance [38]. Here, "image" means the clinical data received from imaging modalities such as computer tomography (CT), magnetic resonance imaging (MRI), and ultrasound (US). These data provide important information about the patient including bone density and neighboring anatomical structures, which is crucial to the success of implant placement, therefore helps preoperative planning, intra-operative navigation, and post-operative evaluation. An ideal placement of a dental implant considers the patient's anatomical structures, in particularly, the schneiderian membrane of the maxillary sinus in the upper jaw and the mandibular nerve in the lower jaw. Cone-beam computer tomography (CBCT) is suitable for use in dental practice, which provides superior 3-dimensional (3D) imaging quality with lower radiation dose and less scan time [8]. Much software is available for image-guided dental implantations (RoboDent, DenX, SimPlant, etc. [10]).

Implant space is one of the concerns in dental implantation. Appropriate spacing between an implant and a neighboring implant, or natural tooth, is required to provide sufficient blood supply and avoid overheating during drilling with subsequent death of the bone cells. A space of 4 mm to 7 mm is recommended by most implant manufactures. The minimum space between an implant and a neighboring natural tooth, and the space between two adjacent implants should be no less than 3 mm and range from 3 mm to 5 mm, respectively [39]. To achieve the requirement for implant space, it adds the upper

limit to the accuracy of the implantation system. Usually, a sub-millimeter accuracy is regarded as clinically acceptable. However, it is not very easy to achieve. The overall accuracy of an image-guided dental implantation system can be affected by many factors in the system structure, including resolution of medical imaging scans, result of 3D models, preoperative planning, registration and accuracy of hardware.

In computer-aided surgery, registration is one of the most important steps. Registration is the process that aligns different sets of data obtained from different objects (for example, the patient's anatomy, medical images, robots, and sensors) or from different time. Registration is "fundamental to all areas of computer-integrated medicine" [40]. Registration error may mainly determine the final accuracy of the system. For image-guided surgery, several different principles are applied to transfer the surgical plan to actual surgical operation:

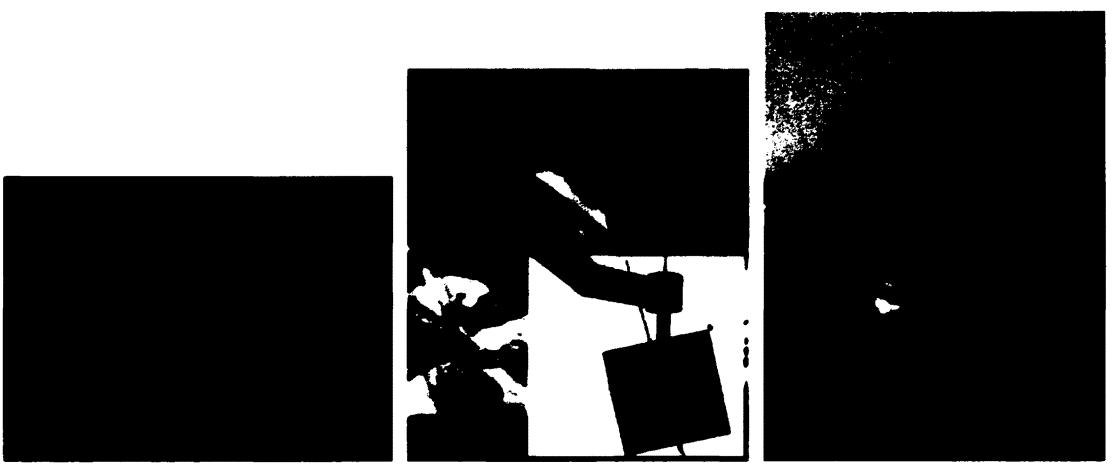

(a) VectorVision [41] (b) Artma Biomedical Inc. [42] (c) FAU [43]

Fig. 3. Examples of image-guided surgery with different methods to transfer the surgical plan to the operation

1) Navigation, involving dynamic tracking, tracks the surgical tool intra-operatively with an optical [44-45] or magnetic tracking system [36] and its position is superimposed onto the virtual model of the patient and shown to the surgeon on a screen. Systems with navigation include VISIT (Vienna, Austria), VectorVision (Brainlab, Munich, Germany), InstaTrak (GE medical systems), etc. [46].

   One significant drawback of such systems is that the navigation is given on the monitor but not directly on the surgical site, therefore it may be difficult to align the display relative to the surgical field, and it also distracts the surgeon's attention from the operative field which might cause errors and danger to the patient. Additionally, optical tracking can be obstructed by objects between the cameras and the target, while the results from magnetic trackers are easily disrupted by metal objects in the surrounding area. Also, the system accuracy is affected by the working distance of the tracking device.

2) Augmented reality also supports navigation but by projecting extracted structures from preoperative images directly onto the patient, thus solving the problem of monitor navigation. The structures could be anything that is important to the surgery but is not otherwise visible by the surgeon, for example, tumors underneath tissue such as the breast [47]. The projection of structures could be on a head-mounted display [48-49], or a specially designed semi-transparent mirror [50-51]. A problem with the augmented reality guided system is the usage of the bulky head-mounted displays, which may deteriorate the surgeon's perception.

3) A surgical guide/template is generated according to the real/virtual geometric information of the patient, which can be physically accessed by the surgeon, therefore navigation is not necessary. This method is usually applied in the field of oral and maxillofacial surgery and is currently the most acceptable by surgeons because it is the closest to the conventional way. Several rapid prototyping technologies could be applied to manufacture the surgical guide, including stereolithography (SLA), 3D printing [52], or computer numerical control (CNC) technology [53]. However, intraoral fixation of the template in edentulous patients could cause serious problems. It not only may provide inaccurate guidance, but may also create a nauseous response in the patient due to template movement [54].

For registration, some artificial markers (namely fiducials) are usually applied to help align the two coordinate systems. Several kinds of registration techniques have been proposed in the literature. Among them, paired-point registration is the simplest method and is widely used for image-guided systems. This method aligns a set of N points ($N \geq 3$) in the first coordinate system with another set of corresponding points in the second coordinate system, using one-to-one mapping. It is straightforward and easy to conduct when fiducials are used or a tracking probe is used to physically contact each of these points. Currently, it is the only registration algorithm that has a closed form solution with well-understood error predictors, if measurement error is independent and identically distributed (IID) with a zero mean Gaussian distribution [55]. Point-to-surface registration, which matches a cloud of points to a 3-D surface constructed from the preoperative image, is another kind of rigid registration technique. The major advantage of this technique lies on that it avoids error introduced by fiducial marker identification

from preoperative images. However, the transformation between the virtual and real object cannot be analytically calculated by using a surface matching method and it is difficult to quantify the quality of the registration [56]. Another category for registration methods is non-rigid (elastic or deformable) registration, which is suitable for situations where objects change their shape during the procedure. Non-rigid registration still remains an open area of research.

Validating the accuracy of an image-guided dental implantation system is a challenge because evaluation *in vivo* is impractical. Instead, phantom experiments are conducted for validation purpose. A unitary definition of system accuracy seems to be non-existent in clinical practice for computer-aided surgery systems (CAS systems). A number of different parameters can be found in the literature to describe accuracy [57]. Among these parameters, the following three are widely used for evaluating the accuracy of point-based registration methods [58]:

1) Fiducial localization error (FLE): the error in locating the fiducial points (displacement error of the fiducial localized point from the correct position);
2) Fiducial registration error (FRE): the distance between corresponding fiducial points after registration;
3) Target registration error (TRE): the distance between a corresponding target point after registration, where the target is a position different from fiducials.

For paired-point registration, FRE and TRE can be calculated as follows: Suppose registration is done between two coordinate systems: CS1 and CS2. $P_1(i)$ and $P_2(i)$ are two sets of fiducial points in CS1 and CS2, respectively; while $Q_1(j)$ and $Q_2(j)$ are two

sets of target points in CS1 and CS2, respectively. Here, i=1~M and j=1~N, where M and N are the number of fiducial points and target points, respectively. For each i, $P_1(i)$ and $P_2(i)$ compose paired-points; while for each j, $Q_1(j)$ and $Q_2(j)$ compose paired-points. After paired-point registration, fiducial points $P_2(i)$ and target points $Q_2(j)$ are mapped into $P'_2(i)$ and $Q'_2(j)$ in CS1. Then, FRE and TRE can be calculated as:

$$FRE = \sqrt[2]{\frac{1}{M}\sum_{i=1}^{M}(P'_2(i) - P_2(i))^2} \quad (1)$$

$$TRE = \sqrt[2]{\frac{1}{N}\sum_{j=1}^{N}(Q'_2(j) - Q_2(j))^2} \quad (2)$$

Accuracy of image-guided implantation was reported in numerous publications, where TRE values at either the entry or the apex of the implant were usually utilized to indicate position accuracy after registration. TRE values reported by different research groups have a huge variance, even with very similar system setups. In a review given by Widmann, et al. [59], the registration errors from 16 systems, all with optical navigation, were listed, and the mean TRE values for each system ranged from 0.35 mm to 5.6 mm, and the maximum error ranged from 0.73 mm to 10.5 mm. On the other hand, registration accuracy with templates seems to be more delightful than the results with navigation. The mean errors at the entry and the apex of the implant are between 0.8~1.51 mm (with the maximum of 1.2~4.7 mm) and 0.9~3.07 mm (with the maximum of 1.6~7.1 mm), respectively [48]. Apart from the position of implant insertion, its orientation is also a very important factor which will affect the final success of the implantation. Similar to positioning errors, the deviation of angulation errors reported is large as well. It ranges from less than one degree to more than ten degrees [48-60]. The registration errors are

evaluated in two ways: in either the image domain or the operation domain. The first is done by fusion of the pre- and post-operative images together and measuring the difference between [61-62], and the latter usually compares the calculated coordinates of the target after registration with the actual coordinate measured by a device [60].

Usually, registration between two coordinate systems is calculated by finding the transformation which minimizes the sum of squared residuals of the sample data set, i.e., fiducials. Because registration is the overall best fit for all the fiducials, and target points are different from fiducial points, target registration error (TRE) can differ from fiducial registration error (FRE), and the distribution of TREs within the surgical space might be different from point to point. Moreover, the placement of fiducial points has a great influence on error minimization for paired-point registration. The centroid of the fiducial points should be as near as possible to the target point and also arrangement for these points should avoid being near-collinear [63]. Additionally, the type of fiducials, including anatomical landmark, skin fiducial, bone fiducial and other external frames, also affects the final registration accuracy [59]. Anatomical landmarks are stable but very difficult to identify, thus would lead to a rather inaccurate result (3.1~10.5 mm as reported by Mascott et al. [64]). The accuracy from skin fiducials are better than anatomical landmarks, however, it still does not meet the sub-millimeter requirement [64-66]. Bone fiducials have been proved to have high accuracy (possibly sub-millimeter accuracy) and represent the current gold standard [59]. The only problem with bone fiducials is its invasive feature. Instead of being placed directly onto the patient, the fiducials could also be integrated with an external frame, which is worn by the patient. Such a frame is noninvasive while providing similar registration accuracy to the invasive

bone fiducials [67-68]. It also allows the usage of larger fiducials, which are not possible if internal fiducials are used in a craniomaxillofacial surgery. However, as mentioned earlier, the locating pattern of fiducials in the frame could affect the registration accuracy.

Another important concept in computer-aided or robot-assisted surgical system is calibration. Different from its meaning as in "instrument calibration", the concept of calibration here is closer to "offset calibration". In a system with a localizer or a robot, the points of interest usually are not accessed by the end-effecter of the localizer or robot directly. Instead, a probe or other device is attached to the localizer or robot to provide direct contact to those points. In this case, the offset between the tip of the probe and the end-effecter of the localizer or robot must be calculated. "Calibration" usually refers to procedures like this in computer-aided or robot-assisted surgical application.

Both calibration and registration are used to determine the geometrical relationship between different entities in a system. However, calibration is for frames connecting to the same object rigidly; while registration is for independent coordinate systems [69]. In other words, calibration is the procedure to determine fixed offsets between different components in the same coordinate system, and registration is the process to link the coordinates of the same object between different coordinate systems. The former is a static procedure, while the latter is a dynamic one.

2-3 Robotic surgery and its safety consideration

Robots were introduced into the surgical area in the 1980s. Now, a large amount of robot-assisted surgery systems are developed by researchers and their applications cover the medical areas of orthopedic surgery, neurosurgery, gynecologic surgery, cardiothoracic surgery, urology etc. [70]. According to one report, the market for medical robotics and computer-assisted surgery (MRCAS) devices and equipments worldwide is expected to be $5.7 billion by 2011, with an average annual growth rate of 34.7% [71]. Robot-assisted surgery can be expected to keep sustainable development because of the unique advantages of robots, including flexibility, stability, rapid response capability, and so on [72].

For robot-assisted surgery, two types of robots exist: "positive" and "active" robots. The positive type robots are used to enhance the visualization and dexterity of surgeons. Because of the complexity of the surgical environment and the diversity of patients' situations, robot-assisted surgeries are usually solutions with human-integrated control, such as in "tele-operation" (remote control mode) or "hands-on" (cooperative control mode). The former composes a tele-operated system, in which the surgeon manipulates the robot from a remote location using data sensed by the robot. In cooperative control mode, the surgeon and the robot both hold the surgical tool, which provides both precision and sensitivity of a machine, and the manipulative transparency and immediacy of hand-held tools. [73] They are typically used during minimally invasive procedures. The da Vinci System from Intuitive Surgical Inc. is the only commercially available and FDA approved tele-operated system. Active type robots execute a predefined plan, thus

combine preoperative medical imaging with the accuracy of the robot to achieve optimal intraoperative positioning. Navigation of the robot is required and is accomplished using images and virtual models of the target object or organ that is registered with the actual patient allowing complex surgeries to be performed safer and faster.

Because robots can only follow pre-programmed commands and cannot react autonomously when unexpected situations happen, certain measures must be taken to guarantee the safety of a robot-assisted surgical application. Due to the limited space and delicate nature of the mouth cavity, one important way for safety consideration is motion constraints which restrict a robot's motion in the dental implantation. Traditionally, drill guides are used to serve as physical fixtures for surgeons' drills (Fig. 4).

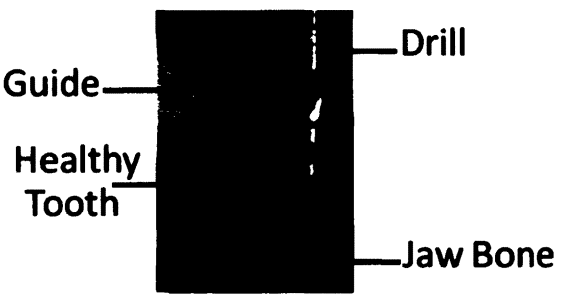

Fig. 4. Drill guide acts as a physical fixture

Another way to introduce motion constraints for the surgery is the implementation of a "Virtual Fixture (VF)". The concept of virtual fixture was first introduced by Rosenberg, in 1993. It was defined as "an overlay of abstract sensory information on a workspace in order to improve the telepresence in a telemanipulation task". [74] There are two categories of virtual fixtures (VFs): guidance virtual fixture and forbidden-region virtual

fixture. The former guides the robot to move along desired paths or surfaces, and the latter prevents the robot from entering into forbidden areas of the workspace [75]. Different technologies for virtual fixtures and their applications in different surgical areas have been discussed in many research papers. A few of these are discussed below.

Robot-assisted craniofacial surgery is a major application area in which virtual fixtures are applied. In the work presented by Matinfar, et al. [76], three types of regions were defined for virtual fixture purposes: safe zone, boundary zone, and forbidden region. The virtual fixture implanted in the paper used linear constraints. Phantom experiments indicated that penetration of the forbidden region was up to 0.7 mm. As the authors stated, a better virtual fixture strategy may be required, such as the one presented by AnkurKappor, et al. [77]

Taylor's group in Johns Hopkins University did intensive research on virtual fixtures. They presented a method to customize VFs by combining several task primitives, for example, stay on a point, maintain a direction, etc. A constraint optimization problem was formulated for each task primitive, where potential-collision boundary constraints, task behaviors and joint limits served as constraint conditions [78]. The constraint optimization problem can be implemented with both linear and nonlinear constraints [77]. In addition, they introduced a "soft" virtual fixture mechanism to allow some freedom for a robotic tool inside safe areas.

One of the most challenging problems with VFs is how to regenerate a new motion trajectory once the violation of virtual fixture occurs. With human-integrated control, this problem can be easily solved since the human can decide which way to go himself. It

ensures safety in the intra-operative site; however, the possibility of automated surgery is eliminated. For all the research mentioned above, VFs were implemented in robot-assisted procedures during which humans act as part of the control. Besides, generating VFs utilizing constraint optimization requires the knowledge of robot's forward kinemics and also feedbacks from the robot, which is difficult to achieve in the dental implantation system. In order to explore the possibility of automated implantology without a surgeon's manual guidance, methods for virtual fixtures need to be adapted and tested in our system.

2-4 Robotic volume machining

Due to the small size scale and relative delicate complex structure of the natural roots, milling for natural-root-formed implants inside the mouth manually by a surgeon is not feasible. On the contrary, it can be easily achieved by a robot, which normally has an accuracy of sub-millimeter order of magnitude.

There are many commercial computer-aided machining (CAM) solutions for machining tool path generation. Also, several dental CAM systems are available especially for manufacture in dentistry. For example, DentMILL by Delcam [79], inciseTM dental milling system by Renishaw [80], etc. These systems usually are designed for machining of dental products in vitro, although algorithms used in these systems for transferring designed 3-D volumes into machining tool path generation might be the same as what is needed by inside the mouth milling. However, the expensive prices of these solutions act as an impediment.

Small amounts of open source CAM are also available through the internet, for example, through www.sourceforge.net. Unfortunately, after downloading and testing, none was found practicable for our application. Besides, some commercial CAM software provide free versions for demonstration or advertisement purpose. However, these versions are usually less capable and some crucial functions are cut off.

Another possible way of CAM is generating the machining scheme according to algorithms presented in publications. There are two main categories for the machining design: direct tool-path generation from a 3-D model, and planning based on volume decomposition. For the 3-D milling process, cutter contact (CC) points and corresponding tool orientations are generated according to geometric features of the volume, in direct tool-path generation. If planning is done using a volume decomposition method, the volume of material to be removed, so called Delta Volume, is divided into several sub-volumes and removed according to the natural sequences of machining [81]. One can tell from the above definition that direct tool-path generation focuses mostly on the surfaces of Delta Volume, while volume-decomposition considers features of the whole volume.

CHAPTER 3

RELATED WORK

Researchers from Shanghai Jiao Tong University in China proposed an image-guided oral implantology system (IGOIS) and applied it in the placement of zygoma implants [62-82]. The IGOIS included 3D models reconstruction, preoperative planning, registration, and intra-operative motion tracking. Two software developed by the authors' institute were used in the system for CT images processing, 3D models reconstruction and preoperative planning. Also, a Polaris optical tracking device was used for real-time motion tracking.

Fig. 5 gives the framework of the IGOIS presented in their paper. There were five main components in the framework:

1. image processing for preoperative CT images;
2. reconstruction of 3D models from the processed CT data;
3. preoperative planning based on the 2D images and the 3D models;
4. registration of fiducial markers between Virtual Coordinate System and Real Coordinate System;
5. real-time navigation for the surgery.

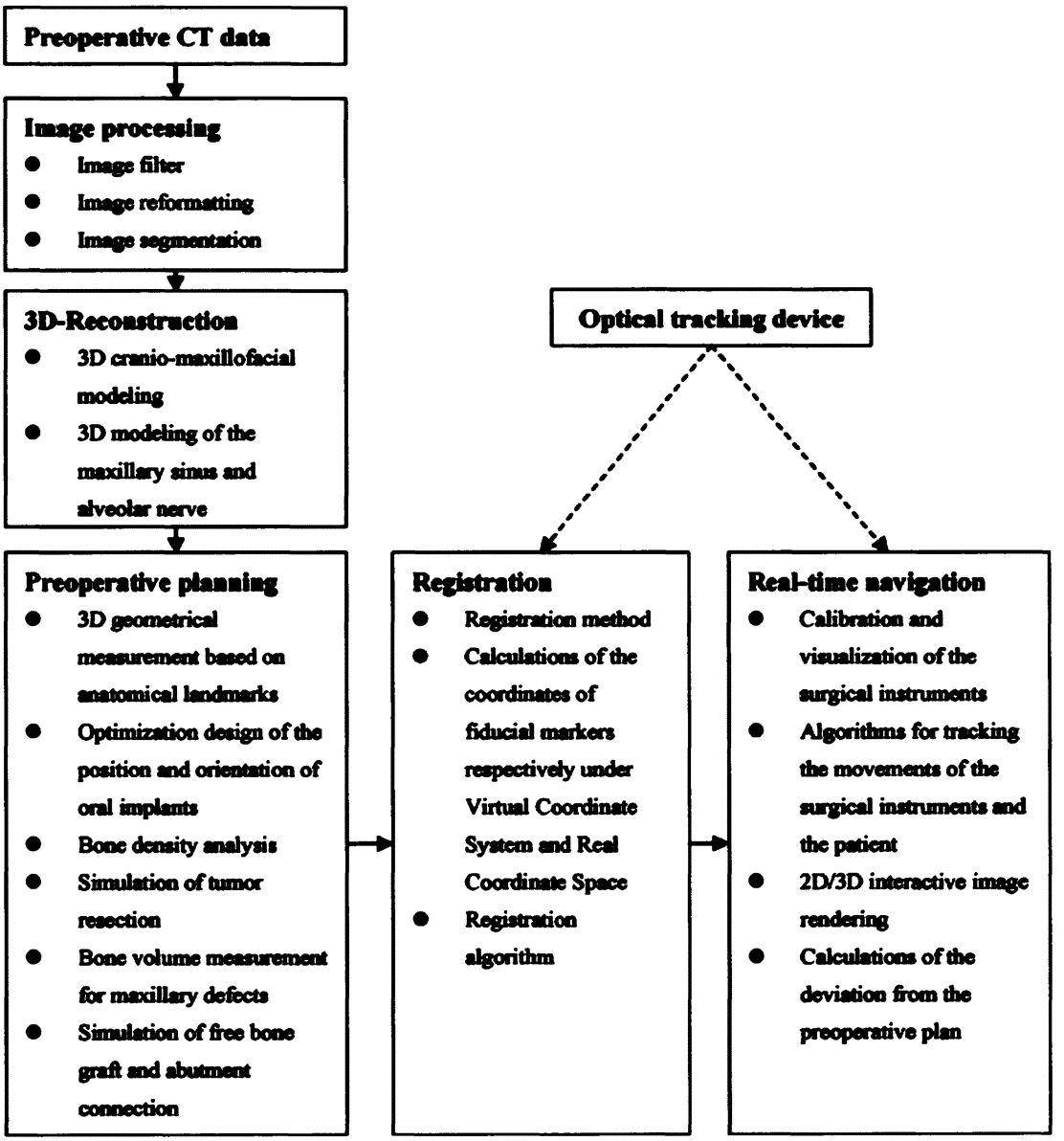

Fig. 5. Framework of IGIOS [62]

It is obvious that the frameworks of their system and the one used in this dissertation are very similar. Preoperative planning based on medical images, and intra-operative navigation using optical tracking and image-guided technology, are the two features of their work.

The major difference between this system and theirs lies in the application of robot. In their system, there was no robot employed and surgical operations are still executed by a surgeon. It means that only computer-aided techniques were used in their application but not robot-assisted techniques. Besides, in their system, intra-operative position and orientation of the surgical tool is recorded by an optical tracking device; while in this system, because the implementation of robot, this information can be reported by the robot itself, which makes an additional tracking device not necessary. However, for registration purposes, a Coordinate Measurement Machine (CMM) was employed in this system to perform the job of coordinate measurement, which is performed in charge by the optical tracking device in their IGOIS. The major reason to not choose the optical tracking or electro-magnetic tracking devices as applied in many image-guided systems is that there is no real-time tracking (navigation) required as in this system design. Therefore, CMM, as a more stable and accurate device, fits the need better. Navigation utilizing optical tracking can be obstructed by objects along the light path, and electro-magnetic tracking might be influenced by the surrounding metal elements (the robot is obvious in the case of this system).

An image-guided robotic system was developed in Taiwan to help with surgical positioning and drilling [83], which has the most closest system design as the one in this dissertation. Their system utilized an ultrasound machine to capture the images of the brain area with tumors. Surgical paths were planned preoperatively using a GUI with patient's images. After the registration procedure to find the optimum transformation matrix among coordinate systems, surgical paths were transformed to the frame of a six-axis robot. The system overview is shown in Fig. 6.

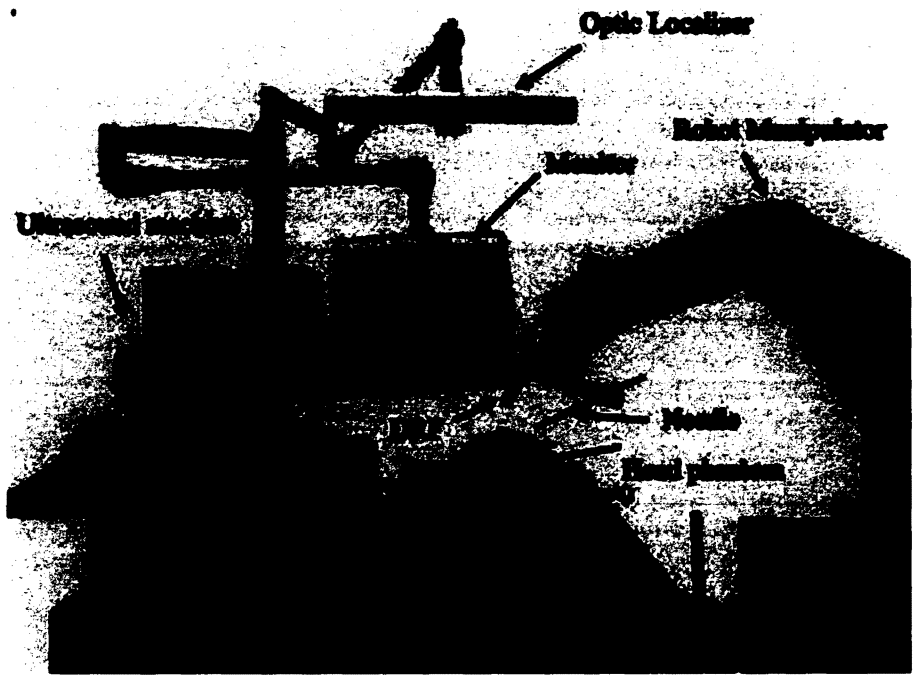

Fig. 6. SPANS robotic system [83]

This system shares the same goal as the one used in this dissertation, which is an automated robotic system. To this end, a six-axis robot was utilized in both systems. However, the job complexity of the robot is different in the two systems. In their system, only the positioning and simple drilling was carried out by the robot; but in this system, a complicated milling operation for the natural-root shapes is required, which necessitates much effort on the robot controlling strategy.

Similar to the system from Shanghai Jiao Tong University, the device for registration is another major difference between the two systems. An optical localizer was incorporated in their system to record the coordinates for registration. As explained earlier, while navigation is not required for this system, the optical localizer might cause unnecessary trouble because of any object along the light path.

CHAPTER 4

NOVEL IMPLANTS DESIGN

According to the research of Choi, et al., the optimum shapes of an implant are in some sense similar to those of the natural human tooth roots [15]. Shi, et al. in a finite element method (FEM) study of dental implants found a corresponding result that natural root shapes evolved under optimal load distribution given certain values of bone bearing stress [16]. However, the authors dismissed the double-root designs because they are "difficult to manufacture" and site-preparation would be manually impossible. The majority of dental implants in use clinically are single cylinder-shaped ones, which cause instability especially for the tooth replacement of multi-root cases such as molars. An attempt was actually made by placing two single screw-type implants instead of a single implant in a large molar case [35]. Although it was a "more functional and biomechanically sound method of molar replacement" as the authors stated, both surgical complexity and cost were increased.

What we are trying to achieve is a complete set of natural-root-formed implant designs to mimic the features that natural roots offer. It should include implants with one-, two-, and possibly three-root types and each should offer different sizes. These implants should be generated based on the natural root shapes of human teeth, but with the following optimizing efforts:

1) Humans usually have 32 permanent teeth, which can be notated according to the "Universal numbering system" [84] as illustrated in Fig. 7. Human teeth are

classified as incisors, canines, premolars, and molars, according to their functional and geometric differences. There are teeth with one-, two-, and three-root shapes in a mouth; further, the shapes of the natural roots for each person could be different. Therefore, extractions of the generalized shapes are necessary.

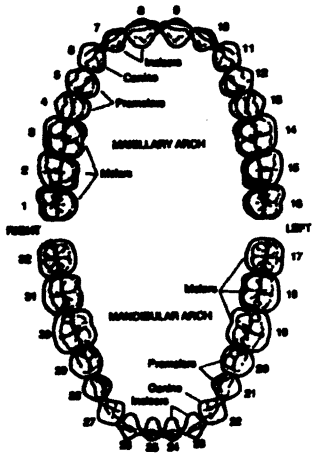

Fig. 7. Numbering and types of human teeth [85]

2) The natural-root-formed implant is much more complex than the currently used cylinder-shape implant in geometry, which is the major reason why previous researchers had to give up such ideas because of its manufacture and placement problem. Robotic-based placement will allow precise site-preparation of the natural-root-formed that is not manually possible. However, under-cuts are not suitable for the robotic milling due to the facts of the small scale and limited space available intra-orally; therefore we would want to optimize/simplify the shapes of natural roots.

4-1 FEM simulation

As described earlier, Shi, et al. in a FEM study of dental implants revealed that optimal designs for implant load distributions followed closely a natural root form [16]. FEM simulation was also run by Yongki Yoon from the Department of Mechanical and Aerospace Engineering of Old Dominion University to check the stress distribution for the natural-root-formed implants. Geometric models of the root-form extracted from a 3D human skeleton model were used in the FEM study. Fig. 8 gives the comparison of stress distribution between a natural-root-formed implant with two roots and a common cylinder-shape implant. It is easy to tell that the natural-root-formed has better mechanical characteristics at every feature point.

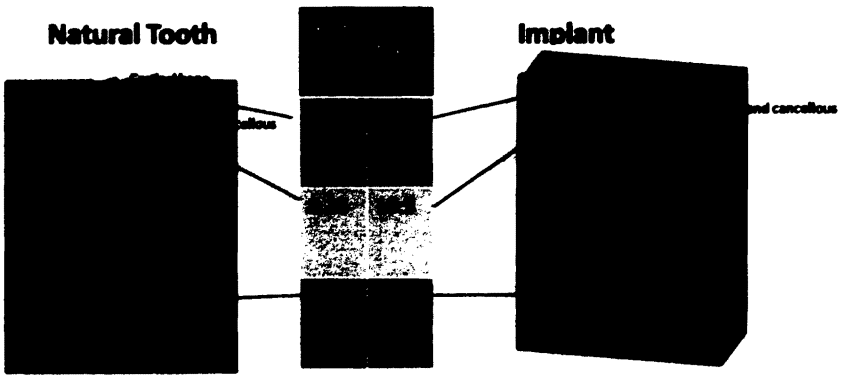

Fig. 8. Stress distribution comparison of a two-root implant with a cylindrical implant using FEM [86]

4-2 Standardized set of novel implants

Generalization and refinement based on natural-root shapes

Our standardized set of natural-root-formed implants were designed based on the 3D shape of human teeth. As described earlier, we need to generalize as well as refine the natural root shapes. In order to do so, firstly, the characteristics of human teeth were analyzed in an attempt to extract some common features, for each group that has a different number of roots. Because human teeth are symmetrical between the left and right side areas, only the 16 teeth from the right side of a mouth were explored. The 3D models of human teeth were extracted from an anatomical correct digital female skeleton (Fig. 9).

There was a totally 9 teeth that have single root, i.e., tooth #4, 6, 7, 8, 25, 26, 27, 28, 29 as identified in Fig. 9. There are differences among shapes of different teeth although they all have only one single root. Particularly, (1) the contour defined in the top view, (2) the ratio of its height (along Z-axis), width (along X-axis) and length (along Y-axis), and (3) the curvature of its tip at the bottom are the three major characteristics which identify one teeth from the others.

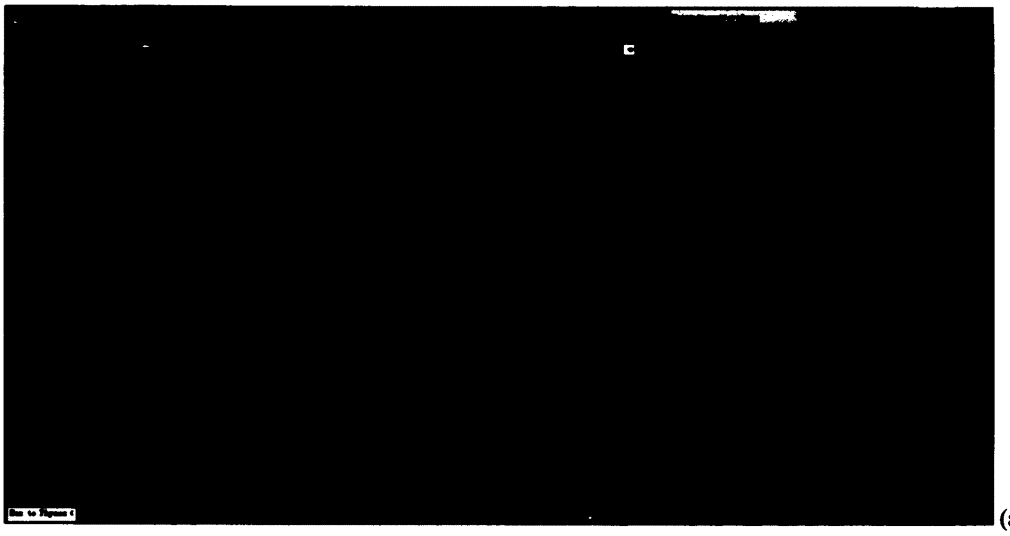

(a)

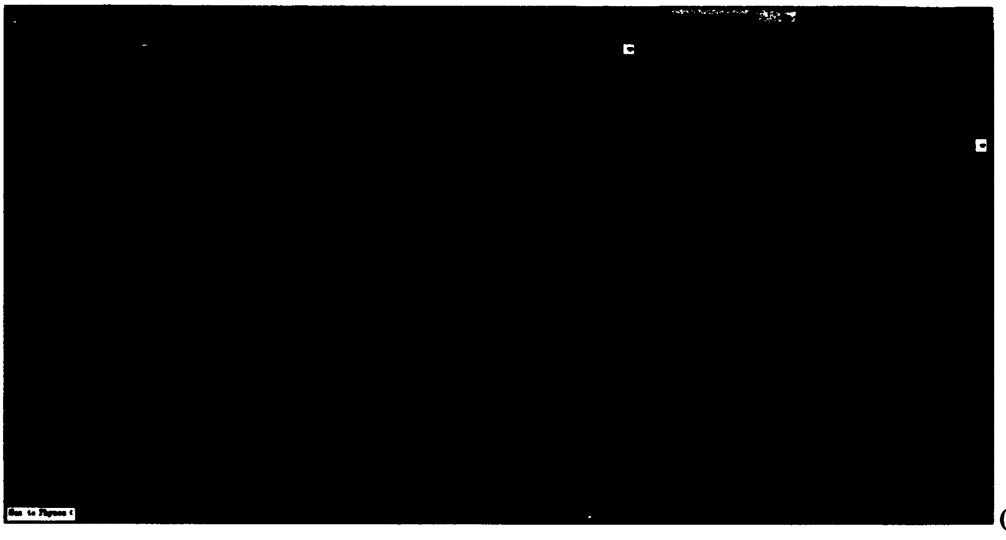

(b)

Fig. 9. Extracting teeth from a female skeleton model: (a) female skeleton; (b) teeth

TABLE I

CHARACTERISTICS FOR HUMAN TEETH WITH SINGLE ROOT

Teeth #	Dimensions			Normalized ratio		Shape of top view	Curvature of the tip
	x	y	z	x	y		
4	3.952	6.952	9.070	1.759	1	rectangular	smooth curved
6	5.192	6.730	16.788	1.296	1	rectangular	obvious hook
7	4.022	5.268	14.284	1.310	1	oval	tiny hook
8	5.143	6.564	15.466	1.276	1	egg-shape	none
25	3.250	5.406	12.289	1.663	1	egg-shape	tiny hook
26	3.350	5.287	12.486	1.578	1	egg-shape	tiny hook
27	4.026	6.234	15.396	1.548	1	egg-shape	tiny hook
28	4.186	6.347	12.595	1.516	1	oval	tiny hook
29	3.985	6.161	12.365	1.546	1	rectangular	smooth curved

TABLE gives the parameters for each tooth with one root. Among these teeth, the root shape of tooth #29 was chosen as the initial template for the natural-root implant with single root.

For the two-root case, 4 teeth fall into this category. Because the root form of tooth #30 has the smoothest curvature and least under-cuts, to facilitate the milling operation of the robot, it was chosen as the initial template for the double-root form implant.

After picking the templates for natural-root-formed implants, shape refinement was required for the design. Although robotic operation allows site-preparation of the

complex shapes of natural-root-formed implants that is not manually possible, there is a need for simplification of the natural-root shapes to make automated robotic milling of the implant site a possibility due to the facts of the small scale and limited space available intra-orally. The biggest issues for natural-root-shape milling are the existence of sharp curvatures and undercuts. Therefore, two strategies were applied in Autodesk 3ds Max to get the refined shapes of the implants.

1) Curvature smoothing. The root of a natural tooth has the tendency of curving at its apex. While it might provide for better anchoring for the teeth, it requires frequent direction changes of the milling tool, which may cause heating and obstructions during the operation thus leading to the failure of the site-preparation. The curvature was smoothed by creating a segmented system (bones) for each root along its central line and then were adjusted the orientations of the segments/bones to make their connections smoother. Fig. 10 shows the bones created for the single-root template in 3ds Max. Three bones were generated according to the curvature of the original model. The conjunction between two adjacent bones lies in wherever a big curvature change occurs. The joint angle between two adjacent bones was rotated (Fig. 10 b), so that the curvature became less sharp. The original model and the modified model after applying curvature smoothing are as shown in (c) and (d) of Fig. 10, respectively. The difference is easy to tell from the left view. Similarly, curvature soothing was also applied to the template for the double-root template, and the before and after comparison is provided in Fig. 11.

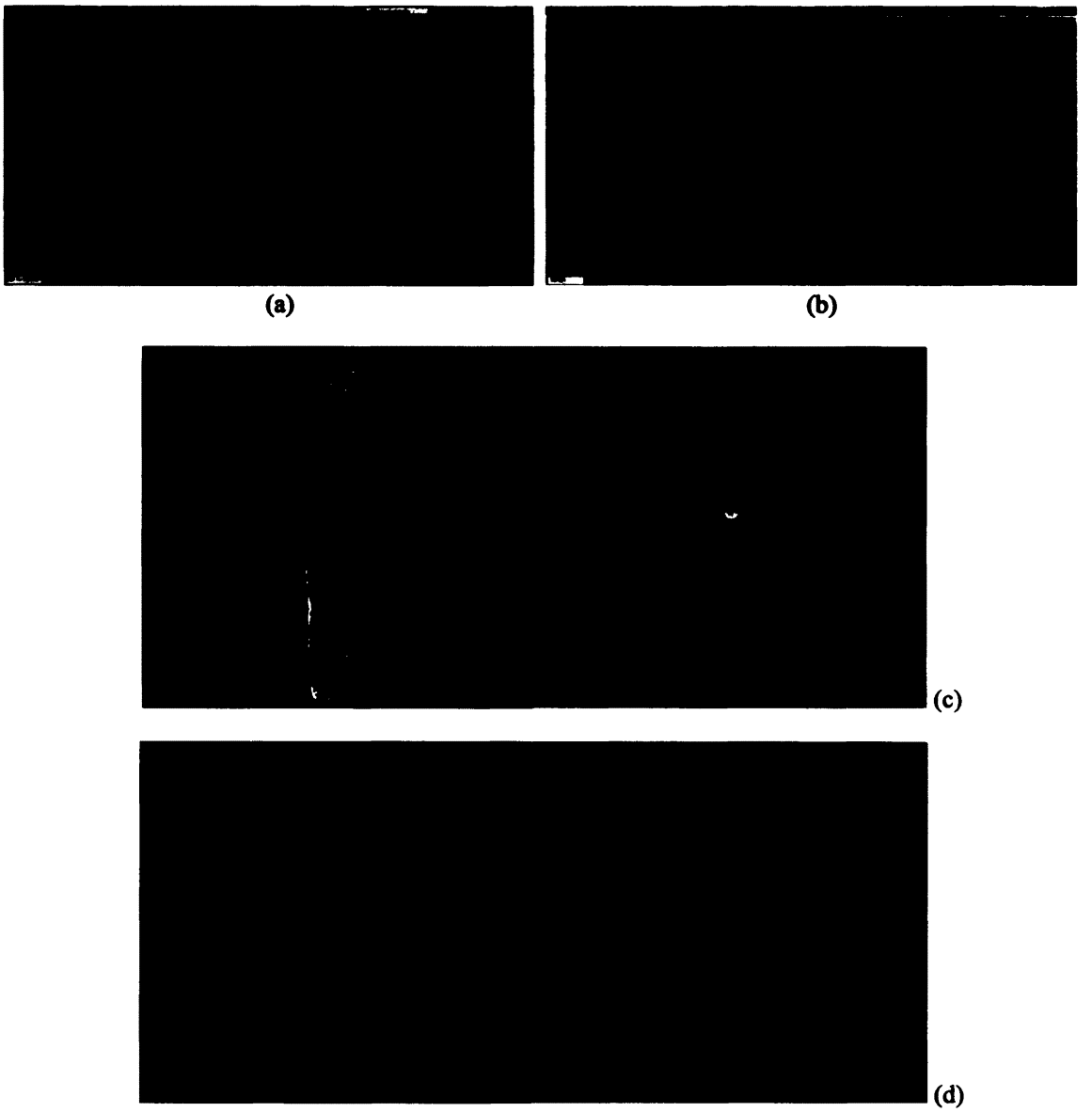

Fig. 10. Curvature smoothing by creating bones in the single-root template. (a) bones created in the original model; (b) change of curvature by rotating joint angle of the bones;(c) original model; (d) modified model after curvature smoothing


(a)


(b)

Fig. 11. Curvature smoothing for double-root template. (a) original model; (b) modified model after curvature smoothing

2) Undercuts removal. When checking the surface of the roots carefully after the curvature smoothing, there were still some under-cuts in the models. Because the intra-oral operation space is so small that no under-cut could be manufactured in the jawbone. All obvious under-cuts were removed manually by dragging the vertices outward with soft selection. Fig. 12 illustrates the under-cuts removal with soft selection, with which adjacent vertices can be translated smoothly together with the center vertices selected. Fig. 13 compares the modified model with the original model for both single-root and double-root cases, where the original models are shown in

grey and the modified ones are shown in yellow. One can tell that the modified models are smoother for the curvature as well as for the boundaries.

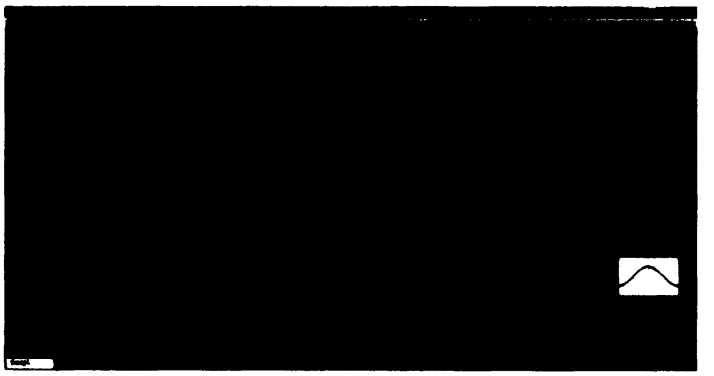

Fig. 12. Remove under-cuts with soft selection

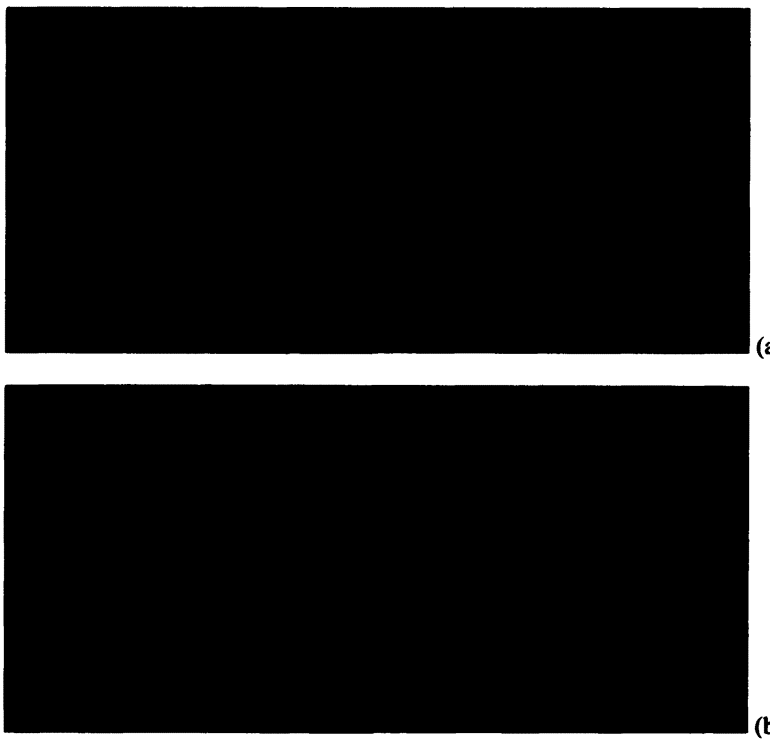

Fig. 13. Comparison of the original (left side) and the modified (right side) natural-root implants. (a) single-root implant; (b) double-root implant.

Soft-Kill Option(SKO) optimization

The shapes of both single- and double-root implants after the generalization and refinement procedure as described in the above section were then sent to a further stage for topology optimization. This was done by applying one of the topology optimization techniques introduced by Mattheck, et.al., called the Soft-Kill Option (SKO) method [87]. This method mimics the biological way bones remodel to find the optimum structure, where the distribution of Young's modulus adapts to the actual load applied over time. The patterns in Fig. 14 reflect the regions of higher stress where stronger materials are needed, such as implant material (titanium). As illustrated, SKO results suggested that the natural-root shapes should have a more rounded and balanced shape at the bottom. Implementation of this SKO method was done by Yongki Yoon.

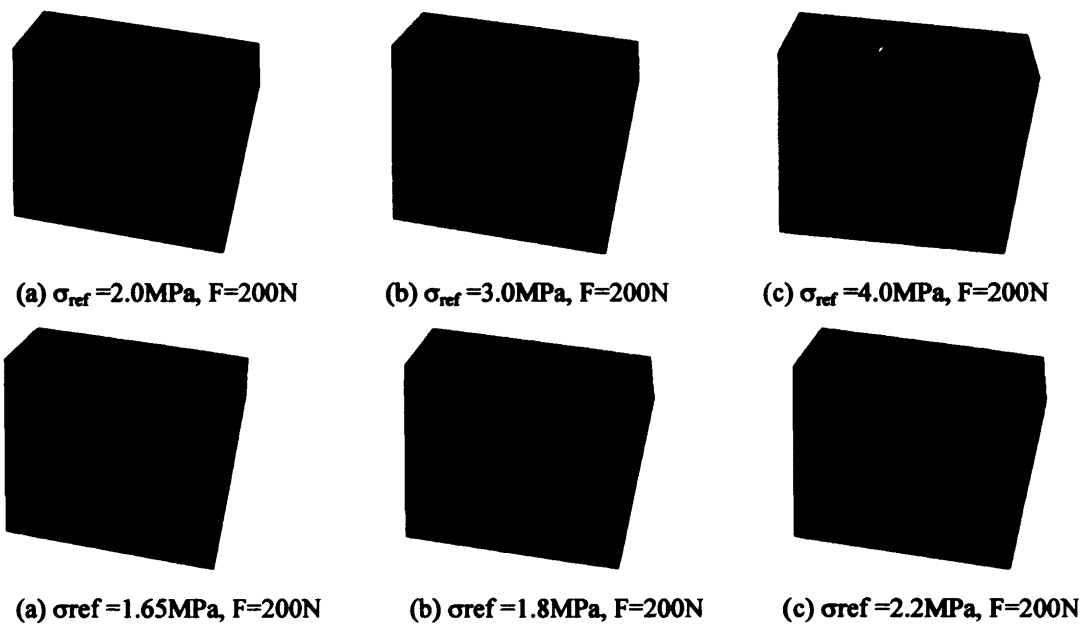

Fig. 14. Optimized material property of natural-root shapes with single-root (a, b, c) and double-root (d, e, f) [88]

Based on SKO results shown in Fig. 14, the modified models as shown in Fig. 13 were further polished by expanding the contour manually with soft selection, to get the optimized shapes for single- and double-root implants. Fig. 15 illustrates the difference between the models before (meshes in white) and after (meshes in blue) this procedure. It is obvious that the models after the bottom rounding have expanded bottom shapes as desired. Normal smoothing was applied to these models in MeshLab to get the final optimized models for the single- and double-root implants.

Additionally, three different scales were applied to each shape to create a complete set of implants with small-, medium-, and large-size in order to fit to different patients' somatotypes as well as different intra-oral sites for the implantation. The optimized model of the single- and double-root implant has a length of 11.8 mm and 10.7 mm, respectively. Dimensions of human teeth from the book "Dental morphology: an illustrated guide" by Geoffrey C. Downer [89] are listed in Table II. According to this data, the average length of the root portion of teeth with single-root and double-root can be calculated as 14.2 mm (N=9) and 12.3 mm (N=3), respectively. Therefore, the current models were considered as the small-sized templates and were scaled to match their average length as the medium-sized templates. It was assumed that if the small one is x% smaller than the average, then large one should be x% larger than the average. The calculated lengths for implants with different size are also listed in Table II. The complete set of the standardized natural-root-formed implants with single- and double-root is shown in Fig. 16.

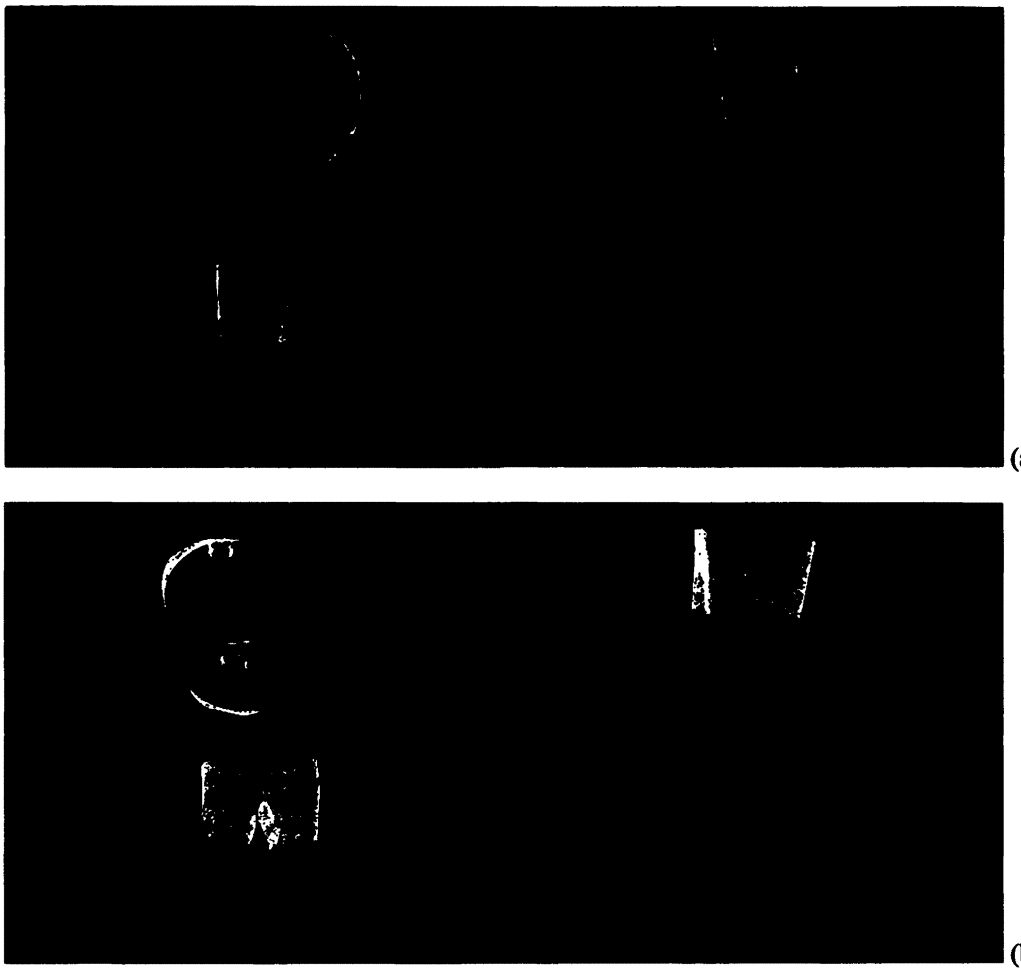

Fig. 15. Final models of the optimized natural-root implants with a rounded bottom. Refined shape: meshes shown in lighter color; Final optimized shape: meshes shown in darker color. (a) single-root implant; (b) double-root implant

TABLE II

LENGTH OF ROOT PORTION OF HUMAN TEETH AND NATURAL-ROOT IMPLANTS

Number of root	Tooth	Length of root (mm)	Length of implant (mm)		
			small	medium (average)	large
1	Maxillary Central Incisor	13.0	11.84 (16.6% smaller than average)	14.2	16.56 (16.6% larger than average)
	Maxillary Lateral Incisor	13.0			
	Maxillary Canine	17.0			
	Maxillary Second Premolar	14.0			
	Mandibular Central Incisor	12.5			
	Mandibular Lateral Incisor	14.0			
	Mandibular Canine	15.5			
	Mandibular First Premolar	14.0			
2	Mandibular Second Premolar	14.5	10.72 (12.9% smaller than average)	12.3	13.88 (12.9% smaller than average)
	Mandibular First Molar	14.0			
	Mandibular Second Molar	12.0			
	Mandibular Third Molar	11.0			

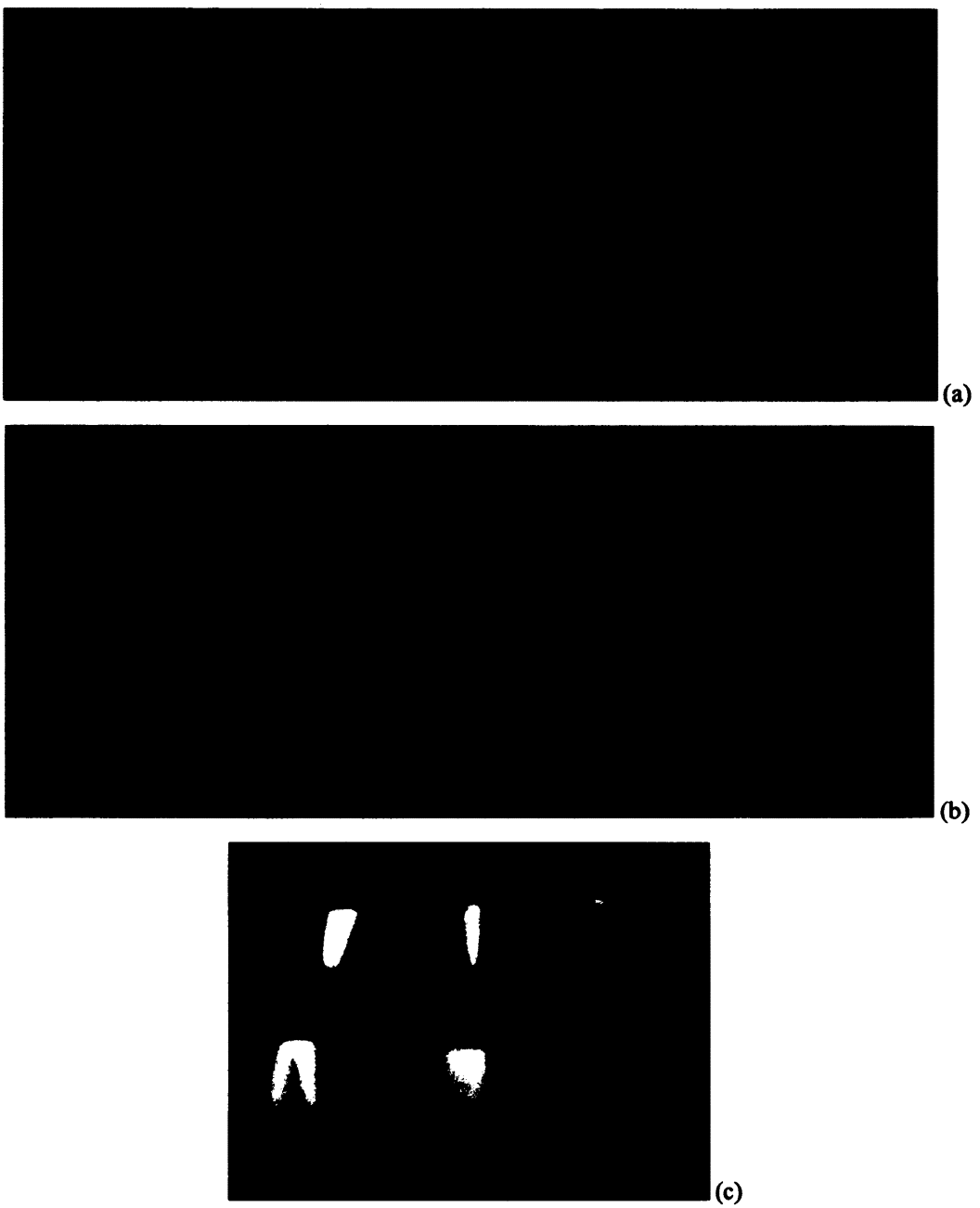

Fig. 16. Complete set of standardized natural-root-formed implants with single- and double-root. Models of implants with single-root (a) and double-root (b) in different size in 3ds Max; (c) printed out models of small-sized implants

4-3 FEM verification

The final standardized natural-root implants with single- and double-root were again analyzed using FEM to check the deviation of their stress distribution under certain loading when compared to the original natural-root shapes. TABLE III indicates that the maximum stress levels are considerably decreased after refinement and optimization procedure as described earlier, comparing with the original natural-root shapes. These results prove that the optimized implants not only resolve the potential problem for the robot milling, but also improve the structural performance under certain loading conditions therefore may provide better stability in the patient's mouth. This FEM verification was also done by Yongki Yoon [88].

TABLE III

COMPARISON OF STRESS LEVEL IN DIFFERENT MODELS [88]

	Original model (MPa)	Refined model (MPa)	Optimized model		
			Value (MPa)	% Change from original model	% Change from refined model
Max. One-root	6.38	6.26	5.03	21.16	19.65
Max. Two-root	3.64	2.45	2.22	39.01	9.39

CHAPTER 5

SYSTEM ARCHITECTURE

The architecture of our image-guided robotic dental implantation system for the natural-root-formed implants as defined in ***Chapter 4*** is shown in Fig. 17. The whole system is composed with preoperative and intra-operative phases. During the preoperative stage, cone-beam computed tomography (CBCT) images of the patient are taken. Patient specific 3D models are reconstructed from the images and a preoperative surgical plan is generated accordingly, utilizing a planning software which is specially developed for this system. A coordinate measurement machine (CMM) is introduced into our system to register between the coordinate system in the planning software and the operation site, thereby transforming the preoperative plan into the operation of the robot. Therefore, the preoperative surgical plan can be accomplished automatically by the robot in the intra-operative stage.

There are four major components in our system:

a) preoperative planning

b) milling sequence generation

c) registration

d) intra-operative operation

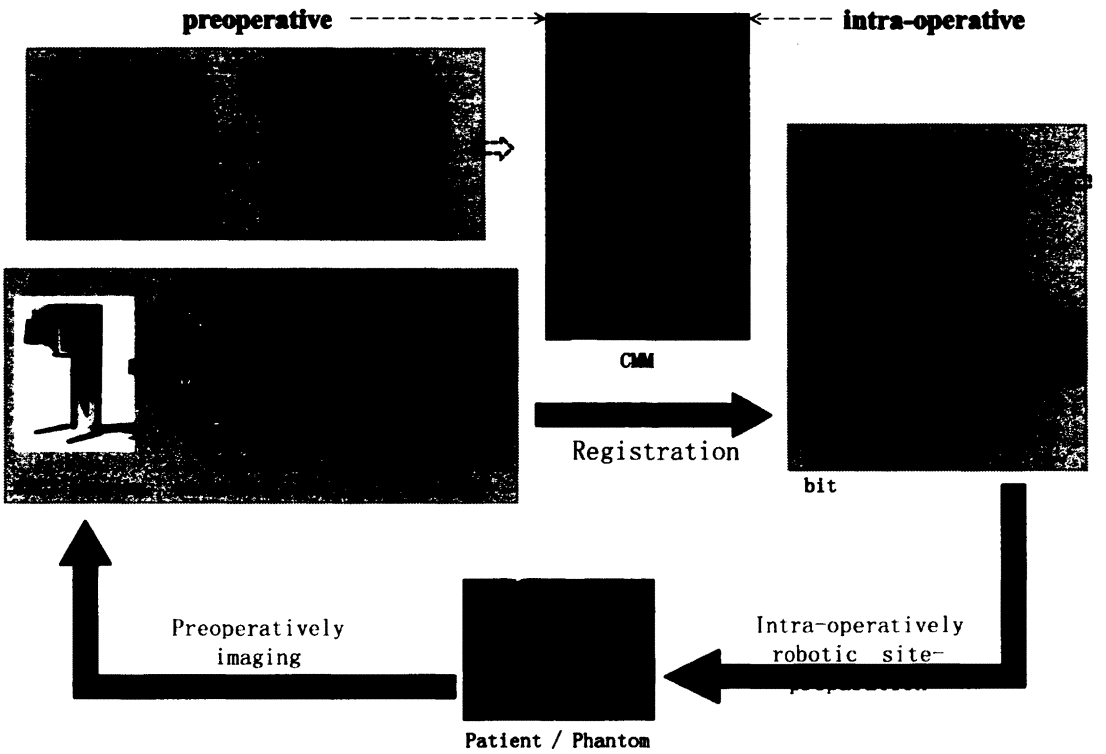

Fig. 17. System architecture

Preoperative planning is completed utilizing a specially developed software. Two jobs are done with this software: the first one is the surgical plan generation which is done by a surgeon according to the patient specific 3D model reconstructed from the CBCT images of the patient's jaw area. The software allows the surgeon to choose a certain type of implant and virtually inserts it into the jaw model thus observing the insertion result in real time. The implant type and size, along with its position and orientation, all of the surgeon's choosing, are exported into .txt files. The other job of the software is to record the coordinates of several fiducials in the virtual coordinate system (the coordinate system of the software). Those fiducials are attached on the patient's jawbone when the CBCT imaging is taken. After the reconstruction and segmentation

procedure, the positions of the fiducials need to be identified by the user of the planning software (either by the surgeon or another staff who does not necessarily need to be clinically educated). The coordinate of each fiducial will be recorded and saved in a .txt file as well. Fig. 18 gives the flowchart for the preoperative planning part.

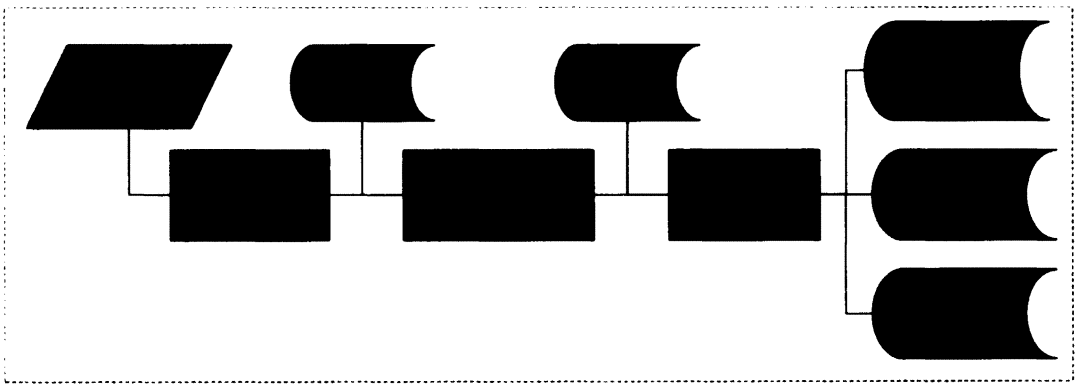

Fig. 18. Flowchart for preoperative planning

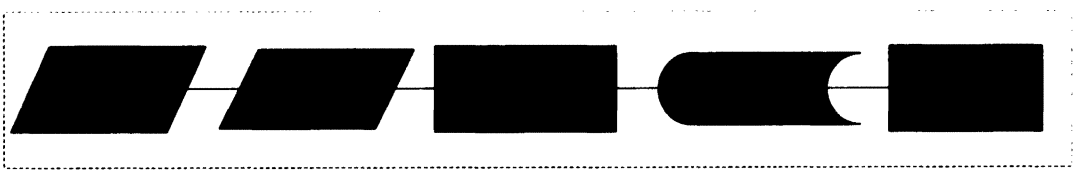

Fig. 19. Flowchart for volume decomposition

Milling sequence generation based on volume decomposition decomposes the shape of a certain implant into the combination of several sub-volumes, any of which is one of pre-set primary shapes (cylinder, cone, points-sequence, etc.). As in our design, there will be a complete set of implants with different shapes and sizes, to meet the desire of different tooth replacement types and locations. Any one single implant corresponds to a

certain sequence of primary shapes and point sets. The robot sub-functions in MELFA for each pre-set primary shape removal were implemented by Yongki Yoon [86]. Therefore, the site-preparation of any implant can be completed by calling a sequence of MELFA sub-functions. The flowchart of this part is as shown below.

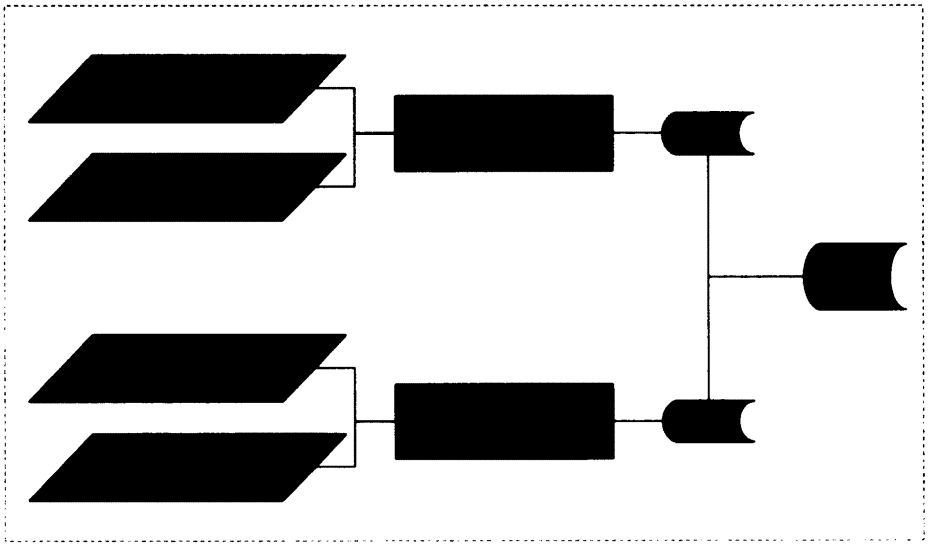

Fig. 20. Flowchart for registration

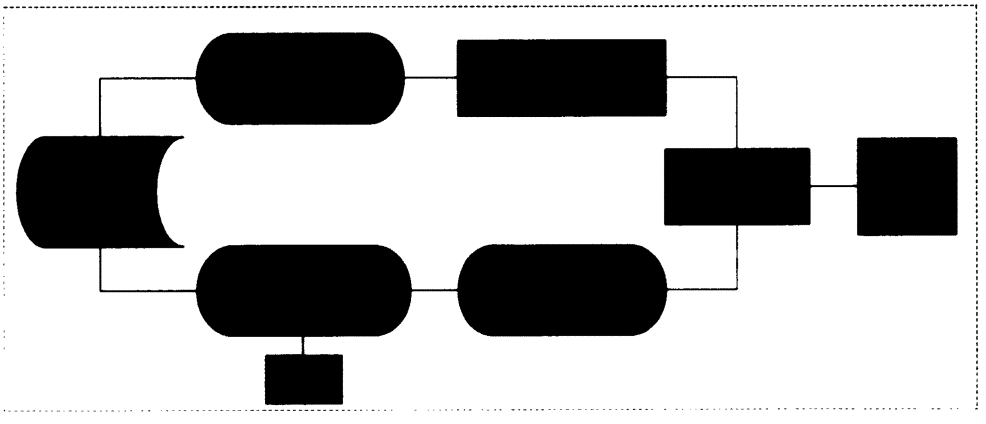

Fig. 21. Flowchart for intra-operative operation

Registration is the procedure which aims to transform the preoperative plan to the intra-operative operation of the robot. The target of this procedure is a transformation matrix which aligns the spatial relation between the virtual coordinate system (preoperative plan) and the operation coordinate system (intra-operative operation), i.e., T_{V2O} in Fig. 20. The coordinates in the Operation CS (OCS) need to be recorded by commanding the robot to move to the target position. In order to avoid any potential danger to the patient, we introduced a so called "reference coordinate system (RCS)" into our application. A novel two-step registration method was developed to get T_{V2O} with the help of RCS, as seen in Fig. 20. The Virtual CS (VCS) and the Reference CS (RCS) are registered with the fiducials attached on the patient's jaw, and RCS and OCS are registered utilizing another set of points which are not on the patient.

The ***intra-operative operation*** for the implantation is automatically performed by the robot, which is controlled by running a MELFA program. The site-preparation for a certain implant is determined by two factors (Fig. 21): (1) the type and size of the implant and, (2) the position and orientation for the insertion of this implant. The first one corresponds to a pre-defined MELFA sub-routine. The second one is determined by the target coordinate in the operation (robot) coordinate system, which can be calculated from the target coordinate in VCS and the transformation matrix gotten from the registration procedure. This target coordinate is passed into the main function for robot control as an input parameter, along with the MELFA sub-routine. In this manner, the robot can be commanded to finish the procedure as designed.

5-1 System operative flow

The whole procedure requires two time points: the first time for preoperative imaging and the second time for system registration and the surgery. The first date should be several days prior to the surgical date.

At the first time point, a small procedure will be taken to attach several fiducials in tiny half spheres to the patient's teeth/jawbone using dental glue or screw. With the fiducials fixed, the patient will be set in a specially designed dental chair with which a device will be used to restrict the movement of his head and most importantly, fix the position of his jawbone. Then, preoperative images will be taken by dental cone-beam computed tomography (CBCT). After taking CBCT images, the patient can leave but the fiducials need to stay in his mouth until the second visit.

Before the second time point, a surgical plan will be generated according to the patient's CBCT images, which defines the preferred implant type and size, and designated target position and orientation. In addition, the coordinate of each fiducial in the virtual coordinate system is recorded for later registration. A calibration block with some fixed registration points is utilized to determine the relative spatial relationship between the reference coordinate system and the operation coordinate system. Coordinates of these points in both the reference CS and the operation CS are recorded and a registration program is run to get the transformation matrix between these two coordinate systems.

On the scheduled surgical date (second time point), the patient will go back to the dental office and also be fixed as in the first time visit. After the fixation, the coordinates of

fiducials in the CMM is recorded by touching the apex of the half-sphere of each fiducial. A registration will be done along with the information recorded earlier, which is the coordinates of fiducials in VCS, to setup the transformation between VCS and RCS. Therefore, the preoperatively designated targets can be transformed into parameters in the operation CS. Finally, the MELFA functions for the surgery with these parameters will be generated accordingly and the robot conducts the site-preparation automately.

5-2 Hardware architecture

The main hardware utilized in our system include a CBCT machine, a CMM, a robot and its controller, a dental drill-bit and its motor piece, a computer, and also some specially designed tools. Fig. 22 indicates the hardware architecture in our system.

The CBCT attains the patient's information preoperatively, and provides the basis for the Virtual CS. Although it is one of the most expensive hardware components in the system, it is also a commonly used equipment in the dental office. The CMM introduced in our system as a Reference CS is a Gold Arm from FARO Technologies Inc. It has a certified 2 sigma single point accuracy of ±0.051 mm, thus providing very high accuracy for measuring coordinates. The robot is the most important component in our system, which is the object of the Operation CS. It is a commercial robot from Mitsubishi (MELFA RV-3S, Mitsubishi), which has 6 DOF and with a position repeatability of ±0.02 mm. It comes with a controller (CR1B-571) utilizing MELFA-BASIC IV language. The controller runs programs which are created either from a computer or

through a teaching pendant. A dental drill-bit with a diameter of 2 mm is attached to a dental hand piece from Aseptico (Woodinville, WA, USA), which comes with a high performance motor. With this hand piece rigidly connected to its end-effector, the robot functions as a high accuracy milling machine. It is commanded to complete the site-preparation for the implantation automatically, when appropriate parameters are given.

Several small fiducials are generated for registering the coordinates between the CBCT images and the CMM. Each fiducial is designed as a small semi-sphere with a radius of 1 mm and is manufactured using dental-friendly material, which can be fixed onto the patient's teeth or jaw easily with the help of dental glue or screw. A set of points for registration between the CMM and the robot are defined on a registration block. It is actually a piece of dental guard, thus having the natural curvature of human jawbone.

Another hardware component needed in our system is a head/jaw fixation device, which makes sure the position of the patient's jaw is unmoved during the registration and the site-preparation procedure. The design of this fixation device is still under discussion. In order for our system to be clinically applicable, such designs will be explored to find the most feasible option.

One more important hardware in our system is a PC. It runs the preoperative planning, records and finishes registration, and also controls the operation of the robot. The PC for system testing in this dissertation is a DELL Precision 690 with 2.33GHz CPU and 4GB RAM. The CMCT images are transmitted to the PC through the internet and the connection from the PC to the CMM and the robot are both through RS232.

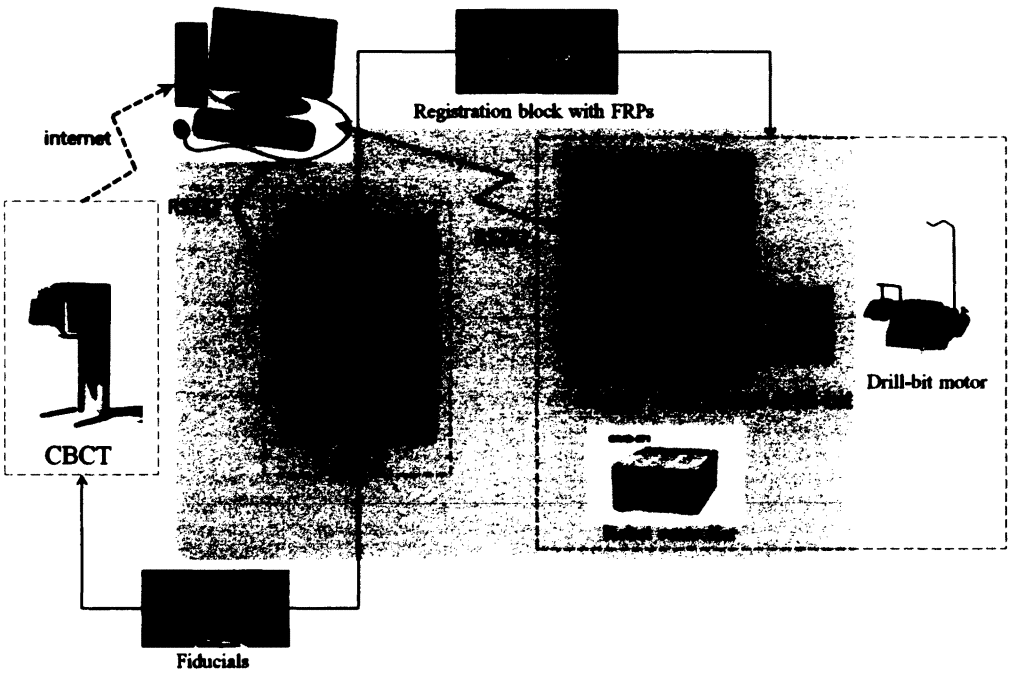

Fig. 22. Hardware in our system

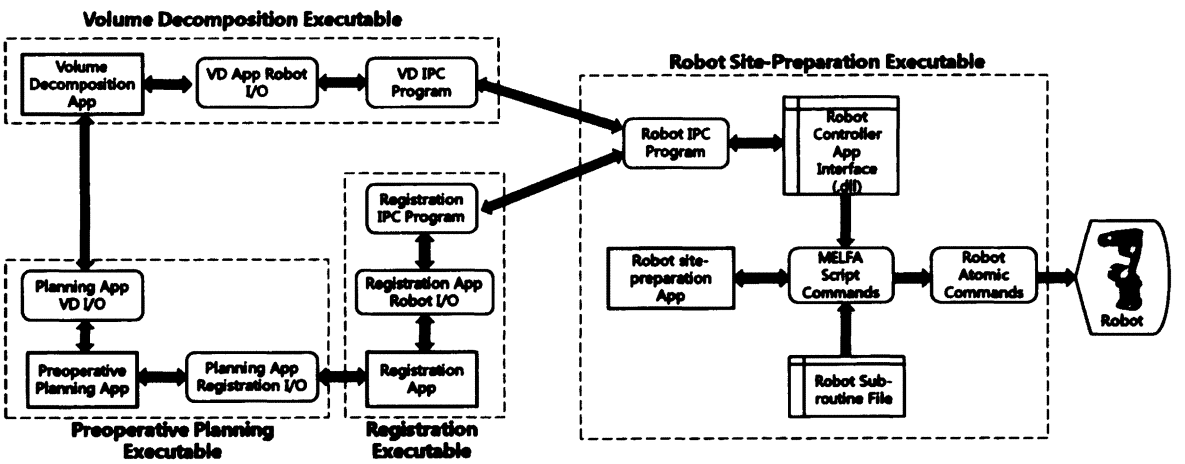

Fig. 23. Software Architecture in our system

5-3 Software architecture

For each phase defined earlier in this chapter, software is developed to accomplish the task. An executable implemented in OpenGL and FLTK visualizes the patient-specific 3D model and provides the user (the surgeon) a graphic interface to develop an appropriate surgical plan. The implant type and the site-preparation parameters are exported through the I/O module of this planning application into two separate files, which will be passed to the executable for volume decomposition and registration. The milling sequence generation application is implemented using Matlab. It decomposes the shape of a given type of implant into the combination of some pre-defined primary sub-volumes. The detailed algorithm for this application will be given later in this dissertation. The decomposition result generated from this application is passed on to the robot site-preparation executable through an IPC program. The registration application is also implemented in Matlab. A novel two-step registration strategy is applied to register the three coordinate systems as defined in Fig. 20. With the target positioning information passed from the planning application, the registration application calculates the target coordinates in the robot coordinate system accordingly and shares this information with the robot site-preparation executable. The robot site-preparation executable is the software that controls the operation of the robot during the intra-operative stage. Several robot sub-function files were implemented using a Mitsubishi Electric Factory Automation (MELFA) script, each of which corresponds to the robot operation of removing a certain shape of volume, but with default spatial parameters. The main program of the robot application calls the sub-routine (a combination of sub-functions) needed according to the implant type and inputs the target coordinates to the

sub-routine, thus the robot is commanded to complete the site-preparation at the designated position and orientation. Fig. 23 illustrates the architecture of these four executables in our system.

CHAPTER 6

IMAGE-GUIDED ROBOTIC DENTAL IMPLANTATION

The detailed description of each component of our system is given in this chapter, including preoperative planning software, registration & calibration, robotic milling for natural-root-formed implants, and virtual fixtures.

6-1 Preoperative planning software

Software for preoperative planning of the implantation procedure was implemented especially to support our novel implants. With this software, the user, generates a surgical plan for each patient and coordinates information is also recorded from this software for later registration.

Segmentation and model reconstruction

The patient specific 3D model is reconstructed from CBCT images of the patient, which are taken during his first time point as defined in ***5-1***. Fig. 24 illustrates an example of the procedure of segmentation and model reconstruction utilizing commercially available software, Analyze 8.1 (AnalyzeDirect, Inc, USA). The part of the patient's jaw is segmented from each image and reconstructed into a 3D model. If the implantation is going to be in the mandible (lower jaw), the inferior alveolar nerves are also segmented separately. Meanwhile, the fiducials attached to the patient during the CBCT imaging are identified and segmented as well. Therefore, three parts are

segmented: the jaw, the nerves and fiducials. Two models are going to be exported from Analyze 8.1 in .vrml format: one is the jaw model with the nerves segmented (as Fig. 24 e), and the other is the combination of the jaw (Fig. 24 d) and fiducials. The two models exported from Analyze need to be converted to .3ds format before loaded into the planning software. Please note, there is no fiducial visible in the CBCT images below because no fiducials was attached to this patient when CBCT was taken.

This segmentation was performed by Xu Han and Suchita Manandhar [26].

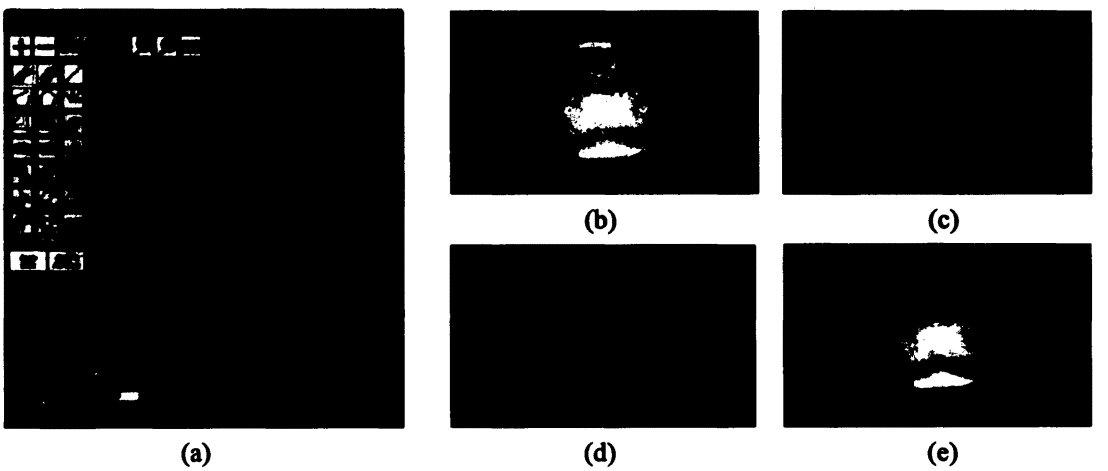

Fig. 24. Segmentation and model reconstruction from CBCT images in Analyze 8.1: (a) one layer of CBCT image, where the red arrows point are the nerves; (b) original parts loaded; (c) parts segmented using seeded region growing; (d) segmented mandible (lower jaw); (e) mandible with nerves segmented (the pink parts)

Surgical planning

The jaw model with nerves segmented is loaded into our preoperative software to generate a surgical plan for the implantation. A graphical user interface (GUI) is provided to visualize the 3D model, with the capabilities of scaling, rotation and translation (Fig. 25 b), so the surgeon can examine the anatomical structure of the patient's jaw thoroughly to gain a general idea about the implant placement. As shown in Fig. 25 (c), once both the jaw model and the implant are loaded, the software provides the surgeon with the capability to interactively planning of the implant insertion into the jawbone. He can adjust the orientation of the implant by using the three sliders at the bottom-left corner to control its rotation along X-, Y- and Z-axis, respectively; and move the implant to the position where the mouse clicks with the "click to move" function at the lower-right corner enabled. The result of the implant placement with current choices of orientation and position will be instantly visualized to the user. If it is not appropriate for any reason, for example, too close to the nerve or adjacent teeth, the surgeon may always adjust it as he wishes until a satisfying outcome is achieved. Besides, our system provides a standard set of implants as introduced in ***4-2***. The surgeon could also try a different type of implant in order to find the best match for the case.

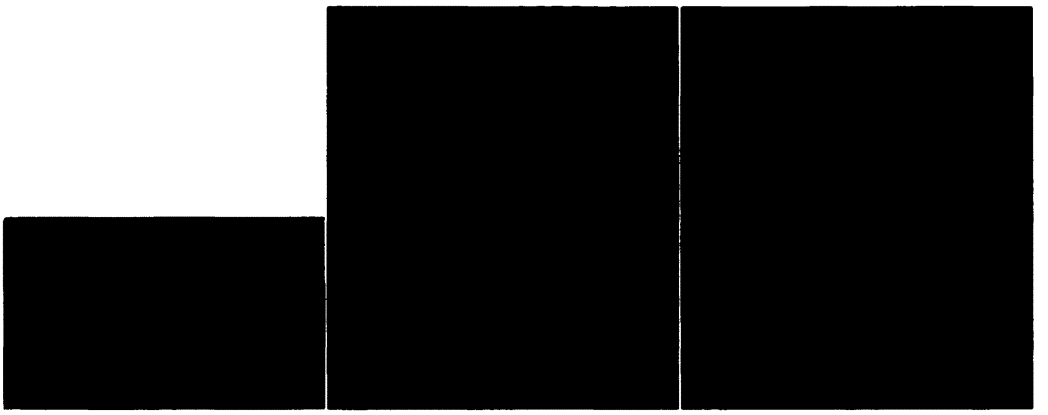

(a) (b) (c)

Fig. 25. Visualization of the surgical planning in the planning software. (a) menu for loading models; (b) patient specific jaw model with nerve segmented is loaded; (c) an implant (the pink one) is virtually inserted into the jawbone

Once the surgeon satisfies with the virtual outcome of the implant placement, the results could be saved into a .txt file by clicking the "save result" button as shown in Fig. 26 (a). The results include the id number of the implant among the standard set of natural-root-formed implants, and the current chosen coordinates of the entry point and apex point of the implant, which define both the position and orientation of the implant in the virtual coordinate system of the planning software simultaneously. Fig. 26 (b) gives an example of the result output, which will be sent to the robot site-preparation software later.

This preoperative planning software was implemented using OpenGL and FLTK.

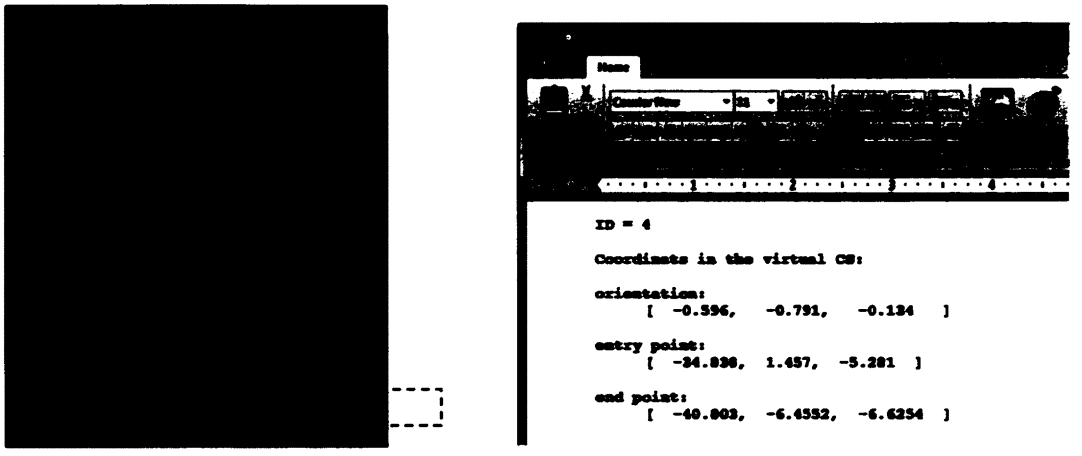

(a) (b)

Fig. 26. Savingsurgicial planning result. (a) "save result" button in the planning software GUI; (b) saved result in a .txt file

Registration predefinition

Another function of the preoperative planning software is to get the coordinates information about the fiducials. As defined earlier, two models are exported after the segmentation and model reconstruction procedure, one of which is the jaw model with fiducials on it. In our software, a menu for loading this model is provided as seen below. Once the model is selected, the user is asked to input the number of fiducials in this model and the number of measures for each fiducial (Fig. 27 b). In Fig. 27 (c), a jaw model with five fiducials (the blue semi-spheres) is displayed. Here, the exact identification point for each fiducial is the apex of the semi-sphere. The coordinate of each fiducial is recorded by mouse clicking. The software allows rotation and scaling of the model (Fig. 27 d), so that a better view of the fiducial could be achieved and the coordinate of the fiducial can be recorded at different angles thus decreasing the

identification error caused by view distortion. For each fiducial, the number of measures as defined by the user will be recorded and their average is calculated as the final coordinate of the current fiducial. Note, for the registration predefinition function, the user of the software is not necessarily a surgeon. No clinical knowledge is a prerequisite here.

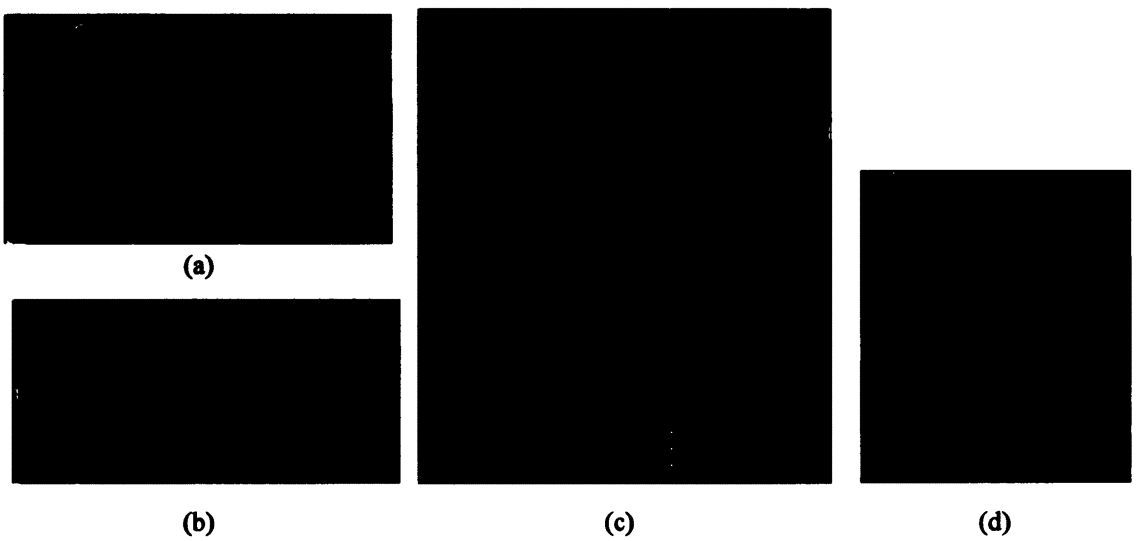

Fig. 27. Identifying fiducials and recording their coordinates in the preoperative planning software. (a) menu for loading the jaw model with fiducials; (b) input the parameters by the user; (c) jaw model with fiducials is loaded; (d) rotating and scaling for better fiducial coordinate identification

6-2 Registration & calibration

The preoperative planning software helps the surgeon to generate an ideal surgical plan for the implant placement, which is patient specific according to the anatomical structures of the patient's jaw. However, an ideal plan alone does not guarantee the

success of the surgery. The surgical plan must be exactly transferred to the placement operation, which requires registering the preoperative coordinate system to the intra-operative coordinate system. The former is the Virtual CS (VCS) of the planning software and the latter is the Operation CS (OCS) of the robot. A Coordinate Measurement Machine (CMM) was introduced into our system acting as a third coordinate system, called the Reference CS (RCS). RCS serves as a bridge to align VCS and OCS instead of registering them directly, avoiding unnecessary touching of the patient with the robot before actual implant preparation and thus ensuring the safety of the patient.

Calibration

The tool frame of OCS is not the end-effecter of the robot, but the dental drill-bit attached to it. Therefore, the coordinate of a target position in OCS is actually the relative position from the tip of the drill-bit to the origin of the robot coordinate system, denoted as P_{tip}. Because the dental drill-bit is attached to the robot's end-effecter rigidly, the coordinate of the drill-bit tip is a known constant in the coordinate system of the robot end-effecter. Let us denote it as v_{cal}. Meanwhile, the rotation and position information of the end-effecter in the robot coordinate system (i.e. OCS) is known from the robot controller software, which can be recorded as R_{rob} and t_{rob}, respectively. R_{rob} and t_{rob} together transfer a coordinate in the robot end-effecter CS to the corresponding coordinate in the robot CS (OCS). The spatial relationship of these variables in the 3D space is illustrated in Fig. 28.

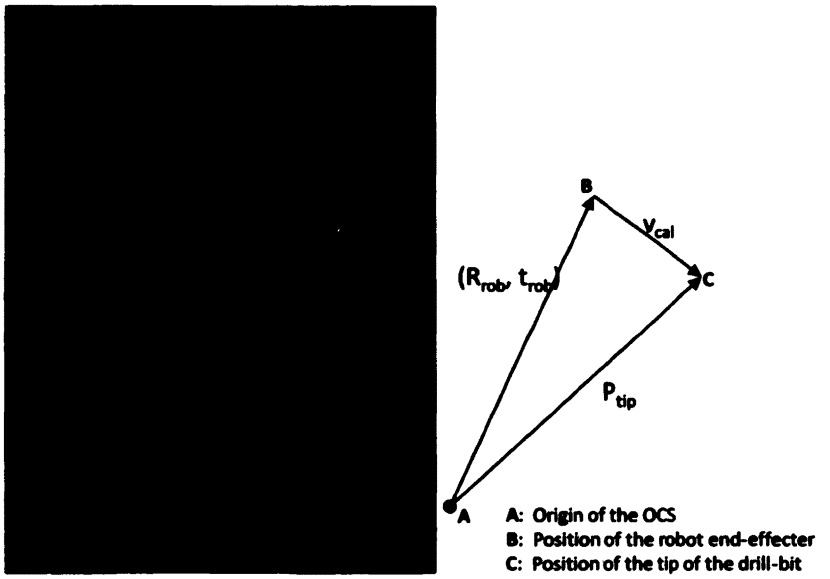

Fig. 28. Illustration of calibration in OCS

Accordingly, once the value of vector v_{cal} is known, P_{tip}, which is the coordinate we are interested in, can be expressed as in (3):

$$P_{tip} = R_{rob} \cdot v_{cal} + t_{rob} \tag{3}$$

The offset v_{cal} can be determined by applying a standard pivot calibration, which is explained as follows:

The tool frame, in this case, the dental drill-bit attached to the robot is commanded to rotate while its tip keeps in an arbitrary position, called the pivot point (Fig. 29). For each posture while pivoting, we have $P_{tip} = R_{rob}(i) \cdot v_{cal} + t_{rob}(i)$, given that the parameters returned by the robot are $R_{rob}(i)$ and $t_{rob}(i)$. Therefore, we get the following set of equations, where N is the total number of postures the tool frame is set to.

$$\begin{cases} P_{tip} = R_{rob}(1) \cdot v_{cal} + t_{rob}(1) \\ P_{tip} = R_{rob}(2) \cdot v_{cal} + t_{rob}(2) \\ \vdots \\ P_{tip} = R_{rob}(N) \cdot v_{cal} + t_{rob}(N) \end{cases} \tag{4}$$

Equation (4) may be written compactly in a matrix form:

$$\begin{bmatrix} P_{tip} \\ P_{tip} \\ \vdots \\ P_{tip} \end{bmatrix} = \begin{bmatrix} R_{rob}(1) \\ R_{rob}(2) \\ \vdots \\ R_{rob}(N) \end{bmatrix} \cdot \begin{bmatrix} v_{cal} \\ v_{cal} \\ \vdots \\ v_{cal} \end{bmatrix} + \begin{bmatrix} t_{rob}(1) \\ t_{rob}(2) \\ \vdots \\ t_{rob}(N) \end{bmatrix} \tag{5}$$

which may be summarized as:

$$\mathbf{P_{tip}} = \mathbf{R} \cdot \mathbf{v_{cal}} + \mathbf{t} \tag{6}$$

v_{cal} can be solved from (6). Therefore, for any given posture of the robot, the coordinate of the tool frame in OCS is determined from the rotation and translation information of the robot, as defined by (3). However, this only creates a directional mapping from (R_{rob}, t_{rob}) to P_{tip}. For the tool frame (the dental drill-bit), apart from the position of its tip, its orientation is also an important parameter which needs to be determined for the surgical operation. A checkboard with a standard line distance of 1 cm was applied to help to determine the rotation matrix between the tool frame and the end-effecter of the robot. The end-effecter of the robot was commanded to be vertically down, and the relative angles between the drill-bit and each axis in the Cartesian coordinate system of the robot was determined manually (Fig. 30). Because the orientation of the tool frame is fixed in the robot's end-effecter CS, which means the orientations of the tool frame and the robot have a one-to-one mapping; thus, with a desired orientation of

the tool frame, there is only one single rotation matrix R_{rob}. In this case, the relationship between (R_{rob}, t_{rob}) and the position and orientation of the tool frame is established.

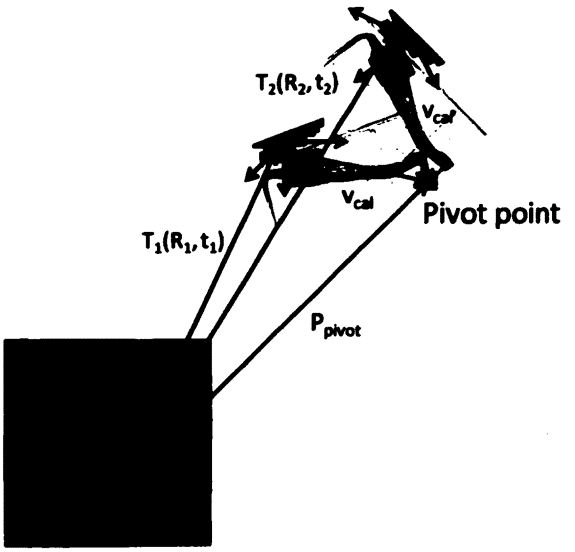

Fig. 29. Pivot calibration for the robot tool frame

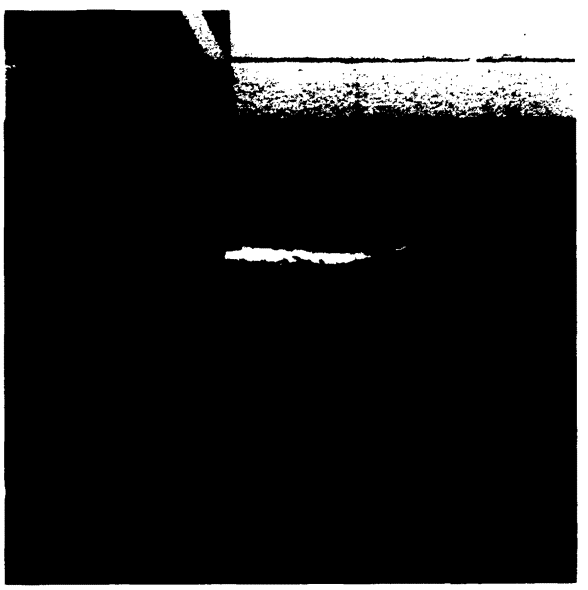

Fig. 30. Orientation calibration for the robot tool frame [86]

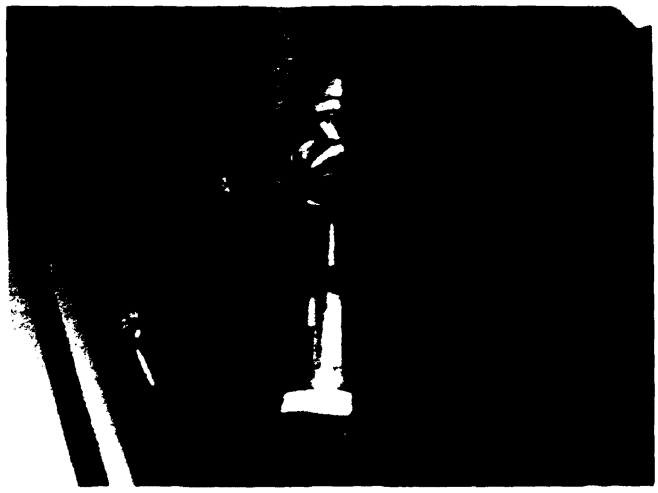

Fig. 31. Calibration in the reference coordinate system

Similarly, calibration is required in the reference coordinate system, which is a CMM (Gold Arm) from FARO Technologies Inc. A point probe (from Faro) was attached to the CMM to accurately measure the objects' coordinates. A sphere method using a 1" Calibration Sphere (from Faro) with FARO CAM2 Measure software was conducted to calibrate the probe (Fig. 31). 27 points on the 1'' calibration sphere were taken according to the instructions of the software, and a calibration error of 0.1290 mm was achieved.

Registration

In our system, three different coordinate systems are involved: the Virtual CS (VCS), the Reference CS (RCS), and the Operation CS (OCS). As mentioned earlier, the aim of registration is to transfer the preoperative surgical plan in VCS to the intra-operative robotic operation in OCS, which is fulfilled with the help of the CMM in RCS. Let t_V, t_R, and t_O be the coordinates of the target position in the virtual, reference and operation CS,

respectively; T_{V2R} and T_{R2O} be the transformation matrix transforming coordinates from VCS to RCS and from RCS to OCS, respectively. We have:

$$t_O = T_{R2O}(t_R) = T_{R2O}(T_{V2R}(t_V)) \quad (7)$$

which can be rewritten as:

$$t_O = T_{R2O}(T_{V2R}(t_V)) = T(t_V) \quad (8)$$

where $T = T_{R2O} * T_{V2R}$, and it is the transformation matrix that transforms coordinates from VCS to OCS, i.e., from the preoperative plan to the intra-operative surgical operation.

The above equations indicate a two-step registration procedure composed of the registration between VCS and RCS, and the registration between RCS and OCS, respectively. Since both the planning site and the surgical operation site that need to be registered is the jaw of the patient, which has an inflexible geometric structure, a classic rigid-body point-based registration method was applied. Several fiducials that were rigidly attached to the patient's jaw or teeth were used as the paired points in VCS-RCS registration. In order not to touch the patient directly with the robot before the intra-operative operation stage, this set of fiducials was designed not to serve the RCS-OCS registration. Instead, another set of markers that were not on the patient, called the Fixed Registration Points (FRPs), was utilized. The two-step registration procedure can be described as follows:

1. Step 1: registration between VCS and RCS

   ① Identify the positions of the set of characteristic points (fiducials, A_i) that were attached to the patient in the preoperative planning software, and record their coordinates in VCS by mouse clicking, denote as $\{A_{v,i}\}$;

   ② Record coordinates of the fiducials on the patient in RCS using the CMM, by touching them with the tip of the point probe, denote as $\{A_{r,i}\}$;

   ③ Register between VCS and RCS using paired-point registration between $\{A_{v,i}\}$ and $\{A_{r,i}\}$; The transformation from VCS to RCS is determined as T_{V2R}.

2. Step 2: registration between RCS and OCS

   ④ Record coordinates of another set of characteristic points which are on the registration block (Fixed Registration Points - FRPs, B_i) in RCS using the CMM, by touching them with the tip of the point probe, denote as $\{B_{r,i}\}$;

   ⑤ Record coordinates of the FRPs in OCS by touching each point from B*i* using the dental drill-bit attached to the robot, denote as $\{B_{o,i}\}$;

   ⑥ Register between RCS and OCS using paired-point registration between $\{B_{r,i}\}$ and $\{B_{o,i}\}$; The transformation from RCS to OCS is determined as T_{R2O}.

Then the coordinate of the target point in the operation CS can be calculated as defined by (7) or (8).

Please notice that step 1 and step 2 described above are actually interchangeable, meaning these two steps do not need to be done in sequence. As a matter of fact, Step 2, which is the registration between RCS and OCS can be carried out without the patient because the FRPs are not patient-related. Moreover, this registration may not necessarily to be conducted independently for each patient, because the relative position between the CMM and the robot is fixed at all times in the operating room. In other words, the registration information between RCS and OCS can be saved as a system parameter so registration needs not be performed every time. Therefore, by applying this novel two-step registration strategy, the patient safety is ensured while no additional procedure is required compared to direct registration between VCS and OCS. In order to ensure system accuracy, in actual applications, Step 2 will be done routinely thus avoiding error caused by any slightly movement between the CMM and the robot.

The relationship among these coordinate systems is shown in Fig. 32.

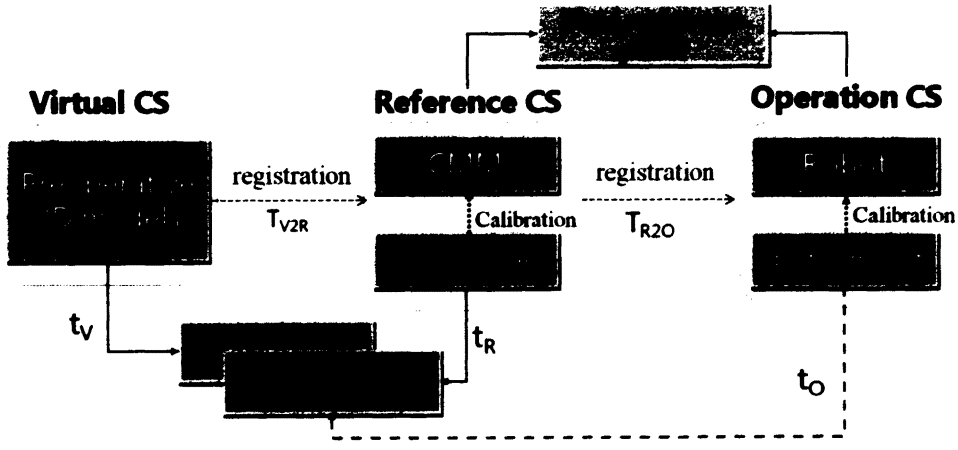

Fig. 32. Relationship among different coordinate systems and objects in the system

A Matlab toolbox developed by Andriy Myronenko for point set registration is used for registration. This toolbox applies the Coherent Point Drift (CPD) algorithm [90], and can be selected to use rigid, affine or non-rigid transformations. Since the patient's jaw is rigid and all the fiducials are rigidly attached to it, a rigid-body point-based registration was chosen. Meanwhile, another two Matlab functions for registration were also used to check the correctness and accuracy of this CPD toolbox, which utilizes Iterative Closest Point (ICP) [61] and finite ICP [60] methods, respectively. Consistent results from all these three methods were achieved.

6-3 Robotic milling for natural-root-formed implants

Natural-root-formed implants have much more complex geometry than traditional cylinder-shaped implants, therefore, site-preparation is manually impossible. The six degree of freedom (DOF) robot with dental drill-bit attached works as a milling machine, which can handle difficult milling schemes with high accuracy. However, the limited space intra-orally restricts the robot from milling the site with arbitrary angles as well as frequent changing of milling orientation. Therefore, to facilitate the robot milling procedure, we optimized the implant design by eliminating under-cuts and smoothing the curvatures as described in ***4-2***. Nevertheless, the geometry of the optimized implants is still irregular thus a single routine like cylindrical milling is not applicable.

Fig. 33 gives an example of an optimized natural-root-formed implant which is voxelized with a resolution of 0.2 mm. The original surface model was voxelized using an open-source software – ArtOfIllusion with a voxelization plugin [91], and then converted into a filled model in Matlab. In this voxelized single-root model, there are a

total of 22627 voxels, corresponding to 22627 coordinates. If we select a direct milling procedure such as milling layer by layer with contour-following, this number of coordinates is too large to be stored in the robot controller memory, which has an upper limit of only 1000 arrays. Therefore, a volume decomposition strategy was applied to simplify the milling procedure.

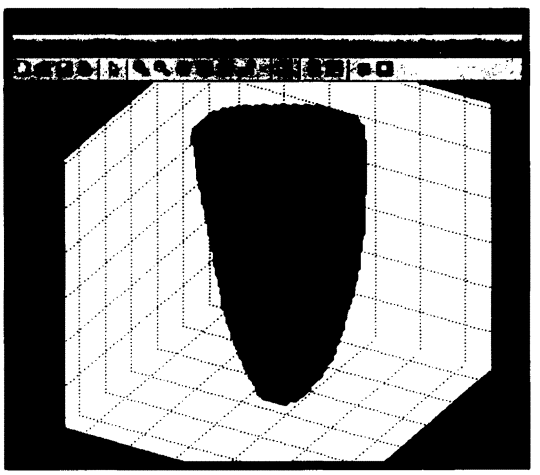

Fig. 33. An example of the voxelized model of an optimized implant

Because the volume of natural-root-formed implants can be approximated by some basic geometric volumes (cylinder, corn, elliptic-cone, etc.), several pre-routines for the removal of these geometric volumes were implemented using Mitsubishi Electric Factory Automation (MELFA) language. For each geometric volume, only a few parameters are required to define such geometry for the robot operation. For example, a cylinder can be determined by three parameters: the radius, the coordinates of the start point, and the end point for drilling, which defines both the depth of the cylinder and the drilling direction at the same time (Fig. 34). These sub-routines extensively simplify the robot commands

and improve the efficiency. They were implemented by Yongki Yoon [86] from the Department of Mechanical and Aerospace Engineering of Old Dominion University. Fig. 35 shows a phantom with which several sub-routines were tested to remove different geometries. TABLE IV compares the time required to remove a certain volume with point-based milling and with a sub-routine using the robot. It is quite obvious that the milling with sub-routines has much shorter operation time than point-based milling, which is only about one-third of the later.

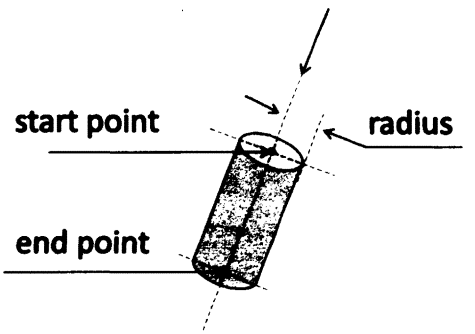

Fig. 34. Parameters for the robot to remove a cylinder shape

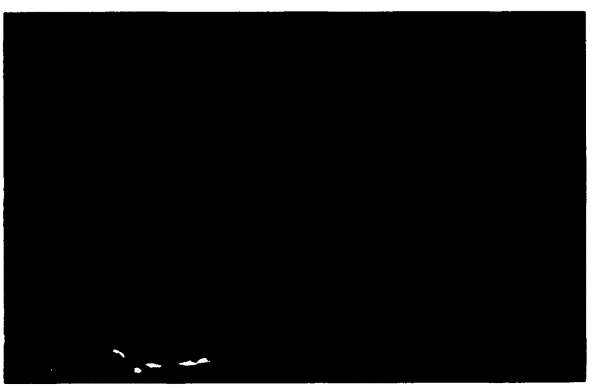

Fig. 35. Phantom results of the robot sub-routines for milling basic geometries

TABLE IV

COMPARISON BETWEEN THE SPEED OF REMOVING THE SAME VOLUME WITH DIRECT DRILLING AND SUB-ROUTINE (OVERRIDE OF THE ROBOT SPEED = 2)

Geometry type	Parameters	Speedy (second)	
		with point-based milling	with sub-routine
Cylinder	r=3, d=6	55.84	291.49
Cone	r=3, d=6	311.33	100.17
Elliptic-cone	a=4, b=3, d=6	403.25	130.56

The volume decomposition strategy we utilized decomposes the volume needed to be removed into the combination of several sub-volumes. Each of these sub-volumes could be either one of the basic geometric volumes that are defined by a MELFA sub-function, or a set of point sequence which has a small amount of points. For each pre-defined natural-root-formed implant, an iterative procedure will be used for sub-volume decomposition. The main steps of the algorithm are as following:

1. voxelize the 3D model of an optimized natural-root-formed implant ($V_{original}$) at the user's desired resolution, and load discretized volume ($V_{discretized}$) into the application program;
2. segment $V_{discretized}$ into (N+1) major parts, i.e., the top part and N roots, where N is the number of roots in the target model;
3. for i=1:N+1, set the alpha volume (the current target volume) to V_i, set variable j=1;

4. for current target volume V_i, calculate the maximum volume which can be removed from V_i under a user defined accuracy, with the general geometry of elliptic-frustum. Denote the maximum volume as $V_i(j)$ and record the corresponding parameters as $F_i(j)$, among which the drilling depth is $d_i(j)$;
5. segment V_i into two portions: the upper one which is the portion that has a depth of $d_i(j)$ from its top layer of V_i; and the lower one which is the remaining part of V_i. Update the alpha volume V_i with the lower portion, and increase the value of j by 1;
6. check if the current alpha volume is small enough. If so, generate milling sequence for the remaining volume and save into $F_i(j)$; otherwise, go back to step 3;
7. check if milling function sequences for all (N+1) sub-volumes have been determined. If so, finish.

Following is the flowchart showing the same algorithm.

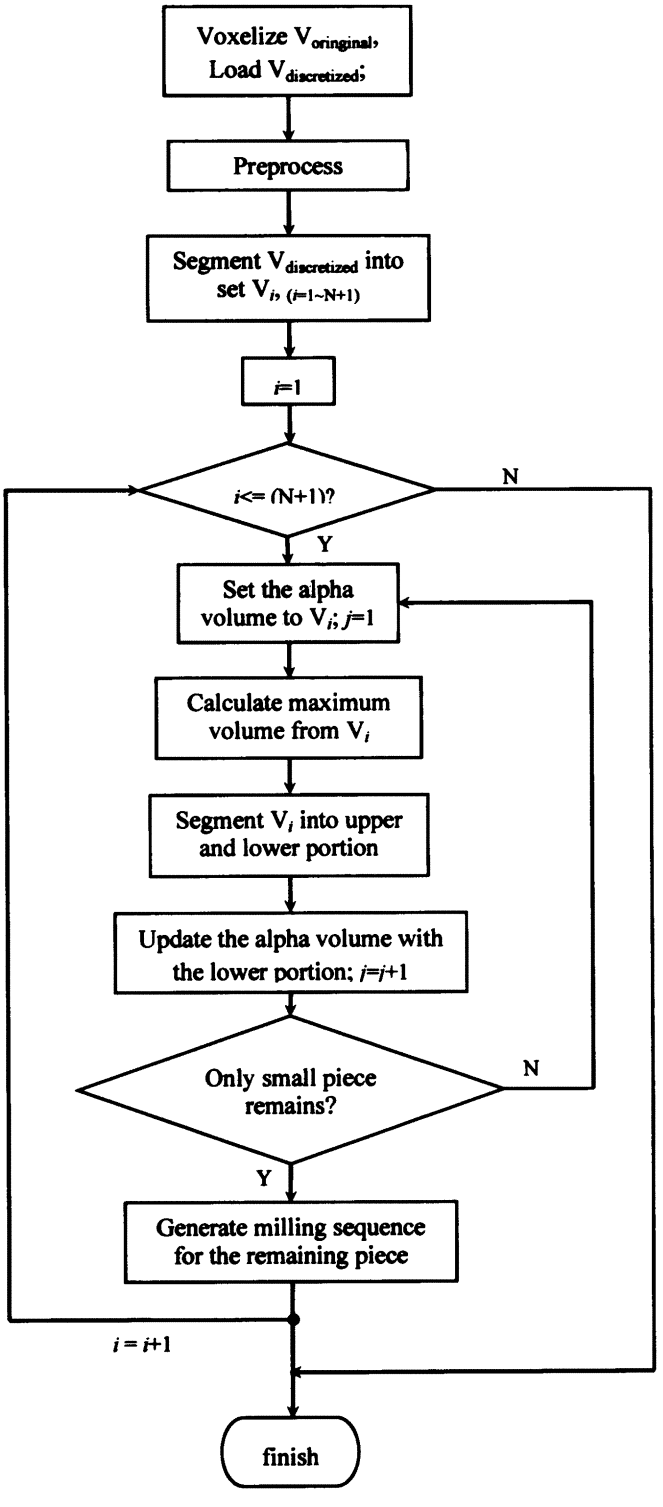

Fig. 36. Flowchart for volume decomposition algorithm

Within this algorithm, there are four major components: (1) preprocessing; (2) volume segmentation; (3) maximum sub-volume extraction; (4) milling sequence generation for the remaining piece. In the preprocessing function, the output of the voxelized surface model from ArtOfIllusion is loaded, which is a Mx3 matrix containing the coordinates of the occupied voxels (M is the number of voxels), and filled into a solid model and then the unclosed layers on the top are removed. The solid model (i.e., the coordinate matrix) is then segmented into 1 top-segment and N root-segments, where N is the number of roots in the model (N=1, 2 for single-, double-root models, respectively). For each segment, the coordinates of the solid model along with the coordinates of corresponding surface model are sent to a generalized function for volume decomposition. This function is applied to extract the maximum sub-volume and generate the milling sequence for the remaining piece.

Maximum sub-volume extraction is the key component, which calculates the volume that can be removed from the alpha volume (the target volume). This volume should be one of the basic geometric volume types, and the distance between any point in the removed volume and its closest point in the current layer of the alpha volume should below a certain threshold (1 mm, for example). Although each geometric volume type as defined by our sub-functions has different parameters for robot milling, when calculate the maximum volume, they can be uniformly expressed using an elliptic-frustum. As shown in Fig. 37, an elliptic-frustum in a 3D space is described by two sets of parameters: the first set of parameters define its geometry, which include its semi-major axis at the top (a1), semi-minor axis at the top (b1), semi-major axis at the bottom (a2), semi-minor axis at the bottom (b2), depth (d); the second set of parameters are the center

point at its top (o1) and bottom plane (o2), which determine its position and orientation in the 3D space. Additionally, the relationship between a1, b1, a2 and b2 is restricted by (9):

$$a1/a2 = b1/b2 \tag{9}$$

Therefore, there are only three effective parameters among these four, and the other one can be determined by these three parameters.

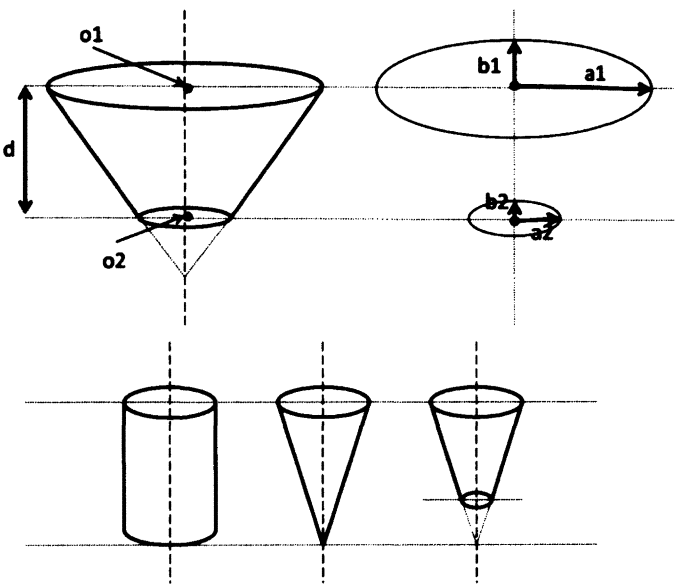

Fig. 37. Uniform expression using elliptic-frustum (upper: a elliptic-frustum; lower: from left to right, cylinder, cone, conical-frustum)

Cylinder, cone, conical-frustum, elliptic-cylinder, elliptic-cone, and elliptic-frustum can all be expressed with the parameters a1, b1, a2, b2, under certain conditions as listed in TABLE . For this reason, uniform expression of an elliptic-frustum to calculate the maximum volume that can be removed from an alpha volume was used.

TABLE V

CONDITIONS FOR DIFFERENT GEOMETRIES USING THE GENERAL ELLIPTIC-FRUSTUM EXPRESSION

parameters (a1, b1, a2, b2)	conditions
cylinder	a1=b1=a2=b2
cone	a1=b1; a2=b2=0
conical-frustum	a1=b1; a2=b2 $\neq$ 0
elliptic-cylinder	a1 $\neq$ b1; a2 $\neq$ b2; a1 = a2; b1 = b2
elliptic-cone	a1 $\neq$ a2; a2 = b2 = 0
elliptic-frustum	a1 $\neq$ b1; a2 $\neq$ b2; a2 $\neq$ 0; b2 $\neq$ 0

The flowchart of the algorithm implemented for maximum sub-volume extraction is shown as in Fig. 38.

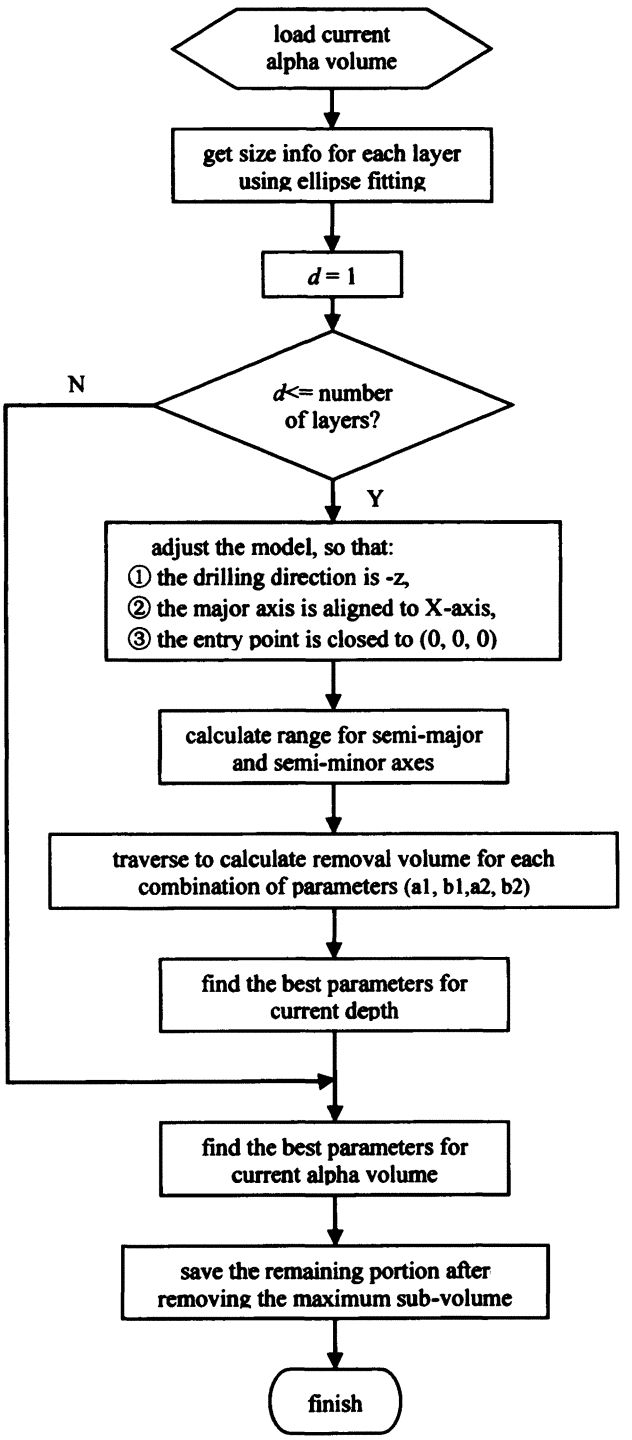

Fig. 38. Diagram of maximum sub-volume extraction algorithm

For the remaining portion, the volume will be milled out layer-by-layer from bottom to top. With regards to each current layer, those voxels on its contour are removed first by applying a contour-following function in Matlab [92]. The contour-following is based on the high resolution model (0.08 mm for the one shown in Fig. 33) to preserve a highly accurate boundary shape. Conversely, such a high resolution is not necessary for the removal of the inner portion because the radius of the drill bit is 1.0 mm, which is much larger than the distance in between two adjacent voxels. Therefore, the contour voxels extracted from the inner portion of the current layer is based on a relatively lower resolution in order to reduce the operation time. With a target resolution of 1.0 mm, the number of voxels can be reduced by a magnitude of about 100 (square of 1.0/008). Once a certain voxel is removed in the current layer, the corresponding voxels along the same line as the drill-bit are all removed with this single operation. Because the models of natural-root implants have been refined, it is assumed there is no under-cut in the model. For that reason, once a lower layer is removed, there would only be a small amount of voxels left around the boundary, which greatly speeds up the milling operation. Fig. 39 illustrates how the volume with the milling sequence generated from our algorithm approximates its original shape. In the original model as shown in Fig. 39 (a), there are total 649526 voxels with a resolution of 0.08 mm. After running the volume decomposition algorithm, the whole volume was decomposed and thus simplified into six portions:

(1) one elliptic-frustum with a depth of 2.0 mm at the top,

(2) a set of milling sequence of 1224 points between the top and roots,

(3) an elliptic-frustum with a depth of 5.6 mm at one root (root #1),

(4) a set of milling sequence of 222 points at root #1,

(5) an elliptic-frustum with a depth of 6.5 mm at another root (root #2),

(6) a set of milling sequence of 109 points at root #2.

The result from this milling sequence generation algorithm for a double-root implant is given in Fig. 39 (b). The denser points located at the middle and bottom of the roots are the discrete point milling sequences. Here, the threshold of error between the approximating elliptic-frustum and the original model was set as 0.8 mm, which makes sure the milled out elliptic-frustum shape, is inside the boundary with an error less than this threshold. It can be seen that the generated milling sequences enclose a volume which is skinnier than the original model. This is because the width of the drill bit is taken into consideration when the milling sequence is generated. The actual volume removed by these milling sequences is shown in (c), which gives a close approximation to the original model.

When the milling sequence for a certain implant is generated, all the coordinates are calculated in the local coordinate system of this 3D model, whose origin lies in its centroid. This coordinate system can be considered as align with the virtual CS. Therefore, the transformation matrix T_{V2O} can be used to map the milling sequence calculated in this local CS to the robot CS.

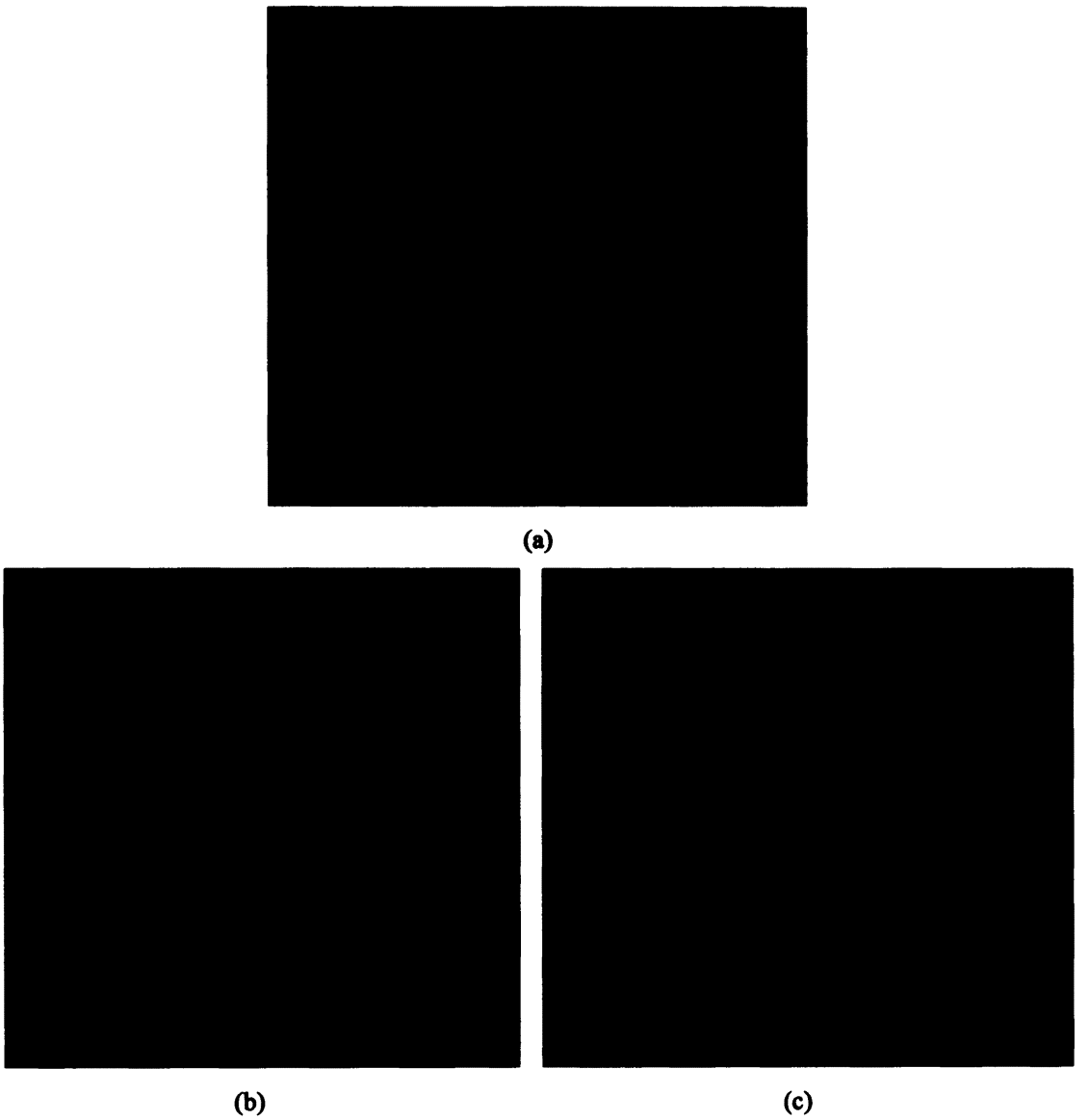

(a)

(b) (c)

Fig. 39. Milling sequence generation for a double-root implant: (a) the optimized model, (b) generated milling sequences, (c) volume removed by the milling sequences

6-4 Virtual fixtures

Two types of virtual fixtures were designed and introduced in the system: one is the motion constraint for the path from robot's original position to the start point of the first milling operation inside the mouth; the other is the motion constraint for the milling operation when it is executed.

A fixated mouth guard device is designed to be used in our application to restrain the patient's head and jawbone in a secured position and orientation. With this device, not only the position of the patient in world coordinate system, thus in reference coordinate system, is fixed; but also the "no-go" areas for the entrance to the mouth and inside the mouth in RCS is determined. Accordingly, their coordinates in OCS can be calculated.

Within the small area inside the patient's mouth, the robot only has a very limited working space there. The relative orientation between the dental drill-bit, which is attached to the end-effector of the robot, and the patient's mouth (or the mouth guard device) must be chosen carefully to make sure that the drill bit as well as any part of the robot do not violate the defined virtual fixtures thus potentially injuring the patient. The possible operational space of the drill bit might be limited to a relatively small angle. Since the robot is fixed on a table whose location is not supposed to change due to calibration requirements, therefore, the operating chair in which the patient sits during surgery is designed as rotatable so the operation site for the implant insertion can be adjusted to the operating space.

For the second type of virtual fixture, which is the constraint for the milling operation into the patient's jawbone, is coded into the program for milling sequences generation. Since the robot is only commanded to move the tip of the drill bit to where the target voxel is, it is important to make sure that none of the upper layers is affected by the milling operation. In another words, none of parts on the drill bit shall touch any portion outside of the designed volume during the procedure. As described in ***7-3***, for each segment, an elliptic-frustum is first removed from the top layers and then the remaining voxels in the bottom layers are milled out. Since this elliptic-frustum always has the feature that its top is wider than its bottom due to the geometry of the implant model, no VF is necessary when removing this elliptic-frustum. A virtual fixture is set to give the boundary for the drill bit only when it is milling the remaining portion of a segment after removing the elliptic-frustums. In our case, two different constraints were combined to define the boundary of the movement of the drill-bit:

type I: the maximum projection of the upper segment (if any) onto the plane perpendicular to the drilling direction of the current segment;

type II: top layer of the remaining portion after the elliptic-frustums removal (if any) of the current segment.

The contour of the combination of these two fixtures is defined as the constraint. The milling sequence for each remaining layer is first generated by trying to follow its contour. If the milling operation for any of the voxels along the contour violates the constraint, meaning any part of the drill bit falls outside of the virtual fixture, the contour will be contracted until the maximum boundary no longer breaches the area that was violated.

The milling sequence generated with virtual fixtures was visualized as shown in Fig. 40, where black dots give the original shape of the model; blue color indicates the area where milling sequences locate; red dots are points that violate the VF; yellow color illustrates the difference between the surface of the extracted elliptic-frustum and the surface of the original model. One can notice that most of the red dots are located around the apex of the root, which is due to the relative big size of the drill bit (diameter = 2 mm) with regards to the small scale of the volume that needs to be removed. For example, the remaining portion of the single-root volume after the elliptic-frustum removal has a dimension of about 1.8 mm * 1.6 mm along the X- and Y- axis (Fig. 41), which is even smaller than the size of the drill bit. Therefore, those points were discarded in order to make sure the drill bit does not go outside of the boundary thus ensuring the safety of the patient.

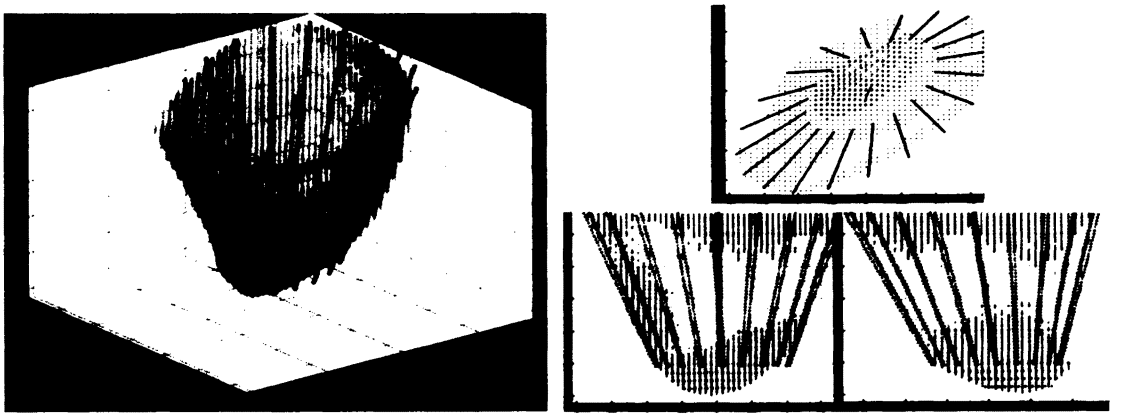

(a)

(b)

Fig. 40. Results of robotic-milling generation. (a), (b): results for volume type S1 and D1, respectively.

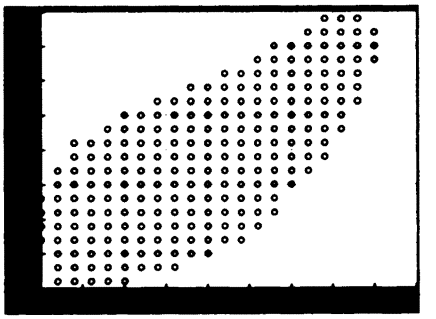

Fig. 41. Remaining portion of the single-root volume after the elliptic-frustum removal (projection onto the X-Y plane)

CHAPTER 7

EXPERIMENTS IN REGISTRATION AND ROBOTIC MILLING

Several experiments were designed to evaluate the registration accuracy of the system on both positioning and orientation with the help of a patient-specific phantom. Besides, robot milling of the shapes of the optimized natural-root implants was conducted, along with the virtual fixture testing.

7-1 Phantom experiment on position accuracy

Registration accuracy was tested with phantom experiments by using a patient specific model. CBCT images of a patient collected from a Toshiba CBCT scanner with a slice thickness of 0.5 mm was reconstructed to a patient-specific 3D model. Five small semi-spheres (diameter = 1 mm) were artificially created and virtually attached to the model, whose apexes acted as both fiducials and targets (one of them was defined as a target while the remaining four as fiducials for registration). The patient-specific jaw model with fiducials attached was printed out by Krzysztof Rechowicz from the Department of Modeling, Simulation and Visualization Engineering, Old Dominion University, using a 3D printer (Spectrum Z510, Z Corp., Burlington, MA, US). Such a shape of the fiducials was chosen because it was not easily broken during the printing process. Their coordinates were measured in the virtual CS by identifying the apex of each semi-sphere using a mouse. In the reference CS, their coordinates are measured by touching the apex of each semi-sphere with the tip of the FARO probe. In order to minimize localization

error, ten measures are made for each fiducial position, and their mean value was recorded as the final coordinate for a given fiducial.

Another eight points were defined by marks on the printed out jaw model (points with red labels in Fig. 42), as the fixed registration points for the second step registration. The coordinates of these points were measured in both the reference CS and the operation CS. In the operation CS, the coordinates were measured by commanding the robot to move along the X-, Y- and Z-axes, until the tip of the drill-bit reached the apex of a semi-sphere.

The two-step registration procedure as described in ***6-2*** was performed for each target and fiducials combination. Two widely used indicators: Fiducial Registration Error (FRE) and Target Registration Error (TRE) were calculated to evaluate the positioning error of the two-step registration procedure. FRE for registrations between the virtual CS & reference CS, and also the reference CS & operation CS were calculated. To evaluate the target registration error, one of the fiducials was set as the target and the registration procedure was conducted using the remaining four fiducials. After registration, the coordinate for each target point in the operation CS was calculated. Accordingly, the robot was commanded to move the tip of the drill-bit to the target coordinate and hold its position there. Because one of the five fiducials (the five semi-spheres) was set as the target, the designated position of the target in the operation CS can actually be measured directly by the robot. Therefore, the measured coordinate in the operation CS was set as "gold standard value" while the current coordinate of the drill-bit tip was recorded as a "registered value", and TRE value after the two-step registration was calculated as the

difference between these two values according to (2). TREs for each pair of the two-CS registration were recorded.

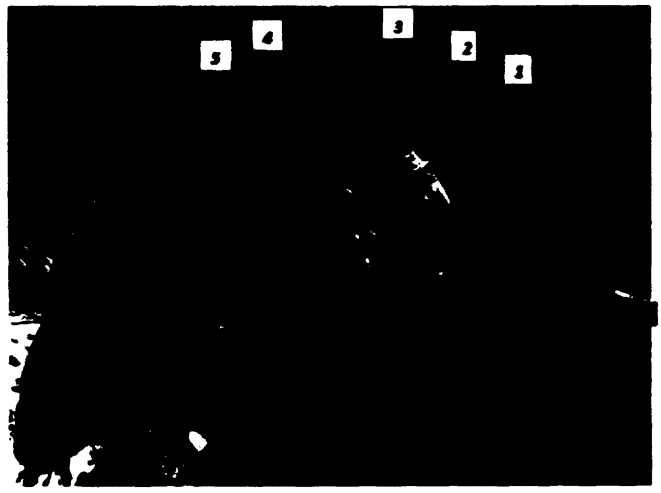

Fig. 42. A patient-specific jaw model with five fiducials (shown in italic) and eight fixed registration points (show in normal)

The phantom experiments were at first carried out with a setup as shown in the left side of Fig. 43. In this setting, the CMM was on a tripod which was placed on the ground next to the table where the robot was fixed. Later, the CMM was fixed on the same table as the robot with a specially made fixation plate (Fig. 43, right), and repeated the registration procedure trying to evaluate if there was improvement after the CMM fixation.

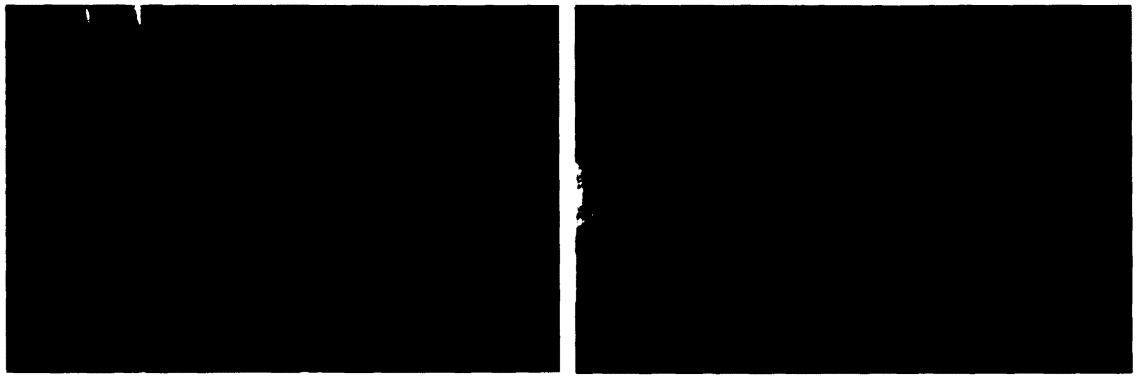

Fig. 43. The original (left) and improved (right) phantom experiments setup

7-2 Experiment on orientation accuracy

In order to calculate the orientation angle, a reference plane was introduced and its norm was considered as the reference direction. The physical jaw model was fixed on a wood board, thus we set this board as the reference plane. For the virtual model, a plane that can hold it as the wood board did in the physical world was generated and its norm was calculated by measuring 10 points on it. The angle between each drilling direction planned and the norm of this plane was calculated. After the two-step registration, orientation error, defined as the difference between the angle in the operation CS and the angle in the virtual CS, was calculated.

In the phantom experiments, five holes were drilled on a drilling base according to the drilling direction calculated for each target. It was decided to not drill directly into the jawbone because its material is not suitable for drilling. Further, this experiment was only for the evaluation of orientation error; therefore, position information did not matter. After drilling, a metal stick magnetically attached to one of the blade edges of a digital

protractor was inserted into the drilled hole. The other blade of the protractor was then adjusted to align to the reference direction of the wood plane, which was defined by one side of a rectangular box (Fig. 44 c). The angle between the metal stick (the drilling direction) and the reference direction in the operation coordinate system was recorded.

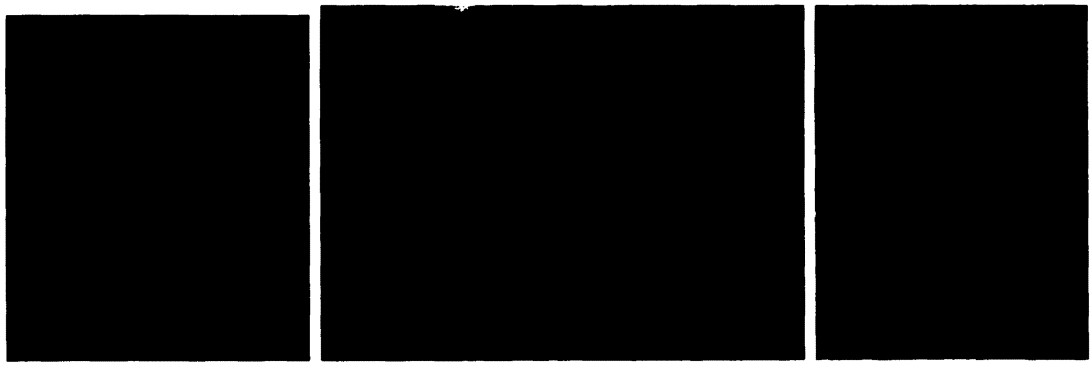

(a) (b) (c)

Fig. 44. 3D model on the reference plane in (a) VCS and (b) OCS, (c) measuring orientation angle in OCS

7-3 Robotic milling of the novel implants

The robotic site-preparation (i.e. robotic milling of the root shape) of the small-sized natural-root-formed implants with single- and double-root was tested. Milling sequences for these two implants were generated utilizing the algorithm based on volume decomposition as described in *6-3*. As a result, the single-root model was decomposed into a top elliptic frustum with a depth of 9.5 mm and a set of discrete points (N=91), while the double-root model was decomposed into three segments, each consisting of an elliptic-frustum and a set of discrete points.

For robotic milling testing, some milling bases similar to those used for testing orientation accuracy were created by mixing one type of powder with water to create a hard plaster. The ratio between the powder and water was tested to find a suitable value with which the hardness of the plaster bases was good for the robot milling operation. An arbitrary point on the surface of the milling base was set as the start point of the robot milling, which equaled to either the entry point of the elliptic-frustum (if any existed) or the first point in the discrete point set of the top segment.

Due to the fact that the volume removed for the site-preparation of our natural-root implant is very small (even the large-sized double-root implant has a dimension of about 10 mm *10 mm *14 mm) and is in an irregular shape, the accurate shape of the removed volume is very hard to measure. Attempts were taken by molding the shape of the volume removed by using a denture material, which helped to approximate and visualize the site-preparation results. Some measurements of the removed volume in the milling base were taken to get its dimensional information, including dimensions of its opening and the depth of the volume. The time of the milling operation for each of the implant designs was recorded as well.

In order to assess the accuracy and efficiency of the volume-decomposition-based algorithm for each implant model, the milling sequence was also generated without trying to extract any elliptic-frustum. The actual volumes removed and the milling time by using these two different strategies were compared.

CHAPTER 8

EXPERIMENT RESULTS AND DISCUSSION

The results of the experiments described in ***Chapter 7*** are provided in this chapter, and some related discussions are given as well.

8-1 Position and orientation accuracy

The coordinates of the fiducials and the fixed registration points measured in the earlier setup (before CMM fixation) and in the later setup (after CMM fixation) are listed in TABLE and TABLE , respectively. Please note that the coordinates in the operation CS were changed slightly after CMM fixation, because the jaw model fixed on the robot table was touched accidentally during the fixation operation of the CMM. The data contain targets' coordinates measured by the robot to represent the "gold standard" values of the targets for TRE calculation.

The results from the phantom experiments for positioning accuracy are listed in TABLE . After fixing the Faro Arm onto the same table of the robot, the spatial relationship of the reference and the operation CS was ensured to remain rigidly unchanged during the whole procedure. As a result, the final TREs decreased from 1.42±0.70 mm to 1.14±0.61 mm.

TABLE VI

COORDINATES MEASURED BEFORE CMM FIXATION (UNIT IN MM, N = 10)

		Virtual CS			Reference CS			Operation CS		
		X	Y	Z	X	Y	Z	X	Y	Z
Fiducials / Targets	1	-18.80	-4.01	24.39	861.73	128.45	-556.88	473.15	25.71	49.89
	2	-10.89	-5.03	29.43	852.57	129.24	-558.69	467.34	18.19	50.66
	3	-0.05	-4.88	32.42	841.52	130.21	-557.09	464.64	7.44	51.62
	4	9.82	-3.69	29.38	833.75	129.89	-550.05	467.75	-2.36	51.13
	5	18.48	-2.80	24.50	827.64	128.55	-542.39	472.24	-11.06	49.90
Fixed registration points	1	/			905.04	129.95	-527.95	516.30	53.42	51.38
	2				882.68	121.65	-525.17	509.67	31.80	42.95
	3				881.09	120.69	-546.34	489.61	38.88	42.14
	4				860.56	126.64	-551.03	477.20	22.00	47.98
	5				831.48	125.46	-534.82	480.19	-10.76	47.02
	6				823.80	120.75	-520.02	490.56	-24.16	42.20
	7				836.29	120.37	-506.64	507.83	-18.36	41.80
	8				820.39	127.67	-495.33	511.54	-37.34	48.99

Also, it was noticed that the original orientation of the X-, Y-, Z-axes relative to the phantom model matters to the registration accuracy. It is important to realign the axes of the "from" CS to align with the "to" CS, in order to get a better registration result. The orientation errors measured using the method as described in VII-2 with three different designated drilling directions are listed in Table IX. The resulting orientation error in the operation CS after registration is 1.99±1.27° (N=14).

TABLE IX also gives the results when the CS orientation is pre-aligned. TREs after step1 decreased from 1.09±0.69 mm to 0.24±0.13 mm, and final TREs decreased from 1.14±0.61 mm to 0.36±0.13 mm. Thus, the system provided a significant improvement in the registration accuracy.

TABLE VII

COORDINATES MEASURED AFTER CMM FIXATION (UNIT IN MM, N = 10)

		Virtual CS			Reference CS			Operation CS		
		X	Y	Z	X	Y	Z	X	Y	Z
Fiducials / Targets	1	-18.80	-4.01	24.39	476.43	-65.99	345.81	476.10	26.11	49.21
	2	-10.89	-5.03	29.43	472.71	-65.13	337.32	470.49	18.55	49.98
	3	-0.05	-4.88	32.42	464.85	-64.07	329.34	467.38	7.86	50.94
	4	9.82	-3.69	29.38	454.56	-64.55	327.05	470.73	-2.12	50.75
	5	18.48	-2.80	24.50	444.61	-65.96	326.66	475.28	-10.78	49.42
Fixed registration points	1				478.82	-64.46	396.87	519.17	53.39	51.06
	2				463.33	-72.71	380.43	512.49	31.95	42.63
	3				479.42	-73.73	366.81	492.83	39.21	41.56
	4		/		470.96	-67.78	347.36	480.24	22.30	47.70
	5				441.15	-68.87	333.53	483.26	-10.43	46.56
	6				424.48	-73.50	335.04	493.40	-23.99	41.89
	7				420.82	-73.90	354.04	510.92	-18.12	41.44
	8				402.50	-66.83	347.80	514.61	-37.16	48.79

TABLE VIII

REGISTRATION RESULTS FOR POSITIONING ACCURACY

	before Faro fixation				after Faro fixation				after Faro fixation and CS orientation pre-alignment			
	step 1		step 2		step 1		step 2		step 1		step 2	
Target #	FRE	TRE	FRE	TRE	FRE	TRE	FRE	TRE	FRE	TRE	FRE	TRE
1	0.23	1.82		2.29	0.20	1.90		1.74	0.10	0.43		0.44
2	0.29	0.80		0.89	0.27	0.86		1.15	0.15	0.23		0.41
3	0.42	0.16	0.186	0.74	0.43	0.26	0.194	0.42	0.15	0.23	0.194	0.50
4	0.28	0.80		1.18	0.33	0.71		0.64	0.18	0.07		0.17
5	0.23	1.80		2.03	0.26	1.72		1.76	0.16	0.25		0.30
MEAN	0.29	1.08	/	1.42	0.30	1.09	/	1.14	0.15	0.24	/	0.36
SD	0.08	0.71	/	0.70	0.08	0.69	/	0.61	0.03	0.13	/	0.13

The orientation errors measured using the method as described in VII-2 with three different designated drilling directions are listed in Table IX. The resulting orientation error in the operation CS after registration is 1.99±1.27° (N=14).

TABLE IX

MEASURED ORIENTATION ERROR AFTER REGISTRATION (UNIT IN DEGREES)

planned angle	15°		30°		45°	
Target #	actual angle	error	actual angle	error	actual angle	error
1	18.0	3.00	30.3	0.30	42.1	2.90
2	18.6	3.60	29.6	0.40	44.0	1.00
3	17.0	2.00	/	/	42.8	2.20
4	18.6	3.60	29.2	0.80	40.9	4.10
5	16.1	1.10	29.0	1.00	43.1	1.90
MEAN=	17.66	2.66	29.53	0.63	42.58	2.42
SD=	1.09	1.09	0.57	0.33	1.16	1.16

8-2 Robotic milling with virtual fixtures

Robotic milling was performed to prepare the insertion site for the small-sized single- and double-root implant, with the milling sequences generated using the volume-decomposition-based algorithm and a point-based strategy for comparison. Therefore, four different volumes were milled out using the robot:

S1: single-root shape with elliptic-frustum from volume-decomposition-based method;

S2: single-root shape without elliptic-frustum from point-based strategy;

D1: double-root shape with elliptic-frustum from volume-decomposition-based method;

D2: double-root shape without elliptic-frustum from point-based strategy.

The results of robotic-milling generation for different models and different methods are reported in Table X. It is clear that the results from the volume-decomposition-based method have a much smaller amount of discrete points than point-based strategy. It not only avoids overloading the robot memory, but also possibly means less operation time.

It was proven by recording the actual milling time for each volume type. The results are given in TABLE . It is obvious that the volume-decomposition-based milling has a much shorter processing time than simple point-based strategy, which is about half the amount of time shorter than the later. This result is consistent with the speed test for simple geometries as listed in TABLE .

TABLE X

RESULTS OF ROBOTIC-MILLING GENERATION

volume	elliptic-frustum	number of discrete points in each segment	total number of discrete points
S1	1 (d = 9.5 mm)	91	91
S2	/	1121	1121
D1	3 (d = 2.0, 5.6, 6.5 mm)	1224, 222, 109	1555
D2	/	813, 1391, 1404	3608

TABLE XI

MILLING TIME FOR EACH VOLUME TYPE (UNIT IN SECOND)

volume	*S1*	*S2*	*D1*	*D2*	*D3*
total milling time (s)	177.00	391.02	941.95	1382.98	1720.16

Although points violating the virtual fixtures have been dismissed in the generated milling sequence, however, by monitoring the whole milling procedure, it was noticed that the top segment was actually affected when the elliptic-frustum decomposed from one of the roots was milled out. The body of the drill bit went outside the boundary of the top segment due to a relatively big orientation of the elliptic-frustum, thus a small piece of milling base was removed (area inside the red square in Fig. 45 a1). This result was different from its designed shape because we only set the virtual fixtures (the two types of boundaries) for the point-sets that remained after the elliptic-frustum removal. Since the elliptic-frustum was removed by calling a predefined sub-routine, the robot can not be commanded to skip some of the points during the procedure. In comparison, the result

from point-based milling (Fig. 45 a2) does not have this issue due to the fact that all the points were considered as belonging to the remaining portion thus were set to follow the virtual fixtures. Therefore, an attempt was made by combining the volume-decomposition and point-based strategies together: the top segment and the root segment that did not affect the top segment were removed using milling sequences from volume-decomposition algorithm and the other root segment which broke the top segment was milled out according to the point-based milling. The volume removed by using this mixed milling strategy is labeled as ***D3***.

From Fig. 45 (a3), it is clear that the resulting shape from the mixed milling strategy approaches a closer shape at its opening to the designed volume. However, the operation time was significantly increased from 942 seconds to 1720 seconds (Table 11), as expected, which was about 13 minutes longer. In future work, more tests would be necessary in order to find the best tradeoff between the volume accuracy and operation time. Also, a methodology can be investigated to allow the predefined sub-routines to follow the virtual fixture constraints.

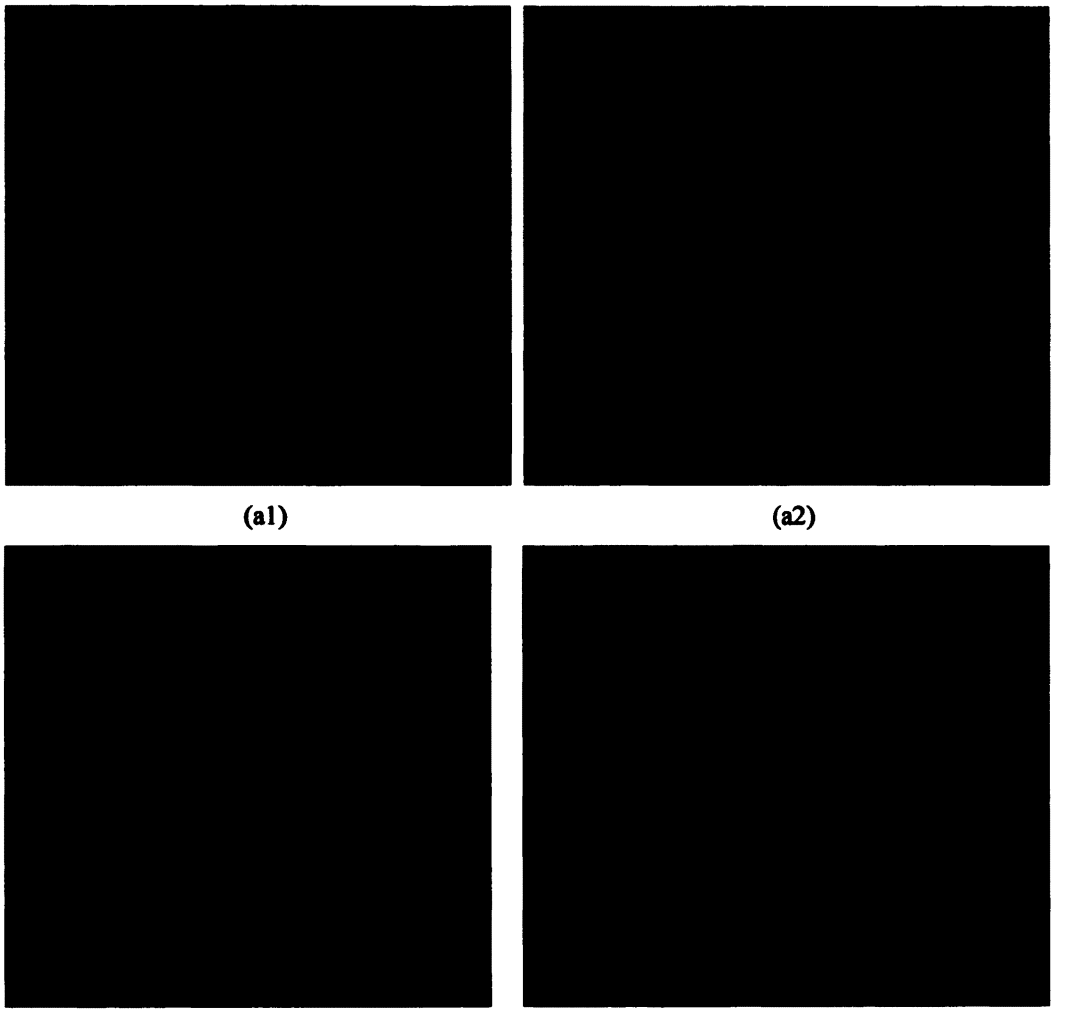

Fig. 45. Milling result for double-root implant. (a1) using volume-decomposition-based algorithm (***D1***); (a2) using point-based milling (***D2***); (a3) using a combination of volume-decomposition and point-based milling (***D3***); (a4) using a volume-decomposition-based algorithm for the model with a straightened root (***D4***)

Another attempt was made by straightening the root which caused the errant milling at the upper segment due to the relatively large angle. The modified model is labeled as ***D4***. Exactly the same parameters (depth, radii, entry point) were used for the milling of this

root, but its orientation was set to be vertical down. The difference between the ***D1*** and ***D4*** is illustrated below:

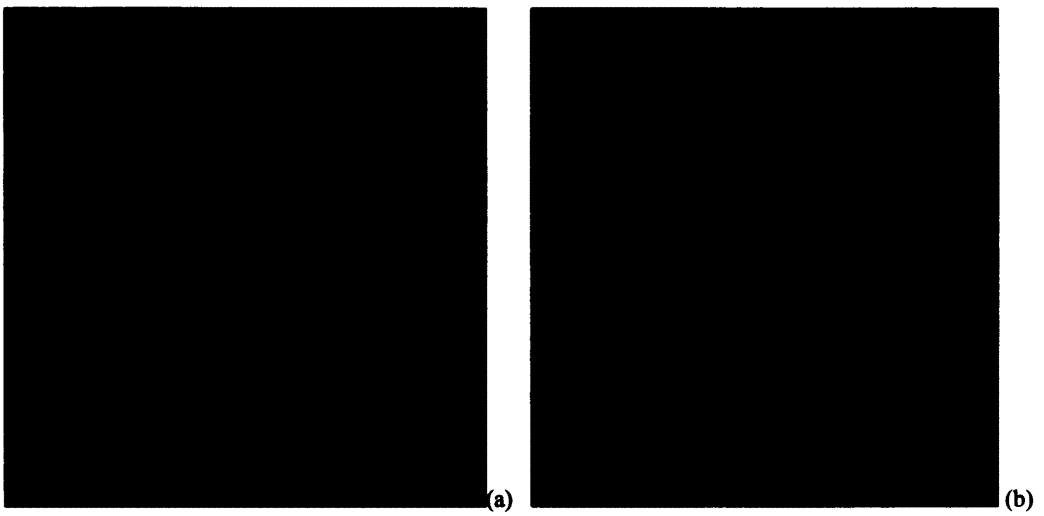

Fig. 46. Milling sequence for (a) the original double-root model ***D1***, and (b) the modified double-root model with a straightened root ***D4***

By monitoring the milling procedure, it was noticed that the elliptic-frustum removal of the straightened root did not affect the upper segment anymore, which proved the effectiveness of this modification. The top view of the removed volume of this straightened model is given in Fig. 45 (b4). Since this model utilized the volume-decomposition-based method for volume removal and has the same parameters for the elliptic-frustums as in ***D1***, the milling time was the same as for ***D1***, which is much shorter than the time for ***D2*** and ***D3***. Therefore, ***D4*** provides good results on both the shape removed and the milling time.

FEM result performed by Yongki Yoon indicated that the stress at the root portion of the model with double-root is much lower when compared to the high stress along the contour of its top [86]. Although it still needs to be proven by FEM analysis with our straightened model, this result suggested that the minor modification of the root should not have much influence on the final biomechanics of the double-root model.

Molds for each of volume removed were made and the figures recording the molding procedure are given below. A dental material was filled into each of the removed volumes and remained overnight to be set. Six molds were attained by breaking down the milling base. As one may notice from Fig. 47 (b), the molds were a little below the actual surface of the milling base therefore the molded openings were not very accurate. Also, there were some breakages in the molds especially around the root areas. Therefore, the casting procedure was repeated to get another set of molds, especially carefulness was paid to cover the volume completely trying to solve the problems of collapsed top surfaces and the undesirable bulbs. However, after checking the new molds, problems still existed: top surfaces were preserved but with some degree of extension, and the root areas were still not complete which we believe was due to the existence of bulbs along with the extremely small space around those areas. Although the molding was not perfect, still it indicated a close approximation to our designed natural-root forms.

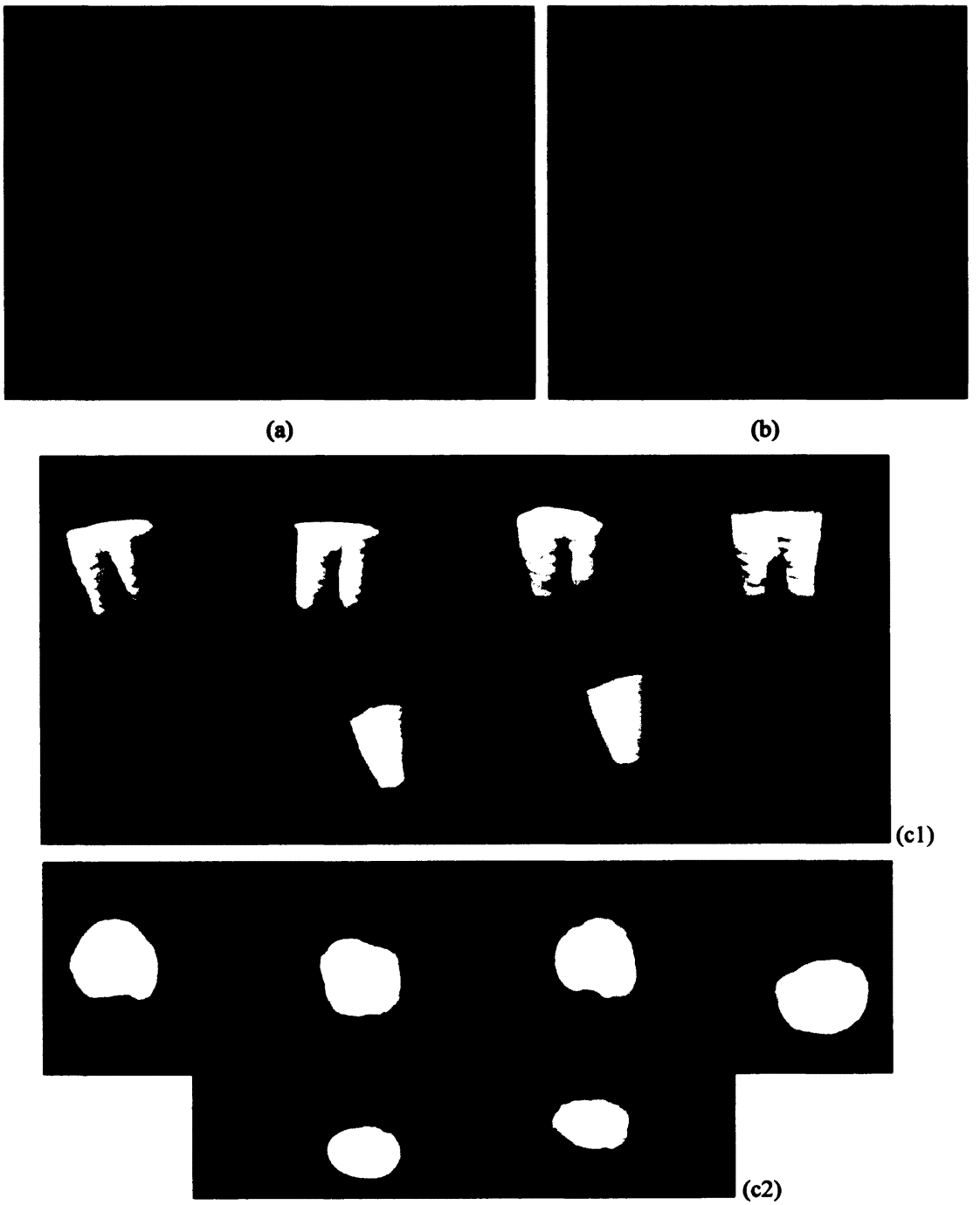

Fig. 47. Casting the removed volumes. (a) site-preparation results; (b) filled with a dental material for molds; (c1), (c2) the extracted molds

The dimensions of the removed volumes were measured with the second set of molds using a caliper, and their designed values were measured with the corresponding virtual models. Because the shapes of the natural-root forms are irregular, measurements on their dimensions were only performed to get the approximate results. Dimensional results for single- and double-root molds are given in TABLE and TABLE , respectively. In these two tables, the measured d1 and d2 is roughly the opening of the long and short axis of the molds' top surfaces. TABLE indicated that all the openings of the molds were smaller than the designed values, which could be due to the fact that when the robot milling was performed, not all the removed powders were successfully cleared out from the volume and may be accumulated inside the volume itself. The accumulation of the powders could result in a removed volume which was actually smaller than designed. When the site-preparation is actually performed in a dental clinic, water flow will be applied to the operation site to clear the removed bones, which may solve the powder problem encountered since only a small balloon was used to blow the powders away. The dimensions of the opening of the molds with double-root did not follow this rule strictly and the possible reason might be the measuring errors for bother the measurements on the molds and the measurements on the virtual models, because the opening shapes were very complex thus their diameters can hardly be determined.

In TABLE , "l" denotes length which was measured from the top surface to the apex of the root. We noticed that all the measured lengths were shorter than the corresponding designed lengths. Apart from the powder accumulation, another reason that caused such results was the existence of bulbs during our casting procedure. As a result, the small and dedicated parts around the root apexes were broken, causing the truncation of the roots.

Besides, for some of the volumes, the apex was the only point in that depth. In this case, the milling operation might not able to reach an effective depth of the root shape as designed. The subscript "$_s$" corresponds to the designed root length when the apex was dismissed from the milling sequence. It is seen that when this factor was considered, the errors between the actual and designed lengths were decreased.

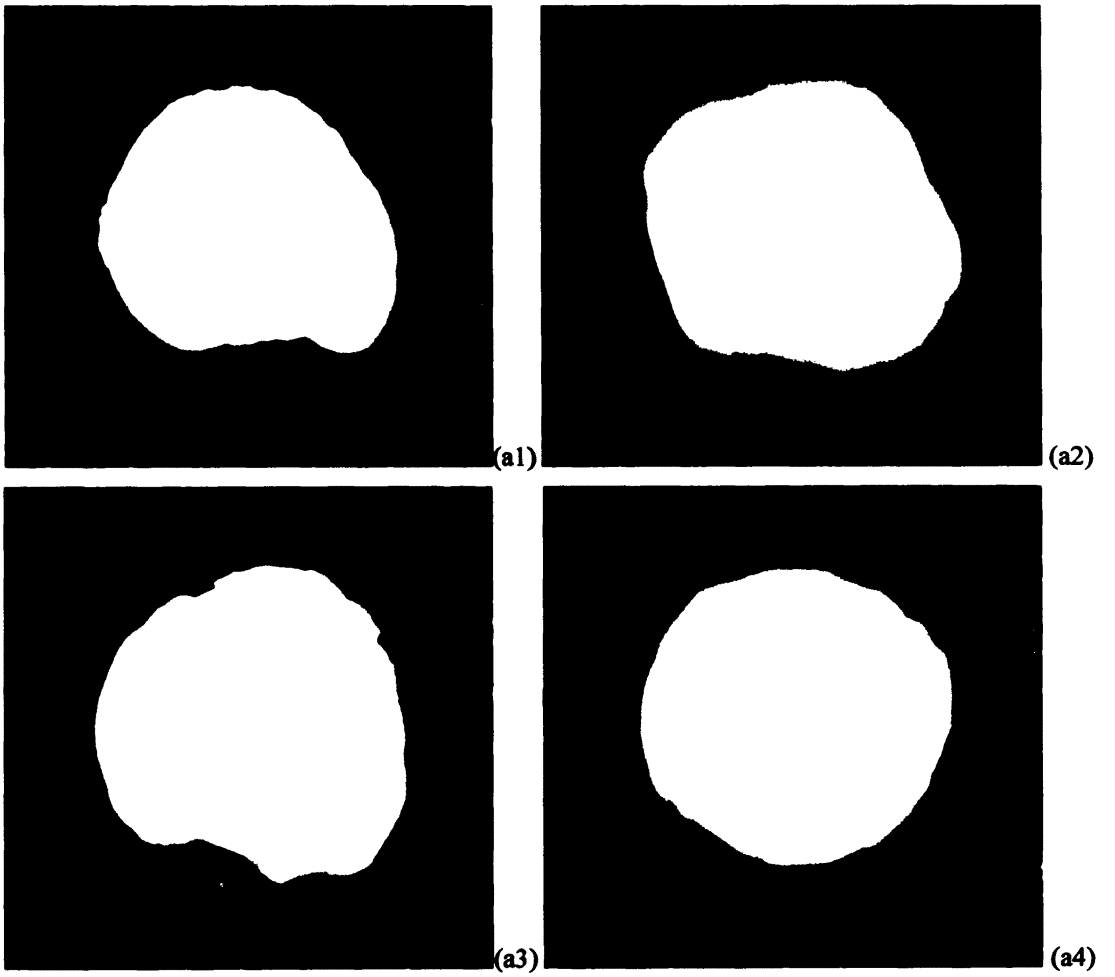

Fig. 48. Molds for different volume types. (a1~a4), top view of the mold for D1, D2, D3, D4, respectively; (b1, b2), comparison of the designed and removed volume for single- and double-root implant

TABLE XII

DIMENSIONS MEASUREMENTS FOR THE MOLDS WITH SINGLE ROOT

		d1	d2	l	l_s
S1	designed	6.82	4.76	11.90	10.94
	measured	6.23	4.40	8.63	/
	error	-0.59	-0.36	-3.27	-2.31
S2	designed	6.82	4.58	11.84	11.28
	measured	6.43	4.43	9.40	/
	error	-0.39	-0.15	-2.44	-1.88

TABLE XIII

DIMENSIONS MEASUREMENTS FOR THE MOLDS WITH DOUBLE ROOTS

		d1	d2	l1	$l1_s$	l2	$l2_s$
D1	designed	8.94	9.06	10.24	9.36	9.78	9.19
	measured	9.78	8.70	9.71	/	9.25	/
	error	0.84	-0.35	-0.52	0.36	-0.53	0.06
D2	designed	8.42	8.16	10.76	9.81	9.74	9.36
	measured	8.97	8.53	9.35	/	8.72	/
	error	0.55	0.37	-1.42	-0.47	-1.03	-0.64
D3	designed	8.94	9.06	10.76	9.81	9.78	9.19
	measured	8.75	8.81	8.69	/	7.27	/
	error	-0.19	-0.24	-2.07	-1.12	-2.51	-1.92
D4	designed	8.94	9.01	10.27	9.78	9.50	9.50
	measured	9.44	8.02	9.97	/	9.60	/
	error	0.50	-0.99	-0.30	0.19	0.10	0.10

CHAPTER 9

CONCLUSION

In this dissertation, an image-guided robotic methodology for dental implantation is presented. A medical image supported preoperative surgical planning and an innovative robot-based intra-operative site-preparation methodology were combined, to enable more accurate placement of current implants and facilitate the insertion of novel natural-root-formed implants.

Natural-root implants mimic the root structure of human teeth and were proven by Finite Element Method (FEM) to provide better stress distribution than current cylinder-shaped implants. Two anatomical accurate teeth models were selected and extracted from a 3D human model, and served as the initial templates of our novel implants with single- and double-root. The shapes of the templates were refined by curvature smoothing and undercut removal, to facilitate the robot site-preparation. The refined shapes were further modified by rounding their bottom area, as indicated by the result of topology optimization using Soft-Kill Option (SKO) method. These modified shapes were proven by FEM to further improve the structural performance under certain loading conditions than the original shapes. These two final templates were scaled according to the statistics of human teeth dimensions to get a complete set of the standardized natural-root-formed implants templates.

An image-based preoperative planning software was implemented to help the surgeon to generate an appropriate surgical plan. A patient-specific 3D model reconstructed from the patient's cone-beam CT (CBCT) images was loaded into the software and the surgeon chose the implant type to be inserted and virtually adjusted its position and orientation in the patient's jawbone until a satisfying result was achieved. A novel two-step registration method with the help of a coordinate measurement machine (CMM) was designed and performed to transform the designated spatial information to the operation coordinates of the robot. The CMM was introduced as a reference coordinate system in order to provide superior accuracy while avoiding unnecessary contact between the robot and the patient, thus ensuring the safety of the patient. Phantom experiments with patient-specific jaw models were performed and positioning and orientation errors after registration of 0.36±0.13 mm (N=5) and 1.99±1.27° (N=14), respectively, were achieved.

The intra-operative stage of the system features an automated robotic site-preparation methodology utilizing a robot with six DOF as a milling machine. A novel strategy for milling the volumes of implants including natural-root-formed implants was presented, which was based on volume decomposition. Implant models were first segmented into their roots and/or the top segment. From each segment, an iterative method was applied to decompose it into several elliptic-frustums, which would remove the maximum volume from the current piece, and a set of discrete point sequence. The milling tests proved that using the milling sequence generated from our volume-decomposition algorithm shortens the milling time when compared to utilizing a simple point-based strategy while still maintaining a good approximation of the original shape of the implant. Furthermore, patient's safety was ensured by implementing some virtual fixtures

(constraints) for the milling. Milling results suggested that by deleting those points violating the virtual fixtures, the removed volume preserved its designed shape to a large degree and no anatomical structure around the implant site was affected by the robotic milling.

The combination of the innovative image-guided robotic site-preparation application along with the novel designs of natural-root-formed implants was presented and proved to be feasible and accurate. Although improvements, including generalizing the implants' shapes to ease the site-preparation, optimizing the milling sequences to find the best tradeoff between accuracy and speed, and implementing virtual fixtures for more complicated templates were necessary before it could be operationally used for dental implantation.

REFERENCES

[1] E. Barboza, A. Caúla, and W. Carvalho, "Crestal bone loss around submerged and exposed unloaded dental implants: a radiographic and microbiological descriptive study," *Implant Dentistry,* vol. 11, no. 2, pp. 162-169, 2002.

[2] "Dental Implants - the tooth replacement solution. Available: http://www.icoi.org/patient-education.php.

[3] "OsseoNews -- The world of implant dentistry online. Available: http://www.osseonews.com/.

[4] D. Schwartz-Arad, N. Kidron, and E. Dolev, "A long-term study of implants supporting overdentures as a model for implant success," *Journal of periodontology,* vol. 76, no. 9, pp. 1431-1435, 2005.

[5] X. Chen, Y. Lin, Y. Wu, and C. Wang, "Real-time motion tracking in image-guided oral implantology," *The International Journal of Medical Robotics and Computer Assisted Surgery,* vol. 4, no. 4, pp. 339-347, 2008.

[6] T. Albrektsson, G. Zarb, P. Worthington, and A. Eriksson, "The long-term efficacy of currently used dental implants: a review and proposed criteria of success," *Int J Oral Maxillofac Implants,* vol. 1, no. 1, pp. 11-25, 1986.

[7] M. VOGELER, U. HELD, T. GERDS, and J. R. STRUB, "Long-term Study Using TPS-SteriOss® Implants in Partially Edentulous Patients," in The IADR/AADR/CADR 82nd General Session, Hawaii, 2004.

[8] W. C. Scarfe, A. G. Farman, and P. Sukovic, "Clinical applications of cone-beam computed tomography in dental practice," *Journal-Canadian Dental Association,* vol. 72, no. 1, pp. 75-80, 2006.

[9] M. E. Guerrero, R. Jacobs, M. Loubele, F. Schutyser, P. Suetens, and D. van Steenberghe, "State-of-the-art on cone beam CT imaging for preoperative planning of implant placement," *Clinical oral investigations,* vol. 10, no. 1, pp. 1-7, 2006.

[10] "Implant Planning & Surgical Guides. Available: http://www.conebeam.com/planning.

[11] H. J. Nickenig, M. Wichmann, J. Hamel, K. A. Schlegel, and S. Eitner, "Evaluation of the difference in accuracy between implant placement by virtual planning data and surgical guide templates versus the conventional free-hand method-a combined in vivo-in vitro technique using cone-beam CT (Part II)," *Journal of Cranio-Maxillofacial Surgery,* vol. 38, no. 7, pp. 488-493, 2010.

[12] J. Hoffmann, C. Westendorff, G. Gomez Roman, and S. Reinert, "Accuracy of navigation guided socket drilling before implant installation compared to the conventional free hand method in a synthetic edentulous lower jaw model," *Clinical Oral Implants Research,* vol. 16, no. 5, pp. 609-614, 2005.

[13] C. Park, A. J. Raigrodski, J. Rosen, C. Spiekerman, and R. M. London, "Accuracy of implant placement using precision surgical guides with varying occlusogingival heights: an in vitro study," *The Journal of Prosthetic Dentistry,* vol. 101, no. 6, pp. 372-381, 2009.

[14] A. Wexler, S. Tzadok, and N. Casap, "Computerized navigation surgery for the safe placement of palatal implants," *American Journal of Orthodontics and Dentofacial Orthopedics,* vol. 131, no. 4, pp. S100-S105, 2007.

[15] J. Choi, B. Lee, and J. Suk Han, "Boundary integral method for shape optimization of interface problems and its application to implant design in dentistry," *Computer Methods in Applied Mechanics and Engineering,* vol. 190, no. 51-52, pp. 6909-6926, 2001.

[16] L. Shi, H. Li, A. Fok, C. Ucer, H. Devlin, and K. Horner, "Shape optimization of dental implants," *The International Journal of Oral & Maxillofacial Implants,* vol. 22, no. 6, pp. 911-920, 2007.

[17] "Dental Implants. Available: http://www.aaoms.org/dental_implants.php.

[18] P. I. Brånemark, B. Hansson, R. Adell, U. Breine, J. Lindström, O. Hallen *et al.*, "Osseointegrated implants in the treatment of the edentulous jaw. Experience from a 10-year period," *Scandinavian Journal of Plastic and Reconstructive Surgery. Supplementum,* vol. 16, pp. 1-132, 1977.

[19] I. K. Karoussis, U. Brägger, G. E. Salvi, W. Bürgin, and N. P. Lang, "Effect of implant design on survival and success rates of titanium oral implants: a 10 year prospective cohort study of the ITI® Dental Implant System," *Clinical Oral Implants Research,* vol. 15, no. 1, pp. 8-17, 2004.

[20] O. Bahat, "Brånemark system implants in the posterior maxilla: clinical study of 660 implants followed for 5 to 12 years," *The International Journal of Oral & Maxillofacial Implants,* vol. 15, no. 5, pp. 646-653, 2000.

[21] "Dental Implants. Available: http://philippinedentalclinic.com/dental-implants.html.

[22] N. Broggini, L. McManus, J. Hermann, R. Medina, T. Oates, R. Schenk *et al.*, "Persistent acute inflammation at the implant-abutment interface," *Journal of Dental Research,* vol. 82, no. 3, pp. 232-237, 2003.

[23] P. O. Östman, M. Hellman, T. Albrektsson, and L. Sennerby, "Direct loading of Nobel Direct® and Nobel Perfect® one-piece implants: a 1-year prospective clinical and radiographic study," *Clinical Oral Implants Research,* vol. 18, no. 4, pp. 409-418, 2007.

[24] "One-piece and two-piece implants demonstrate comparable stress levels in bone: preliminary results of an FEA study. Available: http://www.zimmerdental.com/pdf/lib_artZOPZOPA991.pdf.

[25] J. S. Hermann, D. L. Cochran, D. Buser, R. K. Schenk, and J. D. Schoolfield, "Biologic Width around one and two piece titanium implants," *Clinical Oral Implants Research,* vol. 12, no. 6, pp. 559-571, 2001.

[26] X. Sun, F. D. McKenzie, S. Bawab, J. Li, Y. Yoon, and J. K. Huang, "Automated dental implantation using image-guided robotics: registration results," *International Journal of Computer Assisted Radiology and Surgery*, pp. 1-8, 2011.

[27] T. Albrektsson, J. Gottlow, L. Meirelles, P. O. Östman, A. Rocci, and L. Sennerby, "Survival of NobelDirect implants: An analysis of 550 consecutively placed implants at 18 different clinical centers," *Clinical Implant Dentistry and Related Research,* vol. 9, no. 2, pp. 65-70, 2007.

[28] T. Van de Velde, E. Thevissen, G. R. Persson, C. Johansson, and H. De Bruyn, "Two year outcome with Nobel Direct® implants: A retrospective radiographic and microbiologic study in 10 patients," *Clinical Implant Dentistry and Related Research,* vol. 11, no. 3, pp. 183-193, 2009.

[29] J. A. Hahn, "Clinical and radiographic evaluation of one-piece implants used for immediate function," *Journal of Oral Implantology,* vol. 33, no. 3, pp. 152-155, 2007.

[30] D. S. Sohn, M. S. Bae, J. U. Heo, J. S. Park, S. H. Yea, and G. E. Romanos, "Retrospective multicenter analysis of immediate provisionalization using one-piece narrow-diameter (3.0-mm) implants," *The International Journal of Oral & Maxillofacial Implants,* vol. 26, no. 1, pp. 163-168, 2011.

[31] "Nobel Biocare welcomes the decision of the Swedish Medical Product Agency (MPA) on NobelDirect and NobelPerfect one-piece implants. Available: http://corporate.nobelbiocare.com/en/media/latest-news/corporate-news/2006/nobel-biocare-welcomes-the-decision-of-the-swedish-medical-product-agency-mpa-on-nobe_17.aspx.

[32] "Zimmer One-Piece Implant System. Available: http://www.zimmerdental.com/Products/Implants/im_zopFBOverView.aspx.

[33] "one-piece 3.0 dental implant. Available: http://www.biohorizons.com/onepiece.aspx.

[34] G. Kurtzman, and K. Schwartz, "The subperiosteal implant as a viable long-term treatment modality in the severely atrophied mandible: a patient's 40-year case history," *The Journal of Oral Implantology,* vol. 21, no. 1, pp. 35-39, 1995.

[35] T. Balshi, and G. Wolfinger, "Two-implant-supported single molar replacement: interdental space requirements and comparison to alternative options," *International Journal of Periodontics and Restorative Dentistry,* vol. 17, pp. 427-436, 1997.

[36] T. J. Balshi, R. E. Hernandez, M. C. Pryszlak, and B. Rangert, "A comparative study of one implant versus two replacing a single molar," *The International Journal of Oral & Maxillofacial Implants,* vol. 11, no. 3, pp. 372-378, 1996.

[37] M. T. C. Leung, A. B. M. Rabie, and R. W. K. Wong, "Stability of connected mini-implants and miniplates for skeletal anchorage in orthodontics," *The European Journal of Orthodontics,* vol. 30, no. 5, pp. 483-489, 2008.

[38] S. Hassfeld, and J. Mühling, "Computer assisted oral and maxillofacial surgery-a review and an assessment of technology," *International Journal of Oral and Maxillofacial Surgery,* vol. 30, no. 1, pp. 2-13, 2001.

[39] A. S. E. Askary, R. M. Meffert, and T. Griffin, "Why do dental implants fail? Part I," *Implant Dentistry.,* vol. 8, no. 2, pp. 173-185, 1999.

[40] P. Kazanzides, G. Fichtinger, G. Hager, A. Okamura, L. Whitcomb, and R. Taylor, "Surgical and interventional robotics-core concepts, technology, and design," *IEEE Robotics & Automation Magazine,* vol. 15, no. 2, pp. 122-130, 2008.

[41] "Image Guided Surgery. Available: http://www.sibrainandspine.com/image_guided_surgery.php.

[42] "Virtual reality applications. Available: http://vresources.org/applications/applications.shtml.

[43] H. J. Nickenig, and S. Eitner, "Reliability of implant placement after virtual planning of implant positions using cone beam CT data and surgical (guide) templates," *Journal of Cranio-Maxillofacial Surgery,* vol. 35, no. 4-5, pp. 207-211, 2007.

[44] C. Xiaojun, L. Yanping, W. Yiqun, and W. Chengtao, "Computer-aided oral implantology: Methods and applications," *Journal of Medical Engineering & Technology,* vol. 31, no. 6, pp. 459-467, 2007.

[45] P. Pohlenz, M. Blessmann, F. Blake, S. Heinrich, R. Schmelzle, and M. Heiland, "Clinical indications and perspectives for intraoperative cone-beam computed tomography in oral and maxillofacial surgery," *Oral Surgery, Oral Medicine, Oral Pathology, Oral Radiology, and Endodontology,* vol. 103, no. 3, pp. 412-417, 2007.

[46] A. Nijmeh, N. Goodger, D. Hawkes, P. Edwards, and M. McGurk, "Image-guided navigation in oral and maxillofacial surgery," *British Journal of Oral and Maxillofacial Surgery,* vol. 43, no. 4, pp. 294-302, 2005.

[47] Y. Sato, M. Nakamoto, Y. Tamaki, T. Sasama, I. Sakita, Y. Nakajima *et al.*, "Image guidance of breast cancer surgery using 3-D ultrasound images and augmented reality visualization," *Medical Imaging, IEEE Transactions on,* vol. 17, no. 5, pp. 681-693, 1998.

[48] D. Schneider, P. Marquardt, M. Zwahlen, and R. E. Jung, "A systematic review on the accuracy and the clinical outcome of computer-guided template-based implant dentistry," *Clinical Oral Implants Research,* vol. 20, pp. 73-86, 2009.

[49] F. K. Wacker, S. Vogt, A. Khamene, J. A. Jesberger, S. G. Nour, D. R. Elgort *et al.*, "An augmented reality system for MR image–guided needle biopsy: Initial results in a swine model," *Radiology,* vol. 238, no. 2, pp. 497-504, 2006.

[50] H. Iseki, Y. Masutani, M. Iwahara, T. Tanikawa, Y. Muragaki, T. Taira *et al.*, "Volumegraph (Overlaid three-dimensional image-guided navigation)," *Stereotactic and Functional Neurosurgery,* vol. 68, no. 1-4, pp. 18-24, 1997.

[51] B. Peuchot, A. Tanguy, and M. Eude, "Virtual reality as an operative tool during scoliosis surgery." 1995, pp. 549-554.

[52] A. Azari, and S. Nikzad, "The evolution of rapid prototyping in dentistry: a review," *Rapid Prototyping Journal,* vol. 15, no. 3, pp. 216-225, 2009.

[53] T. Dreiseidler, J. Neugebauer, L. Ritter, T. Lingohr, D. Rothamel, R. A. Mischkowski *et al.*, "Accuracy of a newly developed integrated system for dental implant planning," *Clinical Oral Implants Research,* vol. 20, no. 11, pp. 1191-1199, 2009.

[54] A. Sicilia, B. Noguerol, J. Cobo, and I. Zabalegui, "Profile surgical template: a systematic approach to precise implant placement. A technical note," *International Journal of Oral and Maxillofacial Implants,* vol. 13, no. 1, pp. 109-114, 1998.

[55] R. Galloway, and T. Peters, "Overview and history of image-guided interventions," *Image-guided interventions: technology and applications*, T. Peters and K. Cleary, eds.: Springer, 2008, pp. 1-21.

[56] T. M. Peters, and K. R. Cleary, *Image-guided interventions: Technology and applications*: Springer Verlag, 2008.

[57] M. Hofer, G. Strauß, K. Koulechov, and A. Dietz, "Definition of accuracy and precision-evaluating CAS-systems." 2005, pp. 548-552.

[58] J. M. Fitzpatrick, and J. B. West, "The distribution of target registration error in rigid-body point-based registration," *Medical Imaging, IEEE Transactions on,* vol. 20, no. 9, pp. 917-927, 2001.

[59] G. Widmann, R. Stoffner, and R. Bale, "Errors and error management in image-guided craniomaxillofacial surgery," *Oral Surgery, Oral Medicine, Oral Pathology, Oral Radiology, and Endodontology,* vol. 107, no. 5, pp. 701-715, 2009.

[60] D.-J. Kroon. "Finite iterative closest point. Available: http://www.mathworks.com/matlabcentral/fileexchange/24301-finite-iterative-closest-point.

[61] P. Bergström. "Iterative closest point method, C++. Available: http://www.mathworks.com/matlabcentral/fileexchange/16766-iterative-closest-point-method-c++.

[62] C. Xiaojun, Y. Ming, L. Yanping, W. Yiqun, and W. Chengtao, "Image guided oral implantology and its application in the placement of zygoma implants," *Computer Methods and Programs in Biomedicine,* vol. 93, no. 2, pp. 162-173, 2009.

[63] J. B. West, J. M. Fitzpatrick, S. A. Toms, C. R. Maurer Jr, and R. J. Maciunas, "Fiducial point placement and the accuracy of point-based, rigid body registration," *Neurosurgery,* vol. 48, no. 4, pp. 810-816, 2001.

[64] C. R. Mascott, J. C. Sol, P. Bousquet, J. Lagarrigue, Y. Lazorthes, and V. Lauwers-Cances, "Quantification of true in vivo (application) accuracy in cranial image-guided surgery: influence of mode of patient registration," *Neurosurgery,* vol. 59, no. 1, pp. ONS146-156, 2006.

[65] R. Krempien, S. Hassfeld, J. Kozak, H. P. Tuemmler, S. Däuber, M. Treiber *et al.*, "Frameless image guidance improves accuracy in three-dimensional interstitial brachytherapy needle placement," *International Journal of Radiation Oncology • Biology • Physics,* vol. 60, no. 5, pp. 1645-1651, 2004.

[66] R. Mischkowski, M. Zinser, L. Ritter, J. Neugebauer, E. Keeve, and J. Zöller, "Intraoperative navigation in the maxillofacial area based on 3D imaging obtained by a cone-beam device," *International journal of oral and maxillofacial surgery,* vol. 36, no. 8, pp. 687-694, 2007.

[67] G. Eggers, J. Muhling, and R. Marmulla, "Template-based registration for image-guided maxillofacial surgery," *Journal of Oral and Maxillofacial Surgery,* vol. 63, no. 9, pp. 1330-1336, 2005.

[68] R. F. Labadie, R. J. Shah, S. S. Harris, E. Cetinkaya, D. S. Haynes, M. R. Fenlon *et al.*, "In vitro assessment of image-guided otologic surgery: submillimeter accuracy within the region of the temporal bone," *Otolaryngology-Head and Neck Surgery,* vol. 132, no. 3, pp. 435-442, 2005.

[69] G. Zheng, J. Kowal, M. González Ballester, M. Caversaccio, and L. Nolte, "Registration techniques for computer navigation," *Current Orthopaedics,* vol. 21, no. 3, pp. 170-179, 2007.

[70] A. R. Lanfranco, A. E. Castellanos, J. P. Desai, and W. C. Meyers, "Robotic surgery: A current perspective," *Annals of Surgery,* vol. 239, no. 1, pp. 14-21, 2004.

[71] J. Chiao, J. M. Goldman, D. A. Heck, P. Kazanzides, W. J. Peine, J. B. Stiehl *et al.*, "Metrology and standards needs for some categories of medical devices," *Journal of Research of the National Institute of Standards and Technology,* vol. 113, no. 2, pp. 121-129, 2008.

[72] W. Korb, R. Marmulla, J. Raczkowsky, J. Mühling, and S. Hassfeld, "Robots in the operating theatre-chances and challenges," *International Journal of Oral and Maxillofacial Surgery,* vol. 33, no. 8, pp. 721-732, 2004.

[73] R. Taylor, P. Jensen, L. Whitcomb, A. Barnes, R. Kumar, D. Stoianovici *et al.*, "A steady-hand robotic system for microsurgical augmentation," *The International Journal of Robotics Research,* vol. 18, no. 12, pp. 1201, 1999.

[74] D. Sarment, P. Sukovic, and N. Clinthorne, "Accuracy of implant placement with a stereolithographic surgical guide," *The International Journal of Oral & Maxillofacial Implants,* vol. 18, no. 4, pp. 571, 2003.

[75] G. Hager, A. Okamura, P. Kazanzides, L. Whitcomb, G. Fichtinger, and R. Taylor, "Surgical and interventional robotics: part III [Tutorial]," *Robotics & Automation Magazine, IEEE,* vol. 15, no. 4, pp. 84-93, 2008.

[76] M. Matinfar, C. Baird, A. Batouli, R. Clatterbuck, and P. Kazanzides, "Robot-assisted skull base surgery," in Intelligent Robots and Systems, 2007. IROS 2007. IEEE/RSJ International Conference on, 2007, pp. 865-870.

[77] A. Kapoor, M. Li, and R. H. Taylor, "Constrained control for surgical assistant robots," *Proceedings of the 2006 IEEE International Conference on Robotics and Automation.* pp. 231-236.

[78] M. Li, M. Ishii, and R. H. Taylor, "Spatial motion constraints using virtual fixtures generated by anatomy," *Robotics, IEEE Transactions on,* vol. 23, no. 1, pp. 4-19, 2007.

[79] "DentMILL - 3-5 Axis Dental CAM. Available: http://www.dental-cadcam.com/general/dentmill.asp.

[80] "incise™ - affordable dental cad/cam. Available: http://www.renishaw.com/en/6157.aspx.

[81] C. Mascle, L. Hua, and R. Maranzana, "Machining process planning using Decomposition of Delta Volume," in Assembly and Manufacturing, 2007. ISAM '07. IEEE International Symposium on, 2007, pp. 106-111.

[82] X. Chen, Y. Lin, Y. Wu, and C. Wang, "Real-time motion tracking in image-guided oral implantology," *The International Journal of Medical Robotics and Computer Assisted Surgery,* vol. 4, no. 4, pp. 339-347, 2008.

[83] C. S. Tseng, C. C. Huang, and C. S. Chen, "Development of an image-guided robotic system for surgical positioning and drilling," *Robotica,* vol. 25, no. 03, pp. 375-383, 2007.

[84] "Universal numbering system (dental). Available: http://en.wikipedia.org/wiki/Universal_numbering_system_(dental).

[85] "teeth_numbers. Available: http://www.sundds.com/faq_tooth_teeth_numbers.htm.

[86] Y. Yoon, "Evaluation of autonomous robotic milling methodology for natural tooth-shaped implants based on SKO optimization," PhD thesis, Department of Mechanical and Aerospace Engineering, Old Dominion University, Norfolk, 2012.

[87] A. Baumgartner, L. Harzheim, and C. Mattheck, "SKO (soft kill option): the biological way to find an optimum structure topology," *International Journal of Fatigue,* vol. 14, no. 6, pp. 387-393, 1992.

[88] Y. Yoon, X. Sun, J.-K. Huang, G. Hou, K. Rechowicz, and F. D.McKenzie, "Designing natural-rooth-shaped dental implants based on soft-kill option optimization," *Computer-aided Design and Applications*, 2012.

[89] G. C. Downer, and D. Anderson, *Dental Morphology: an illustrated guide*, London J. Wright, 1975.

[90] A. Myronenko, and X. Song, "Point set registration: coherent point drift," *Pattern Analysis and Machine Intelligence, IEEE Transactions on,* vol. 32, no. 12, pp. 2262-2275, 2010.

[91] C. Martinez. "AOI-Matlab Voxelizer. Available: http://people.exeter.ac.uk/cm265/aoi/index.html.

[92] F. Mourougaya. "contour_following. Available: http://www.mathworks.com/matlabcentral/fileexchange/14947-contourfollowing.

APPENDICES